Structure Based Studies on FMN-Binding Fluorescent LOV Proteins and Their Application as Optogenetic Tools

Inaugural-Dissertation

zur Erlangung des Doktorgrades
der Mathematisch-Naturwissenschaftlichen Fakultät
der Heinrich-Heine-Universität Düsseldorf

vorgelegt von

Katrin Röllen
aus Viersen

Düsseldorf, Januar 2016

aus dem Institute of Complex Systems (ICS-6)
der Heinrich-Heine-Universität Düsseldorf

Gedruckt mit der Genehmigung der
Mathematisch-Naturwissenschaftlichen Fakultät der
Heinrich-Heine-Universität Düsseldorf

Referent: PD Dr. Renu Batra-Safferling
Korreferent: Prof. Dr. Karl-Erich Jäger

Tag der mündlichen Prüfung: 04. April 2016

Zwei Dinge sind zu unserer Arbeit nötig:

Unermüdliche Ausdauer und die Bereitschaft, etwas,

in das man viel Zeit und Arbeit gesteckt hat, wieder wegzuwerfen.

(Albert Einstein)

Meinen Eltern

List of Publications

Röllen, K., Granzin, J., Panwalker, V., Arinkin, V., Rani, R., Hartmann, R., Krauss, U., Jaeger, K.-E., Willbold, D., Batra-Safferling, R. (2016) Signaling states of a short blue light photoreceptor protein PpSB1-LOV revealed from crystal structures and solution NMR spectroscopy*, J. Mol. Biol. 2016 Jun 9. pii: S0022-2836(16)30206-6. doi:10.1016/j.jmb.2016.05.027 [Epub ahead of print]*

Röllen, K., Granzin, J., Arinkin, V., Krauss, U., Drepper, T., Jaeger, K.-E., Willbold, D., Batra-Safferling, R., Structural evidence for the role of Met49 in dark recovery kinetics of a LOV protein DsLOV, *manuscript under preparation*

Röllen, K., Granzin, J., Arinkin, V., Krauss, U., Jaeger, K.-E., Batra-Safferling, R., Stadler, A., Light-induced responses in a full-length short LOV protein measured with time-resolved small angle X-ray scattering, *manuscript under preparation*

Poster presentation

Röllen, K., Granzin, J., Arinkin, V., Willbold, D., Batra-Safferling, R. (2015). Signal propagation in the blue-light-sensitive protein PpSB1-LOV – a comparison between crystal structures in light and dark states. GRC Proteins, Holderness, New Hampshire, USA *(Best poster award)*

Arinkin, A., Granzin, J., **Röllen, K.**, Batra-Safferling, R. (2015). Crystal structure of a fast recovering full-length LOV protein PpSB2-LOV from *Pseudomonas putida* - 1st CSSB International Symposium - Systems in Infection Biology From Molecules to Organisms, Hamburg, Germany.

Röllen, K., Granzin, J., Panwalker, V., Arinkin, V., Krauss, U., Jäger, K.-E., Willbold, D., Batra-Safferling, R. (2016) Signalling states of a short blue-light photoreceptor protein PpSB1-LOV – GRC Photosensory Receptors & Signal Transduction, Galveston, Texas, USA

Acknowledgements

First of all, I would like to thank PD Dr. Renu Batra-Safferling for providing me with this interesting topic and her continuous help and support during the last three years of my PhD.

Many thanks to Prof. Dr. Karl-Erich Jäger for helping me first to get in touch with PD Dr. Renu Batra-Safferling and of course for kindly taking over the secondary examination of my thesis.

I would like to thank Prof. Dr. Dieter Willbold for the possibility to work at the Institute of Complex Systems – 6 at the FZ Jülich.

Thanks to PD Dr. Joachim Granzin for his continuous help in theory and the practical aspects of X-ray crystallography. I could not have done this work without his support.

A big “thank you” goes to Andreas Stadler who helped me with the theory and practice of small angle X-ray scattering. The discussions about this method and the results of this work have always been interesting and helpful.

I also would like to thank Dr. Ulrich Krauss and Dr. Thomas Drepper at the Institute of Molecular Enzyme Technology and their collaborators, especially Esther Knieps-Grünhagen, who helped me in the beginning to get started with my project. The knowledge and experience you shared with me was really helpful in the development of this thesis.

A special thanks goes to Anne Cousin who was a huge support in the first steps in the lab. Thanks for your knowledge, optimism, humour, and your support. It has been a true valuable experience.

To the people in the “TA-office”: Thank you so much for your support, the interesting conversations and most important for your “round table” which was always full of nice things!

I also would like to thank Michael Owen for reading and correcting my thesis.

Thanks to all the people who supported me during my time at the university and during my PhD in all possible ways even if they are not named individually.

And of course a special thanks to Dr. Vineet Panwalkar for sharing the same office with me for three years filled with interesting, crazy and weird conversations and of course a lot of laughter!

Markus, I have to thank you for your support, your strength and patience! Your understanding and encouragement helped me so much, especially in the last couple of months.

Das wohl größte Dankeschön gilt meinen Eltern, für ihre Unterstützung, ihr Verständnis, und so vieles mehr, von Beginn des Studiums an bis zum Ende der Promotion. Ohne euch hätte ich vieles wohl gar nicht erst geschafft!

Abstract

The growing field of optogenetics is the focus of current scientific areas such as in biotechnology and biomedicine. Application of optogenetic tools has made spatiotemporal control of several biological processes now possible. Recent research has focused on employment of photoactivatable proteins from the Light-Oxygen-Voltage (LOV) family, where LOV domains represent the photo-responsive domains that mediate sensory responses to various signal transduction domains. In order to design LOV-based optogenetic devices, it is essential to gather a detailed knowledge of allosteric communication between the LOV sensor and effector domains. For this, characterization of all relevant signaling states is required at molecular level. The main objective of this thesis is the structural analysis of full-length short LOV proteins, for which X-ray crystallography and small angle X-ray scattering (SAXS) methods were employed.

In this thesis, two LOV proteins PpSB1-LOV from the soil bacteria *Pseudomonas putida*, and DsLOV from the marine bacteria *Dinoroseobacter shibae* and their respective mutants are characterized. The LOV protein PpSB1-LOV has been previously characterized biochemically and photochemically, and the light state structure was already published. The dark state crystal structure is determined in this thesis and structural comparison of both the states is performed. Large conformational change in the C-terminal helix Jα, a different dimer organisation, combined with differences in coordination of the chromophore enabled prediction of the signal propagation in PpSB1-LOV. This signal transfer is induced by illumination with blue light, subsequent absorption of a photon and the formation of a covalent bond between the Sγ atom of the photoactive cysteine and the C4a atom of the FMN chromophore. A conformational change of key amino acid side chains in the LOV core domain, in particular of Gln116, induces a reorientation of the C-terminal helix propagating the signal to the outer regions of the protein. Subsequently, this is directed towards a putative effector domain. Extended SAXS experiments in solution supported the obtained results. The same structural rearrangements are observed for PpSB1-LOV-C53A in which the photoactive cysteine was substituted into an alanine thus generating a protein which is unable to undergo photoactivation, and is permanently fluorescent. The comparison of the PpSB1-LOV structures in dark, light and illuminated states provide further insights into the light-induced activation and signal propagation in SB1-LOV protein. Furthermore, two additional arginines (Arg61 and Arg66) coordinating the phosphate of the chromophore were previously identified to be partly responsible for the slow dark recovery of PpsB1-LOV. Crystal structure of PpSB1-LOV-R61H/R66I in dark state shows that

coordination of the phosphate moiety is compensated by the remaining conserved arginines. The second short LOV protein DsLOV exhibits a methionine at position 49, which is usually occupied by a leucine or isoleucine in other LOV protein sequences. Substitution of the methionine into an isoleucine and a serine has a severe influence on the dark recovery. The wildtype exhibits a recovery time of τ_{REC} = 9.6 s and is accelerated in the DsLOV-M49S mutant to τ_{REC} = 1.1 s and decelerated in DsLOV-M49I to τ_{REC} = 153 s. The crystal structures in dark state of both mutants reveal a change in steric interaction as the possible origin for these differences. The isoleucine shields the covalent bond suppressing deprotonation of the N5, whereas the serine enhances this protonation due to its smaller size. In addition, a different dimer interface as published for the wildtype structure is observed in the crystal structure of DsLOV-M49I. In case of wildtype DsLOV, the N-terminal cap mediates formation of the dimer. This N-cap region is not observed in DsLOV-M49I, most likely due to higher flexibility in this region. Instead, the dimer is formed by residues in the β-sheet of the conserved LOV core domain. Crystal structure of DsLOV-C72A is also determined that shows high similarity to the wild type DsLOV in dark state, and is currently being applied as a fluorescence reporter.

Zusammenfassung

Das kontinuierlich wachsende Feld der Optogenetik nimmt eine immer stärker werdende Rolle in verschiedenen Bereichen der Naturwissenschaften, unter anderem der Biotechnologie und Biomedizin, ein. In den letzten Jahren wurden vor allem licht-aktivierbare Vertreter der Familie der Light, Oxygen, Voltage (LOV) Proteinfamilie auf ihre Anwendbarkeit als optogenetisches Werkzeug hin untersucht. LOV Domänen leiten durch Lichteinstrahlung ausgelöste Signale zu unterschiedlichen Effektordomänen weiter. Ein detailliertes Wissen über diese Interaktion zwischen Sensor- und Effektormolekülen ist von großer Bedeutung um optogenetische Werkzeuge zu designen. Dazu ist es nötig die einzelnen Schritte der Signalaufnahme- und Weiterleitung auf molekularer Ebene zu charakterisieren und verstehen. Darauf beruhend ist ein Hauptaspekt dieser Arbeit die Strukturanalyse von Kurz-LOV Proteinen mittels Röntgenkristallstrukturanalyse und Kleinwinkel-Röntgenstreuung.

In dieser Arbeit wurden die Kurz-LOV Proteine PpSB1-LOV aus *Pseudomonas putida* und DsLOV aus *Dinoroseobacter shibae* und ihre Mutanten (PpSB1-LOV-C53A, PpSB1-LOV-R66I, PpSB1-LOV-R61H/R66I, DsLOV-M49S, DsLOV-M49I, DsLOV-C72A) strukturell charakterisiert. Ein Vergleich der Lichtstruktur und der in dieser Arbeit bestimmten Dunkelstruktur von PpSB1-LOV zeigt eine Konformationsänderung der C-terminalen Jα Helix, eine veränderte Organisation der einzelnen Moleküle im Dimer zueinander und Veränderungen der Chromophorkoordination. Die oben genannte Signalweiterleitung in LOV Proteinen wird initiiert durch die Bestrahlung mit Blaulicht und der darauffolgenden Ausbildung einer kovalenten Bindung zwischen Cys53-Sγ und dem C4a Atom des Flavinmononukleotid (FMN). Konformationsänderungen der Aminosäuren Seitenketten, vor allem des Gln116 in der Kernregion, induziert die beobachteten Änderungen von PpSB1-LOV, wodurch das Signal zu den äußeren Bereichen des Proteins weitergeleitet werden kann. Diese Ergebnisse werden durch Kleinwinkel-Röntgenstreuung (SAXS) Daten unterstützt. Die Struktur der Mutante PpSB1-LOV-C53A, bei welcher der Austausch des photoaktiven Cysteins einen permanent fluoreszierenden Photosensor generiert, stimmt mit der Dunkelstruktur des Wildtyps überein. Ein Vergleich der Struktur von Licht- und Dunkelzustand mit der sogenannten belichteten Struktur zeigt, dass Erkenntnisse über strukturelle Änderungen auch aus belichteten Strukturen gewonnen werden können. Zusätzlich ist in dieser Arbeit die Struktur der Mutante PpSB1-LOV-R61H/R66I im Dunkelzustand bestimmt worden. In PpSB1-LOV wurden Arg61 und Arg66 als diejenigen Aminosäuren identifiziert, die zusätzlich zu den konservierten Argininen (Arg54 und Arg70) die Phosphatgruppe des FMN koordinieren. Diese vierfache Koordination

hat einen ausschlaggebenden Anteil an der langsamen Rückkehr des Proteins in den Dunkelzustand. Die Kristallstruktur zeigt, dass die verbliebenen zwei Arginine die Koordinierung des FMN-Phosphatrestes ausgleichen.

Ein Vergleich von Aminosäuren Sequenzen verschiedener LOV Proteine zeigt, dass bei DsLOV an Position 49 ein Methionin liegt, welche in anderen LOV Proteinen durch ein Leucin oder Isoleucin besetzt ist. Ein Austausch dieser Aminosäure mit einem Isoleucin und einem Serin bewirkt einen deutlichen Unterschied der Rückkehrzeit in den Dunkelzustand. Für den Wildtyp wurde ein Zeitkonstante von τ_{REC} = 9.6 s beobachtet. Der Austausch in ein Isoleucin verlangsamt die Rückkehrreaktionszeit zu τ_{REC} = 153 s, wohingegen der Austausch in ein Serin die Reaktion beschleunigt mit τ_{REC} = 1.1 s. In der Literatur wurden diese Unterschiede mit sterischen Effekten begründet. Die Seitenkette des Isoleucins hat einen starken abschirmenden Effekt auf die kovalente Bindung (siehe oben) wobei außerdem die Deprotonierung des N5-Atoms des FMN verlangsamt wird. Die kleinere Seitenkette des Serins hingegen hat einen schwächeren abschirmenden Effekt, wodurch die Rückkehr in den Dunkelzustand beschleunigt wird. Die Kristallstruktur der Mutante DsLOV-M49S konnte in dieser Arbeit ebenfalls bestimmt werden und zusätzliche Hinweise liefern, um den oben beschriebenen Unterschied der Zeitkonstante in der Rückkehr in den Dunkelzustand zu erklären. Weiterhin wurde die Struktur der Mutante DsLOV-C72A in dieser Arbeit bestimmt, die der des Wildtyps sehr ähnlich ist. Diese Mutante wird zurzeit auf die Anwendbarkeit als Fluoreszenzreporter geprüft. Vor kurzem wurde die Kristallstruktur des Wildtyps publiziert. Dabei konnte ein Dimer identifiziert werden, das durch N-terminale Sekundärstrukturelemente bestehend aus zwei Schleifen und einer Helix (sogenannter „Ncap“) gebildet wird. Die Kristallstruktur der Mutante DsLOV-M49I hingegen zeigt einen Dimer, der durch Interaktionen zwischen Aminosäuren gebildet wird, die im konservierten β-Faltblatt zu finden sind.

List of Figures

List of Tables

List of Abbreviations

°C	Degree Celsius
µg	Microgram
µL	Microliter
Å	Angstrom
A	Ampere
ARNT	Aryl hydrocarbon nuclear transporter
BLUF	Blue-light receptor using FAD
cm	Centimetre
CV	Column volume
ddH2O	Double distilled water
DESY	Deutsches Elektronen Synchrotron
DNA	Deoxyribonucleic acid
E. coli	*Escherichia coli*
et al.	et alii
FAD	Flavin adenine dinucleotide
FbFP	FMN binding fluorescent protein
fc	Final concentration
FMN	Flavin mononucleotide
FRET	Förster resonance energy transfer
g	Gram
GFP	Green fluorescent protein
h	Hours
Hg	Mercury
I	Intensity
K	Kelvin
kDa	Kilo Dalton
Km	Kanamycin
L	Litre
LB	Luria-Bertani
LOV	Light, Oxygen, Voltage
M	Molar
mA	Miliampere
Mb	Megabases
min	minutes
mL	Millilitre
mM	Milimolar
mW	Miliwatt
MW	Molecular weight
nm	Nanometre
OCP	Orange carotenoid protein
OD	Optical density
p. A.	Per analyses
PAS	Per-ARNT-Sim
PDB	Protein data base

PEG	Polyetyhlenglycol
ps	Picoseconds
PYP	Photoactive yellow protein
q	Scattering angle
RBF	Riboflavin
res.	Residue
rpm	Rotation per minute
RT	Room temperature
s	Seconds
SAXS	Small angle X-ray scattering
SDS-PAGE	Sodium dodecyl sulphate-polyacrylamide gel electrophoresis
SEC	Size exclusion chromatography
STAS	Sulphate transporter and anti-sigma-factor antagonist
UV	Ultraviolet
v/v	Volume per volume
w/v	Weight per volume
ε	Extinction coefficient
λ	Wavelength

Table of Contents

1. Introduction

1.1. LOV-proteins

Light is one of the most essential and crucial requirement for the viability of most existing organisms. Different evolutionary adaption processes in nature enable living cells to absorb, process and react to light. In this context, eight different sensor protein families are known: rhodopsins, phytochromes, xanthopsins, cryptochromes, phototropins, BLUF (blue-light receptor using FAD) proteins, photoreceptors sensing UV radiation like UVR8 from *Arabidopsis thaliana*, and the orange carotenoid proteins (OCP). Each reacting to light of precise wavelength range with a photochemistry characteristic for the respective family and different photon absorbent molecules. In the first three families a cis/trans isomerization of retinal, linear tetrapyrrol, and *p*-hydrocinnamoyl anion is the basis of the photochemistry (Birge, 1990; Rockwell, et al., 2006; Coto, et al., 2008). The cryptochromes, phototropin and BLUF families exhibit a flavin molecule (FMN or FAD) inside their photosensitive core domain (Christie , et al., 2015; Fudim, et al., 2015).

Rhodopsins play a key role in the phototransduction and light/dark vision in vertebrates (Schreiber, et al., 2006), but are also present in haloarchaea, proteobacteria, cyanobacteria, fungi, and algae (Spudich, et al., 2002). The red/far-red light absorbing phytochromes in plants mediate the regulation of seedling de-etiolation, flowering, and shade-avoidance (Franklin, et al., 2010; Chen, et al., 2011). In comparison, less is known about the xanthopsin family. The best known representative is the photoactive yellow protein (PYP) of *Ectothiorhodospira halophila* and although a lot of effort is made neither the natural interaction partner, nor the actual functional role in the organism is identified (Möglich, et al., 2010). However, PYP is the structural archetype of the PAS domain which is further discussed in the following.

The blue-light sensitive, FAD-binding cryptochromes play a major role within the gene repression, growth and development in plants, and the circadian clock in animals (Conrad, et al., 2014; Shcherbakova, et al., 2015), any members of this family are part of early investigation of receptors at molecular level (Ahmad, et al., 1993). The well characterized phototropins affect phototropism which is the ability of plants to bend towards the sunlight, stomatal opening, chloroplast migration and leaf expansion in plants (Briggs, et al., 2001 a); Briggs, et al., 2001 b); Sakai, et al., 2001; Kinoshita, et al., 2001; Sakamato, et al., 2002; Briggs, et al., 2002). They are composed of a C-terminal serine/threonine kinase fused to two blue-light sensing core domains. The photocycle of the latter two protein families include the formation of a covalent bond in the core domains between the protein and the flavin chromophore as the primary event

after illumination. In comparison, for the BLUF receptors (blue light receptor using FAD) (Fudim, et al., 2015) no covalent bond formation was observed, the basic reaction after exposure of the protein to light are changes in the direct interaction between conserved residues in secondary structure elements of the apoprotein and the flavin chromophore (Masuda, 2013). The UV photoreceptors with UVR8 as representative most probably exhibits at least one intrinsic tryptophan in the role of a chromophore. UVR8 enables the plant to adapt to UV radiation to minimize stress and damage of the cells (Kliebenstein, et al., 2002; Rizzini, et al., 2011; Tilbrook, et al., 2013). The orange carotenoid protein is part of energy dissipation processes evoked by fluorescence quenching. Most cyanobacteria exhibit highly conserved homologues of OCP in their genome (Kirilovsky, 2007; Berera, et al., 2012).

Interestingly, three protein families - the phototropins, phytochromes, and xanthopsins possess a common structural feature, the light-sensitive PAS domain. The name PAS was derived from sequence based comparison between the *Drosophila melanogaster* genes *period* and *single-minded*, and the vertebrate aryl hydrocarbon nuclear translocator ARNT (Nambu, et al., 1991) (Pellequer, et al., 1998). The structure of these receptors is composed of an anti-parallel β-sheet surrounded by α-helices usually denoted Cα, Dα, Eα, and Fα (figure 1A). Thereby, in comparison to the β-sheet which is highly conserved, the α-helices can vary in length, number and orientation (Möglich, et al., 2009). The canonical PAS-fold shows a strict topologic order Bβ-Aβ-Iβ-Hβ-Gβ for the β-strands comprising the β-sheet (figure 1A). As already mentioned, the described 3D structure was first observed and described for the photoactive yellow protein (PYP) of *Halorhodospira halophila*, formerly known as *Ectothiorhodospira halophila* (Borgstahl, et al., 1995) (figure 1B). In some photoreceptor proteins, the PAS domain is flanked by N- and C-terminal extensions or they are linked C- or N-terminally to an effector domain (Möglich, et al., 2009). A cofactor molecule is located inside the PAS core, covalently or non-covalently linked to the protein.

Different PAS domains can incorporate a variety of cofactors sensitive to different physical and chemical stimuli ascribed to diverse physiological functions (Möglich, et al., 2009). PAS domains are proposed to play a role in selection of regulatory paths, including the adaption to hypoxia (Semenza G.L., 2003), circadian rhythm-dependent gene transcription (Imaizumi T., et al., 2003), phototropism, and chloroplast organization in plants (Liscum, et al., 1995). In this context, dimer or oligomer formation of PAS domains play an integral role in the functional diversity (Huang, et al., 1993; Pongratz, et al., 1998; Talyor, et al., 1999). In majority of cases, homo- and heterodimers are formed which are stabilized by diverse hydrophobic interactions between the conserved β-sheet (Möglich, et al., 2009).

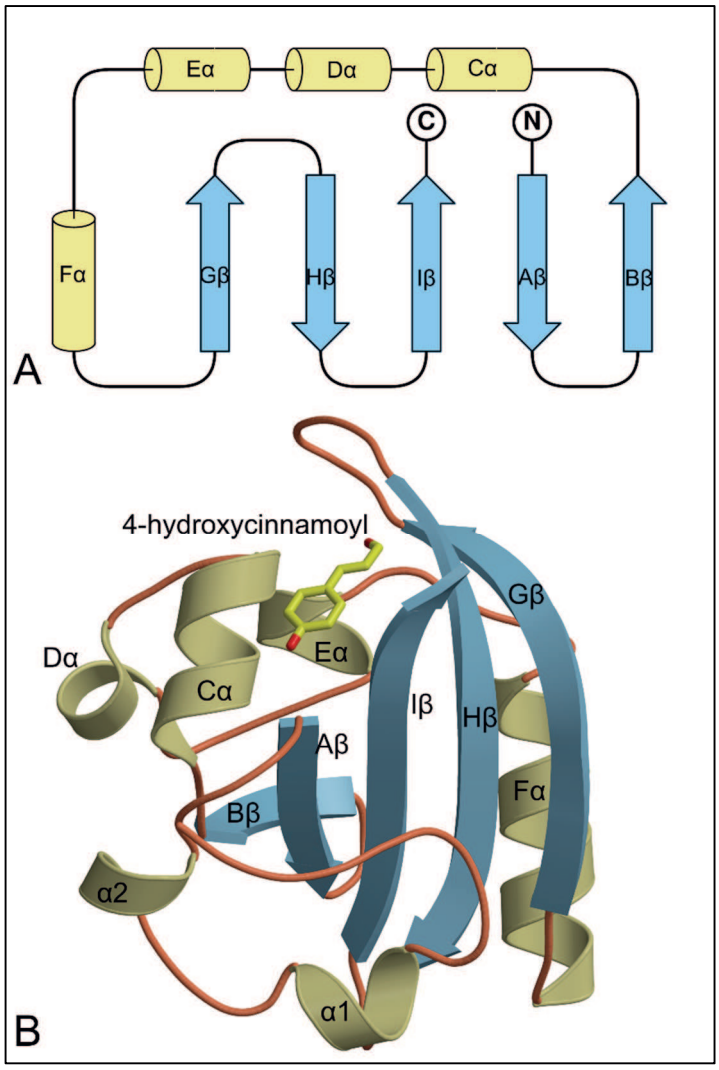

Figure 1: Topology of the canonical α/β-PAS-fold. (A) The highly conserved β-sheet is highlighted in blue; the surrounding helices are highlighted in beige. (B) Ribbon representation of the photoactive yellow protein (PYP, PDB-entry: 2PHY), the structural archetype of PAS domains, the color code is in accordance to panel A.

Within the group of PAS proteins, a special subset of domains was identified specifically binding flavin chromophores and termed LOV domains named after the reaction triggered factors light, oxygen and voltage (Taylor, et al., 1999). One of the first reports of a LOV protein can be found in the description of two tandem PAS-like domains in plant phototropins regulating different parts of photomorphogenesis (Huala, et al., 1997; Herrou, et al., 2012). Since these initial observations, several additional LOV domains were identified and characterized not only in plants, but in archaea, prokarya and eukarya. The diversity of LOV proteins and the infinite dispersion in all kingdoms of life indicate a horizontal gene transfer of ancestral cyanobacteria and proteobacteria into the genome of eukaryotic cells as a consequence of endosymbiosis (Krauss, et al., 2009).

The basic structure of LOV proteins comprise the above described α/β-PAS-fold, with a β-sheet formed by five β-strands and α-helices connecting the strands. Inside the core domain a

blue-light absorbing flavin molecule is non-covalently linked close to a conserved sequence motif GXNCRFLQ where X is any amino acid (figure 2) (Herrou, et al., 2012; Conrad, et al., 2014). The conserved motif comprises the photoactive cysteine required for the formation of a covalent photoadduct as the primary event after excitation with blue light (figure 2 and 3) (Salomon, et al., 2000; Crosson, et al., 2002).

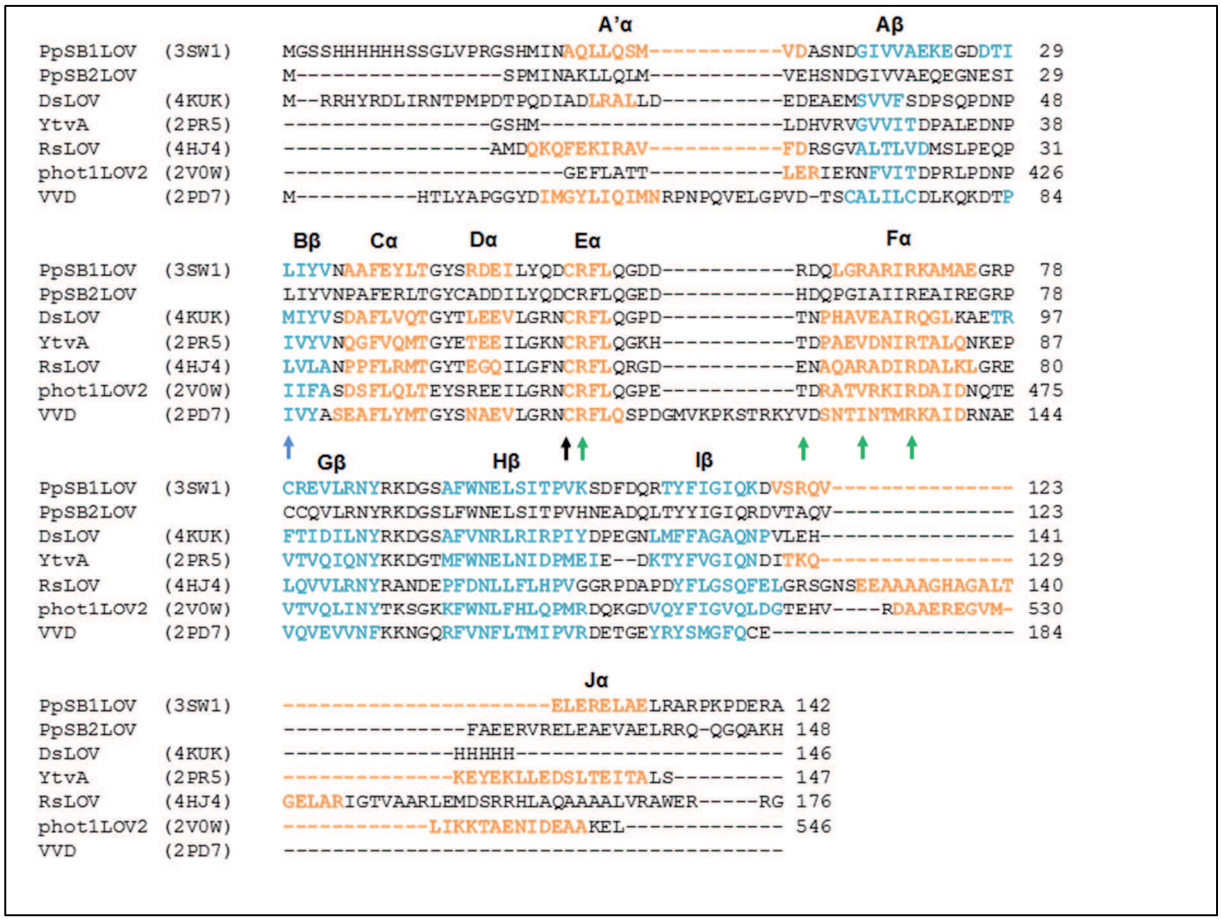

Figure 2: Alignment of amino acid sequence of LOV proteins using the multiple sequence alignment program MAFFT (Katoh, 2013). In particular, of *D. shibae* (DsLOV), *P. putida* (PpSB1-LOV and PpSB2-LOV*), B. subtilis* (YtvA), *A. sativa* (AsLOV), *N. crassa* (VVD) and *R. sphaeroides* (RsLOV), the secondary structure elements are marked in blue (β-strands) and orange (α-helices); the photoactive cysteine is highlighted with a black arrow; the arginines coordinating the phosphate moiety in PpSB1-LOV are highlighted with green arrows. The blue arrow marks the Met49 in DsLOV. This position is discussed further in section 1.3.

In addition to the conserved structure of the core domain, N- and/or C-terminal extensions are observed for most LOV proteins (Möglich, et al., 2007; Zoltowski, et al., 2008). These usually helical or coiled-coil structural elements, either protrude away from the core domain (Möglich, et al., 2007; Circolone, et al., 2012) or are linked to the β-sheet via hydrophobic interactions (Halavaty, et al., 2007; Nash, et al., 2011; Conrad, et al., 2012). If the LOV domain is part of a multidomain protein these extensions are usually linker regions between photoreceptor and effector as found in YtvA where a helical element connects the LOV domain with the STAS effector domain (Möglich, et al., 2007). Additionally, these extensions are often involved in the

formation of LOV protein oligomers, usually dimers (Myatake, et al., 2000; Key, et al., 2007; Zoltowski, et al., 2008; Zoltowski, et al., 2008; Vaidya, et al., 2011; Circolone, et al., 2012). In case no effector domain is observed, the full length LOV construct is designated as a so-called short-LOV protein.

In different organisms LOV proteins mediate various intracellular functions upon the illumination with blue light, like phototropism, chloroplast movement and stomatal opening in *Arabidopsis thaliana* (Huala, et al., 1997), circadian expression of pigments in *Neurospora crassa* (Heintzen, et al., 2001), virulence regulation in *Brucella abortus* (Swartz, et al., 2007), cell adhesion in *Caulobacter crescentus* (Purcell, et al., 2007), and the stress response in *Bacillus subtilis* (Avila-Perez, et al., 2006; Buttani, et al., 2007; Tang, et al., 2010). When fused to an effector domain, the signal is presumably propagated from the LOV domain towards the effector domain fused N- or C-terminally to the protein. This propagation most likely is derived by structural changes in the LOV core domain influencing the connecting linker to the effector domain and activating the respective function.

The LOV domain of YtvA found in the soil bacterium *Bacillus subtilis* was the first described LOV protein with a bacterial origin. It was identified solely based on sequence homology with plant phototropins (Akbar, et al., 2001; Losi, et al., 2002). The LOV domain is fused N-terminally to a sulfate transporter and anti-σ factor antagonist (STAS-domain) thus regulating the general stress response of the organism. The filamentous fungus *Neurospora crassa* exhibits two LOV domains, the short LOV domain VVD and the multidomain LOV protein WCC-1, both regulating the adaption of blue-light responses in the organism (Zoltowski, et al., 2008). In fact, VVD is an antagonist to WCC-1 inhibiting the transcription of light induced gene transcription. For the LOV domains of VVD and WCC-1 high homology is observed. This homology enables the formation of WCC-1 homodimers and WCC-1/VVD heterodimers. The WCC-1/VVD complex then antagonizes the gene transcription (Vaidya, et al., 2011).

The plant phot1LOV2 domain of *Avena sativa* is part of a multidomain phototropin protein (phot1) with two LOV domains (LOV1 and LOV2) connected N-terminally to a serine/threonine kinase domain. The second LOV domain phot1LOV2 is already identified as the main photoreceptor which initiates the autophosphorylation of the STAS domain upon blue-light illumination (Halavaty, et al., 2007). For all LOV proteins fused or non-fused to an effector domain, the basic photocycle remains the same. However, major differences are observed for the recovery time which is defined as the required time for a protein to convert from the activated light state into the ground dark state (figure 3).

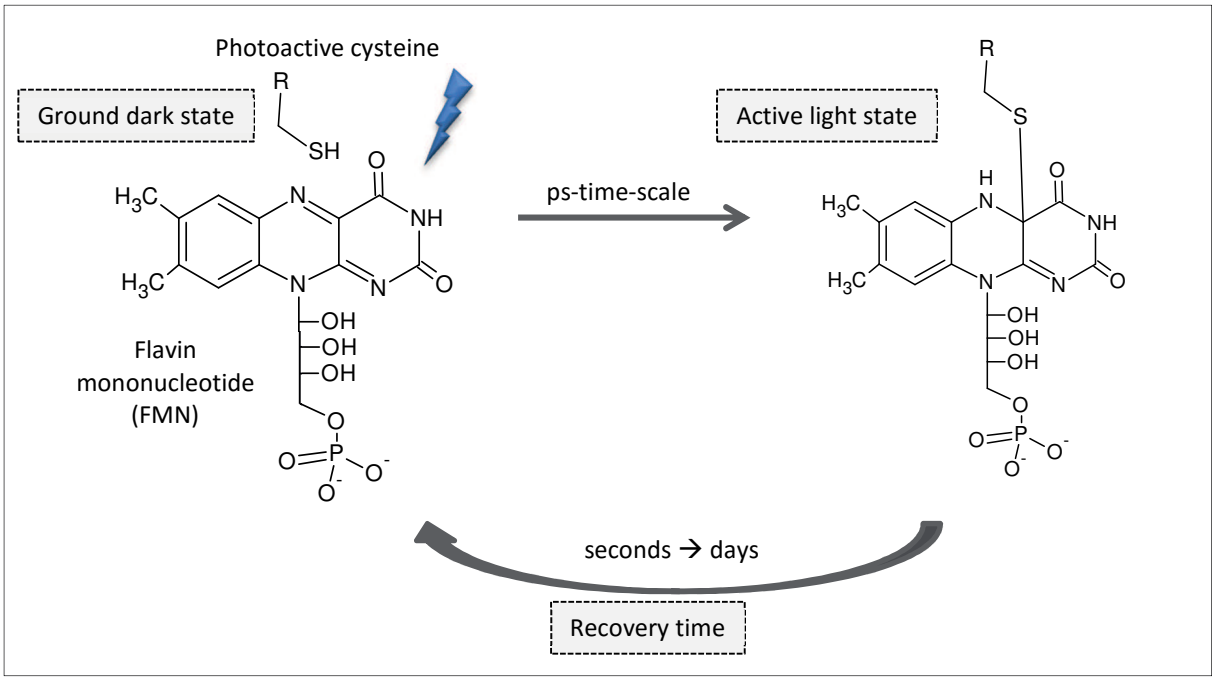

Figure 3: General photocycle of LOV proteins. If the LOV protein is excited with blue light, a photon is absorbed inducing the formation of a covalent bond between the photoactive cysteine and the formerly non-covalently linked flavin chromophore (in this case FMN). The dark recovery describes the required time of the LOV domain to return into the ground dark state.

So far three different mechanisms are reported for the photocycle of LOV proteins after excitation with blue light. Initially, an ionic mechanism was suggested by Swartz and coworkers with a deprotonated cysteine as a driving force in the photocycle (Swartz , et al., 2001). However, in different infrared spectroscopy approaches the cysteine was observed to be protonated in the dark state (Iwata, et al., 2002; Ataka, et al., 2003). For this reason, a concerted mechanism was described by Crosson and coworkers. In this case, the Sγ hydrogen is subtracted from the cysteine while the N5 atom of the FMN is protonated resulting in a nucleophilic attack of the sulfide (Crosson, et al., 2001; Crosson, et al., 2003). The third described mechanism suggests the formation of a radical by an electron transfer between the photoactive cysteine and the FMN molecule. The adduct is furthermore transformed by the transfer of a proton and the subsequent recombination of the radicals (Kay, et al., 2003; Schleicher, et al., 2004). Unfortunately, a final evidence for neither mechanism was found, but the basic interactions between flavin and protein, and especially the effect of blue light absorption of the core residues, are conserved upon the LOV protein family (Vaidya, et al., 2011). Different studies revealed changes in the hydrogen bond interactions between flavin and protein upon illumination besides the formation of the covalent adduct (Crosson, et al., 2002; Freddolino, et al., 2006). The most frequently discussed residue in this context is the motion or flipping of a conserved glutamine on a C-terminal β-strand of the LOV core domain usually labelled as Iβ (Crosson, et al., 2002; Fedorov, et al., 2003; Harper, et al., 2003; Harper, et al., 2004;

Nozaki, et al., 2004; Jones, et al., 2006; Zoltowski, et al., 2007; Nash, et al., 2008).

Thus, the signal propagation from the core cavity to the outer segments of the protein is ascribed to conformational changes of the side chain of Gln513 in phot1LOV2 (Nash, et al., 2008), Gln182 in VVD (Zoltowski, et al., 2007), Gln118 in RsLOV (Conrad, et al., 2012), and Gln123 in YtvA (Raffelberg, et al., 2011). Additional mutagenic analysis of YtvA also revealed a destabilized covalent adduct upon substitution of the glutamine by an asparagine (Raffelberg, et al., 2011). However, the final impact of the glutamine in the signal propagation is not fully resolved (Freddolino, et al., 2013).

This signal propagation after excitation of the protein with blue light is in focus of current research. A detailed knowledge can assist in the development of optogenetic tools based on LOV proteins. The variety of effector domains in contrast to the highly conserved LOV structural fold makes a common signal transduction via reorganization of secondary, tertiary or quaternary structure elements highly likely (Lee, et al., 2001; Harper, et al., 2003; Kurokava, et al., 2004; Möglich, et al., 2007; Möglich, et al., 2009). The proof for this assumption was provided by the substitution of the PAS domain of FixL, a chemo sensitive histidine kinase from *Bradyrhizobium japonicum* by the blue-light sensitive LOV domain of YtvA from *Bacillus subtilis*. This resulted in preservation of the kinase activity and substrate affinities (Möglich, et al., 2009).

As already mentioned, LOV domains are usually fused to effector domains. These domains include a STAS domain as in YtvA from *Bacillus subtilis* (Akbar, et al., 2001), a serine/threonine kinase as in the phototropin module of *Adiantum* phy3 (Crosson, et al., 2001) or a histidine kinase as in LOVHK from *Brucella abortus* (Sycz, et al., 2015). But recently several full-length LOV domains were characterized designated short-LOV proteins like PpSB2-LOV (Krauss, et al., 2005) and PpSB1-LOV (Jentzsch, et al., 2009) from *Pseudomonas putida*, and DsLOV from *Dinoroseobacter shibae* (Wingen, et al., 2014). These short-LOV proteins provide 13 % of all LOV proteins. But despite their widespread appearance, deeper knowledge about their functional role in the cell remains poorly understood.

1.2. PpSB1-LOV - a short LOV protein from *Pseudomonas putida*

The complete genome of the saprophytic soil bacterium *Pseudomonas putida* KT2440 was sequenced and analysed in 2002. The 6.18 Mb genome describes a metabolically versatile organism with a decent potential for biotechnological applications based on the biosafety declaration in comparison to *Pseudomonas aeruginosa*. Both organisms share 85 % of the predicted coding regions but key virulence factors are missing in *P. putida* making it the

favoured strain for cloning and gene expression for gram-negative soil bacteria (Nelson, et al., 2002).

In the genome of *Pseudomonas putida*, two genes coding for putative LOV domains are identified: PP2739 (Swiss-Prot: Q88JB0) and PP4629 (Swiss-Prot: Q88E39) (Nelson, et al., 2002; Krauss, et al., 2005; Jentzsch, et al., 2009). The expressed proteins are named in accordance to Losi and coauthors, *Pseudomonas putida* sensory box 1 and 2 protein or PpSB1-LOV and PpSB2-LOV (Losi, 2004). The molecular weights are calculated as 19.18 kDa for PpSB2-LOV and 18.59 kDa both including the fused N-terminal His_6-Tag. Based on analytical gel filtration and HPLC-based size exclusion chromatography, molecular weights of 39 kDa and 37.1 kDa are observed for the proteins, indicating the formation of dimers in solution, respectively (Krauss, et al., 2005). These two proteins are the first described bacterial short-LOV proteins. But despite the already explained characteristics further knowledge about the physiological role inside the organism is absent and requires further experiments. The main difference is observed in the photochemical behaviour where the recovery time was decelerated by three orders of magnitude with τ_{REC} = 2471 ± 22 min for PpSB1-LOV in comparison to a recovery time of τ_{REC} = 114 s at T = 20 °C for PpSB2-LOV (table 1) (Krauss, et al., 2005; Jentzsch, et al., 2009).

Table 1: Comparison of required time for different LOV proteins to recover into dark state.

Protein	PDB-ID	Strain	τ_{sec} (s)	Temp. (°C)	Reference
DsLOV	4KUK	*D. shibae*	9.6	20	(Endres, et al., 2015)
DsLOV-M49S	-	*D. shibae*	1.1	20	(Endres, 2013)
DsLOV-M49I	-	*D. shibae*	153	20	(Endres, 2013)
PpSB1LOV	3SW1	*P. putida*	148 000	20	(Circolone, et al., 2012)
PpSB1-LOV-R66I	-	*P. putida*	1380	20	(Circolone, et al., 2012)
PpSB1-LOV-R61H/R66I	-	*P. putida*	540	20	(Circolone, et al., 2012)
PpSB2-LOV	-	*P. putida*	137	20	(Jentzsch, et al., 2009)
YtvA	2PR5	*B. subtilis*	2700	25	(Losi, et al., 2003)
Phot1 LOV1	2VOU	*A. sativa*	27	20	(Salomon, et al., 2000)
VVD	2PD7	*N. crassa*	18000	4	(Schwerdtfeger, et al., 2003)
RsLOV	4HJ4	*R. sphaeroides*	2374	20	(Conrad, et al., 2013)

The differences in the recovery time of two LOV domains with a sequence similarity of 66 % and a common origin in the same organism raises the interest in structural and mutational characterization of both the proteins. Sequential comparison of both proteins with each other and other known LOV domains identified several amino acid positions varying amongst the domains (figure 2). First major difference was observed in the conserved sequence motif in which the amino acid position ahead of the photoactive cysteine usually is occupied by an asparagine, but observed to be an aspartic acid in PpSB1-LOV. In all LOV proteins two conserved arginines can be found and structure analysis revealed the formation of a salt bridge

between the amino acid side chains and the phosphate moiety of the FMN chromophore. In PpSB1-LOV two additional arginines are found, Arg61 and Arg66 and structural observations revealed supplementary interactions of these residues with the phosphate (figure 2 and 4B). In the homologue PpSB2-LOV a histidine is observed at position 61 and an isoleucine at position 66. Substitution of Arg66 in PpSB1-LOV into an isoleucine resulted in an accelerated dark recovery (5.9 ± 0.1 min) whereas the exchange of the isoleucine in PpSB2-LOV into an arginine decelerated the dark recovery (1760 ± 16 s) (Jentzsch, et al., 2009).

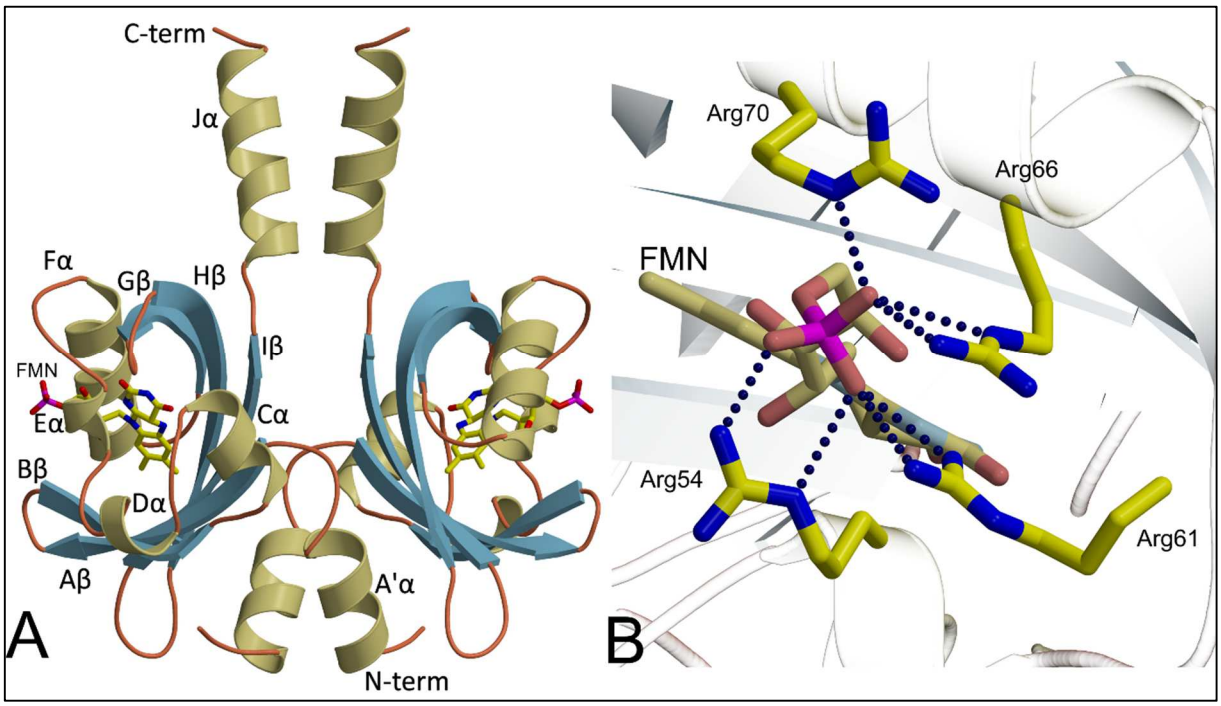

Figure 4: Light state crystal structure of PpSB1-LOV (pdb-ID: 3SW1) (A) and phosphate coordination by a novel arginine cluster (B). Amino acid side chains and FMN are represented in stick model and standard color code. Hydrogen bonds are represented in dark blue, dotted line. For a better discrimination between chromophore and protein the FMN is kept in pale colors (Circolone, et al., 2012).

Crystal structure of PpSB1-LOV in light state was reported by Circolone et al. with a resolution of 2.6 Å and a ribbon representation is shown in figure 4A. The structure comprised the canonical α/β PAS core with N- and C-terminal helical extensions protruding away from the core. The highest structural similarity with other LOV domains was observed with *Chlamydomonas reinhardtii* phot1LOV2 and *Bacillus subtilis* YtvA. PpSB1-LOV revealed a novel dimer interface mediated by hydrophobic interactions between N- and C-terminal structural elements and hydrogen bonds between the core domains. The N-terminal cap of both dimer chains, the N-terminal cap and the β-sheet of the opposite chain and the C-terminal Jα helices interact mainly via hydrophobic interactions. Additionally, hydrogen bond formation between polar side chains of different amino acids in the β-sheet and a salt bridge in the Jα helix are defined, constituting a rigid dimer interface. Inside the LOV core, a flavin mononucleotide

is located, mainly coordinated by hydrogen bonds between surrounding amino acid side chains and the chromophore. The light state of LOV proteins is defined by the formation of a covalent bond between the photoactive cysteine and the chromophore (figure 3). Although the C4a atom of the FMN is sp^3 hybridized in the light state crystal structure, a covalent thioether bond was not observed (Circolone, et al., 2012) with a bond distance of 2.35 Å between Cys-Sγ and the C4a atom of FMN. But based on the growth of the crystal under light conditions and a continuous electron density around the C53-Sγ/FMN-C4a region, the authors concluded a light state structure. Additional hydrophobic and hydrogen bonding interactions between chromophore and protein coordinate the chromophore in the vicinity. The already described conserved glutamine on Iβ (Gln116) forms two hydrogen bonds with the N5 atom of the FMN chromophore. The most pronounced difference as previously mentioned in the core FMN binding site is a cluster of four arginines (Arg54, Arg61, Arg66, Arg70) forming salt bridges with the phosphate group of the FMN (figure 4B). In comparison with other LOV proteins, PpSB1-LOV exhibits two additional arginines at amino acid positions 61 and 66. The structure thus allowed the authors to hypothesize the role of this unique arginine cluster in tight coordination of the FMN molecule and thereby controlling the slow dark recovery.

1.3. DsLOV – a short LOV protein from *Dinoroseobacter shibae*

Members of the *Roseobacter* family are the most abundant and metabolically versatile organisms in the world's oceans. *Dinoroseobacter shibae* DFL12^T is a gram-negative α-proteobacteria assigned to this clade. *D. shibae* was isolated from different microalgae, and a symbiotic relationship is observed between these organisms and *D. shibae*. In general, *Roseobacter* members are observed to host a variety of extrachromosomal elements with *D. shibae* exhibiting one of the largest number of plasmids (Wagner-Döble, et al., 2010).

In the genome of *D. shibae*, three different putative LOV domains were identified comprising a short LOV protein, a LOV-Histidine kinase, and a multidomain protein with a LOV domain, two PAS domains, a histidine kinase and a C-terminal response regulator (figure 5).

The diversity of LOV proteins in this organism implicates importance of light for this organism in regulatory processes. As an example, Endres et al. reported the role of Dshi_2006 in photopigment synthesis by comparative experimental analysis between the wildtype strain and a Dshi_2006 gene deletion strain. In the absence of blue light, DsLOV upregulates the photopigment accumulation inside the cell, in comparison to the deletion strain where no clear difference was observed. This study mainly focusses on the short LOV Dshi_2006 protein,

designated DsLOV in the following. Photokinetics of DsLOV shows a fast dark recovery of $\tau_{REC} = 9.6 \pm 0.1$ s (table 1).

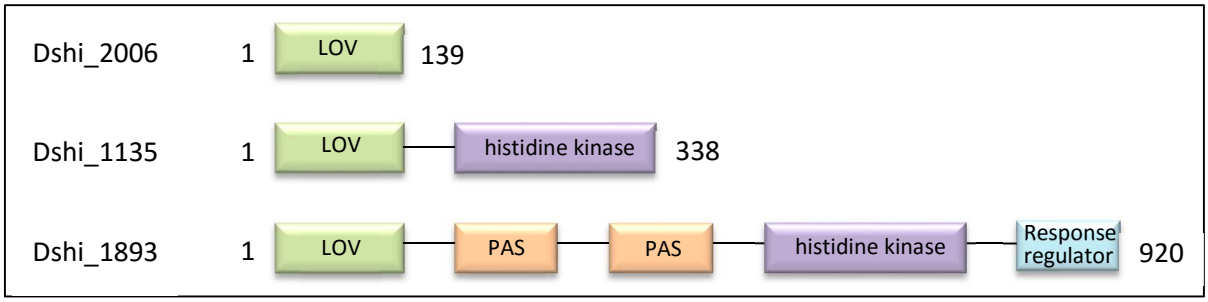

Figure 5: Identified LOV proteins in the genome of *Dinoroseobacter shibae*. The genes Dshi_2006, Dshi_1135, and Dshi_1893 code for LOV proteins in the genome of *Dinoroseobacter shibae* and the length of each protein is specified. Present work focuses on the characterization of the short LOV protein (Endres, 2013) (Endres, et al., 2015).

Recently, the dark state crystal structure of DsLOV was published with a resolution of 1.5 Å by Endres, et al., 2015. As observed for other LOV proteins, DsLOV exhibits a conserved α/β PAS fold with five β-strands comprising the β-sheet and four surrounding helices (figure 6). Interestingly, DsLOV does not exhibit a C-terminal extension but a N-terminal noncanonical secondary structure element consisting of a N-terminal turn, an α-helix and a connecting loop designated N-cap. Although only one chain was located in the asymmetric unit, the protein forms dimers in solution determined by analytical SEC and SAXS experiments. Based on PISA analysis (Krissinel, et al., 2007), a unique dimer interface was predicted, constituted by the N-cap elements of both molecules in the dimer (figure 6). Surprisingly, in the vicinity of the crystal structure of DsLOV a RBF molecule was located instead of the expected FMN. Preliminary analysis of the binding affinity of the LOV core domain revealed a prevalent binding of FMN (74.3 ± 0.2 %) ahead of FAD (23.7 ± 0.2 %) (Endres, et al., 2015). The authors hypothesized hydrolysis in acidic crystallization conditions for the presence of RBF during the crystallization process. FMN and RBF differ solely in the terminal phosphate group that is absent in the latter. The Iβ strand of DsLOV exhibits the conserved glutamine Gln135 which is the equivalent to Gln116 in PpSB1-LOV. Upon comparison between the dark state and the illuminated state crystal structure (in which the structure was derived from crystals grown in dark and was illuminated prior to cryocooling) reorientation of the side chain of Gln135 was shown to be the primary event of photoactivation and is most likely responsible for the displacement of the Iβ strand. Structural comparison with other LOV proteins revealed high similarity with VVD from *Neurospora crassa*. The dimer formation of VVD after illumination with blue light exhibits a similar constitution of the dimer interface mediated by a N-terminal extension (Zoltowski, et al., 2007; Vaidya, et al., 2011). Thus the interaction and signal transfer in DsLOV resemble those in VVD (Endres, et al., 2015).

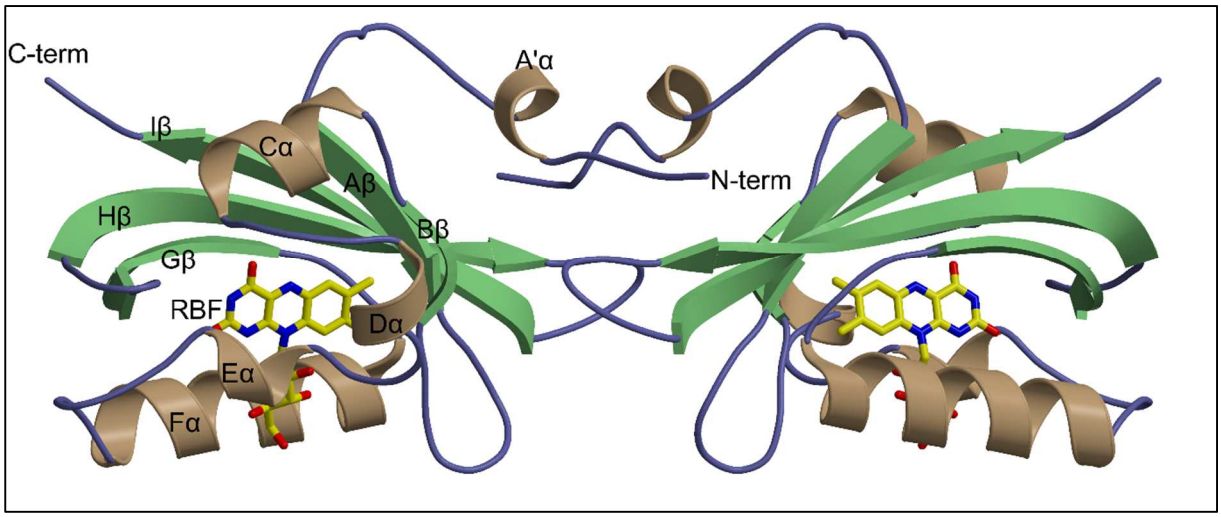

Figure 6: Dark state crystal structure of DsLOV (pdb-ID: 4KUK). Ribbon representation of the dark state crystal structure of DsLOV, with α-helices highlighted in beige, loops in purple and β-strands in green. The FMN molecule is represented in accordance to figure 4.

The most prominent difference between DsLOV and other LOV domain sequences is the presence of a methionine in the Bβ strand at position 49. In other LOV proteins this position is occupied by either a leucine or an isoleucine (figure 2). Substitution of the equivalent isoleucine in a truncated version of VVD with a valine accelerated the dark recovery by a factor of 25 (Zoltowski , et al., 2009). A similar result was observed in mutagenic analysis of phot1LOV2 form *Avena sativa*. The mutants I16V, I16L, and I16T exhibited a faster dark recovery than observed for the wildtype. The authors concluded the isoleucine side chain affects the stabilization of the photoadduct. In addition, a continuing reduction of the amino acid side chain causes acceleration of the dark recovery (Christie, et al., 2007). Stephan Endres reported about mutants with a substitution of Met49 in DsLOV with an isoleucine and a serine in his PhD thesis where he compared the recovery kinetics of the mutants with wildtype (Endres, 2013). The most significant difference of the M49I mutant was a 15-fold deceleration of the photocycle with recovery time of 153 sec. In comparison, the respective substitution into a serine resulted in a 5-fold acceleration with a recovery time of 1.1 s. Stephan Endres summarized that both mutants evoke differences in the steric stability of the photoadduct. The stability is enhanced by the substitution into an isoleucine and reduced by substitution into a serine resulting in a faster dark recovery compared to the wildtype. Additional solvent isotope effect experiments further suggest a different accessibility of the chromophore for surrounding buffer molecules (Endres, 2013). The smaller side chain of the serine evoked reduced solvent isotope effects (SIE), increasing the accessibility of the chromophore accounting for a faster dark recovery. The deprotonation of the FMN-N5 atom is the rate-limiting step in the decay of the photoadduct. Based on this assumption a more shielded FMN molecule as in the case of M49I requires a

longer decay time in comparison to the short amino acid side chain in the mutant M49S resulting in a faster deprotonation and thus faster recovery time (Endres, 2013).

1.4. LOV proteins as optogenetic tools

The field of optogenetics has attracted rising attention in the scientific area in the last two decades. In general, optogenetics describes the application of light sensitive proteins introduced into the system on a genetic level in diverse approaches. These vary from *in vivo* genetic control, monitoring and imaging of different cell compartments, and light-induced activation or deactivation of proteins. Based on the characteristics of the individual optogenetic tool a precise spatial and temporal control is possible (Pudasaini, et al., 2015) (Shcherbakova, et al., 2015). This application is based on the ubiquitous presence of natural photoreceptors in organisms like plants, fungi, and bacteria (Quail, 1998; Krauss, et al., 2005; Purcell, et al., 2007; Zoltowski, et al., 2008; Jentzsch, et al., 2009; Shcherbakova, et al., 2015). A continuous growth on characterized photoreceptor proteins provide templates for a growing number of optogenetic tools. One of the first optogenetic tools was the green fluorescent protein GFP used as *in vivo* fluorescent marker (Chalfie, et al., 1994). Since then several classes of GFP have been designed, each exhibiting different excitation and emission wavelengths (Tsien, 1998). However, additional photosensory modules were recently reported comprising the photoreceptor families of LOV, BLUF, Phy, and UVR8 (Möglich , et al., 2010; Fenno, et al., 2011; Christie, et al., 2012).

Depending on the variety of chromophores and the effect of light absorption, these photoreceptors were altered by different strategies to design optimal optogenetic tools, as explained in the following. In a detailed review about natural photoreceptors, Shcherbakova et al. listed three different exemplary approaches for the design of optogenetic tools (a) deactivation of steric inhibition in the protein thus activate the desired downstream process, (b) activation of enzymes like in the synthesis of second messengers, (c) provoking of protein-protein interactions by oligomerization of the photosensors (figure 7). A good example for the first approach is the use of the LOV2 domain of phototropin 2 from *Avena sativa* (Halavatny, et al., 2007) in which the C-terminal helix Jα is docked to the core domain in the dark state. Excitation with blue light induces a structural unwinding of the helix.

If the target protein or protein of interest is fused C-terminally to the LOV domain, this structural change can expose a previous caged epitope for substrate binding or enables protein-protein interactions (figure 7A). Another strategy bases on the oligomerization of LOV domains. The short LOV protein VVD from *Neurospora crassa* is monomeric in the dark and

homodimerizes upon illumination. This approach can play a role in reconstituting split enzymes or relocalize fused proteins to other cell compartments (figure 7C).

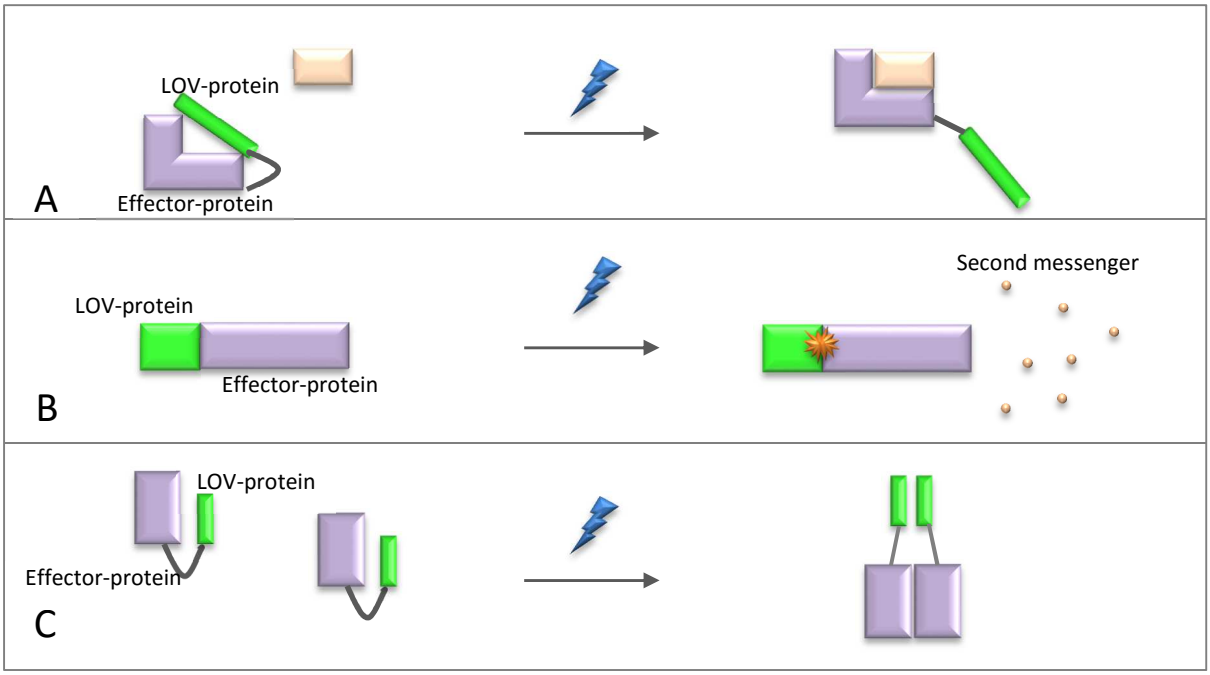

Figure 7: Different approaches for the design of optogenetic tools. (A) Blue light (represented as blue arrow in all examples) induces a structural reorientation of the LOV protein (green) thus deactivating the steric inhibition of the effector protein (purple); (B) blue light, absorbed by the LOV protein (green), activates the enzymatic activity of the effector protein (purple) as for example the synthesis of second messengers (yellow dots). The activated enzyme is indicated by the orange star; (C) blue light induces oligomerization of the LOV proteins and provokes protein-protein interaction of the effector domains.

To date, different natural photoreceptors are used as templates to design optogenetic tools. LOV proteins raised the interest of many researchers to design LOV based optogenetic tools due to several advantages over the GFP system (Drepper, et al., 2010). The most severe problem upon application of GFP is the oxygen requirement to autocatalyse the chromophore 4-(*p*-hydroxybenzylidene)imidazolidin-5-one (HBI) (Tsien, 1998). LOV proteins do not require oxygen and can be applied in anaerobic or low-oxygen methods, such as probing cell biomass in bioreactors and product formation in yeast fermenter cultures, analysis of microbial pathogenesis, hypoxia induced inflammatory processes, tumor pathophysiology, microbial fermentation, and monitoring and optimization of bioremediation and bacterial production processes (Coates, et al., 2000; Löffler, et al., 2006; Brown, 2007; Karakashew, et al., 2007; Ernst, et al., 2009; Hassett, et al., 2009; Rustad , et al., 2009; Tielker, et al., 2009; McKinlay, et al., 2010; Schobert, et al., 2010; Lu, et al., 2010; Drepper, et al., 2010; Eltzschig, et al., 2011. Additionally, for GFP and its derivatives a molecular weight (~ 27 kDa) is observed which is bulky in size that can have an impact on the protein it is fused to or on the cells or applied tissue itself. The LOV proteins on the contrary exhibit molecular weights of ~ 12-16 kDa (Wingen, et al., 2014) and thus are less likely to interact with cellular components or fusion proteins.

Additionally, LOV protein family members exhibit pH resistance against low pH values and bind a flavin molecule as chromophore which is ubiquitously present in most living cells facilitating and promoting the application of LOV proteins as optogenetic tools. All LOV proteins exhibit prompt folding kinetics and spontaneous incorporation of the chromophore resulting in a fast fluorescence active conformation (Drepper, et al., 2010; Mukherjee, et al., 2013; Wingen, et al., 2014). Although natural photoreceptors already exhibit interesting features, several approaches are undertaken to improve and further develop these properties. It has been demonstrated for various LOV proteins that substitution of the photoactive cysteine into an alanine for example prevents the protein from undergoing the photocycle and is thus permanently fluorescent (Drepper, et al., 2007; Chapman, et al., 2008; Jentzsch, et al., 2009; Wingen, et al., 2014).

These above described characteristics and findings were helpful in the design of optogenetic tools based on LOV proteins. Two LOV proteins that have been successfully engineered from natural photoreceptors into fluorescent markers are phiLOV (Christie, et al., 2012) and miniSOG (Shu, et al., 2011). For the fluorescence reporter phiLOV, LOV2 domain of phototropin2 from *Arabidopsis thaliana* was used as a template. Initial random mutagenesis resulted in the formation of monomeric iLOV (improved LOV), a reporter for viral movement in plants with a better performance than GFP (Chapman, et al., 2008). Inoculation of tobacco leaves with iLOV produced a ubiquitous green fluorescence in the leaves, but for GFP fluorescence was only observed in close distance to the inoculation. Additional random mutagenesis revealed an even more photostable version of iLOV which was subsequently renamed into phiLOV (Christie, et al., 2012). The second monomeric photoreceptor miniSOG (mini singlet oxygen generator) is derived from the phototropin2 LOV2 domain of *Arabidopsis thaliana* (Shu, et al., 2011). MiniSOG generates singlet oxygen evoked by blue-light excitation. In electron microscopy experiments, this oxygen species polymerizes diaminobenzidine into a precipitate. This precipitate is further stainable with osmium and enables the localization of proteins in diverse cells and tissues correctly. MiniSOG has already been successfully used to visualize synaptic cell adhesion molecules in neuronal cell culture and mouse brain (Shu, et al., 2011).

The above explained differences in oxygen requirements of LOV proteins and GFP derivatives enabled the design of a FRET-based biosensor for oxygen designated FLuBO (Potzkei, et al., 2012). This particular sensor is based on the fusion of EcFbFP and the yellow fluorescent protein YFP. EcFbFP was generated from the LOV domain of YtvA from *Bacillus subtilis* which was codon optimized for the expression in *Escherichia coli* strains and the

photoactive cysteine was substituted by an alanine. FLuBO was successfully used in online measurements of changing concentrations of cellular oxygen in the cytoplasm during batch cultivation (Potzkei, et al., 2012). Recently, a new oxygen photosensitizer was introduced Pp2FbFP L30M with a high quantum yield (Φ_Δ = 0.09 ± 0.01) in comparison to all other published photosensitizer (Torra, et al., 2015). Based on this high quantum yield, this optogenetic tool can be applied in chromophore assisted light inactivation of proteins (CALI (Surrey, et al., 1998)) or photodynamic therapy (PDT (Greenbaum, et al., 2000)). In addition, EcFbFP in combination with Pp1FbFP has recently been reported as a fluorescent reporter in mammalian cells with a fluorescence intensity comparable to GFP especially under hypoxic conditions (Walter, et al., 2012).

1.5. Goals of this study and outline of this thesis

The blue-light sensing LOV photoreceptors raised more and more attention in the field of optogenetics, based on their interesting characteristics in comparison to other well-known biosensor molecules like GFP. After the first description and characterization of the phototropin, further information was collected about plant LOV proteins. In comparison, little is known about bacterial LOV proteins although the number of identified proteins is constantly increasing. Recent developments raised the interest in short-LOV proteins and their possible application as optogenetic tools. They are deficient of fused effector domains but can still serve as ideal models to characterize their function inside the cell based on their full-length character and provide information about dimerization and signal propagation in LOV proteins.

Structural analysis of different proteins is a basic method to gain information on these different aspects. Especially, the comparison of light and dark state crystal structures on fundamental changes between both states provides a decent amount of information about signal propagation and the inter- and intramolecular interactions. These 3D structures might be auxiliary in the optimization and design of new LOV proteins with novel and desirable properties serving as optogenetic tools.

The present thesis will broaden our understanding and simplify the prediction of the functionality of LOV proteins. Focus of the thesis is to perform extended structural investigations on the two short-LOV proteins PpSB1-LOV and DsLOV and its mutants in dark and light state.

The first part of the thesis focuses on PpSB1-LOV and its derivatives. In addition to the already published light state structure, the dark and illuminated state structures of PpSB1-LOV are characterized and compared with the light state structure. The active site mutant

PpSB1-LOV-C53A in dark and illuminated state is reported and also compared with the wildtype structure. Another mutant crystal structure with interesting recovery kinetics PpSB1-LOV-R61H/R66I is described in dark state and provides further information about chromophore coordination. Besides the crystal structures, small angle X-ray scattering was performed for the LOV proteins in solution. The resulting *ab initio* models provide additional and supportive information about signal propagation in PpSB1-LOV.

The second part of this thesis mainly focuses on the M49I and M49S mutants of the short LOV protein DsLOV. As already explained, the equivalent position in other LOV proteins to position 49 usually exhibits a leucine or isoleucine. Structural comparison of both proteins with the wildtype helps to determine the influence of the methionine in the fast dark recovery of DsLOV. In addition, the crystal structure of the active site mutant DsLOV-C72A, previously reported as DsFbFP (FbFP = FMN-binding fluorescent protein), is determined and explained. Small-angle X-ray scattering provides further information about the oligomeric state of the mutants. Finally, the recovery kinetics of the methionine mutants are determined with a UV/Vis spectrometer.

2. Material and methods

2.1. Material

2.1.1. Bacterial strains

Table 2: Bacterial strains and their genotype

Strain	Genotype	Reference
E. coli DH5α	F-*sup*E44 Δ*lac*U169 (Φ*80lac*ZΔ15) *hsd*R17 *rec*A1 *end*A1 *gyr*A96 *thi*-1 *rel*A1	Clontech, Heidelberg, Germany
E. coli BL21(DE3)	F-*omp*T *hsdS*$_B$($r_{B-}m_{B-}$) *gal dcm* (DE3)	Novagen, Darmstadt, Germany

2.1.2. Vectors and recombinant plasmids

Table 3: Vectors, recombinant plasmids and their genotype

Vector	Genotype	Reference
pET28a(+)	P_{T7}, N-Terminal His_6-Tag, MCS, *lac*I, *bla*, Km_r pBR322 ori, f1 ori, pp1fbf	Novagen, Darmstadt, Germany
pET28a(+)PpSB1LOV-WT	Km^r; *pp1* under the control of the T7 promotor, N-Terminal His_6-Tag	(Jentzsch, et al., 2009)
pET28a(+)PpSB1LOV-C53A	Km^r; *pp1fbfp* under the control of the T7 promotor, N-Terminal His_6-Tag	Circolone, unpublished
pET28a(+)PpSB1LOV-R66I	Km^r; *pp1 r66i* under the control of the T7 promotor, N-Terminal His_6-Tag	(Jentzsch, et al., 2009)
pET28a(+)PpSB1LOV-R61H/R66I	Km^r; *pp1 r61h/r66i* under the control of the T7 promotor, N-Terminal His_6-Tag	(Circolone, et al., 2012)
pRhotHi	pBBR1mcs (*rep*, *mob*, Cm^r), pET22b (MCS, *pelB*), pBSL15 (aphII) orientation II, P_{T7}	(Katzke, et al., 2010)
pRhotHi-2DsLOV-WT	Km^r; *dslov* under the control of the T7 promotor; C-terminal His_6-Tag	(Endres, et al., 2015)
pRhotHi-2DsLOV-M49S	Km^r; *dslov m49s* under the control of T7 promotor; C-terminal His_6-Tag	(Endres, 2013)
pRhotHi-2DsLOV-M49I	Km^r; *dslov m49i* under the control of T7 promotor; C-terminal His_6-Tag	(Endres, 2013)
pRhotHi-2DsLOV-C72A	Km^r; *dsfbfp* under the control of T7 promotor; C-terminal His_6-Tag	(Endres, 2013)

2.1.3. Kits and equipment

Table 4: Kits and equipment

Equipment	Company
NanoPhotometer™	IMPLEN, München, Germany
Eppendorf Centrifuge 5804R	Eppendorf, Hamburg, Germany
Tissue grinder	Milleville, New Jersey, USA
PD10 column	GE healthcare, Freiburg, Germany
Electrophoresis power supply EPS-1001	GE healthcare, Freiburg, Germany
molecular weight marker	Thermo Scientific, Braunschweig, Germany
Hiload 26/60 Superdex 200	GE healthcare, Freiburg, Germany
äkta pure system	GE healthcare, Freiburg, Germany
PRIM Vis spectralphotometer	SCHOTT instruments, Bath, United Kingdom
Blue light LED (λ = 440 nm, 180 mW cm^{-1})	Luxeon Lumileds, Philips, Aachen, Germany
UV/Vis-spectrophotometer UV-18000	Shimadzu, Duisburg, Germany
Vivaspin 20	Sartorius, Göttingen, Germany
innuPREP plasmid mini kit	Analytic Jena, Germany
Bio-Rad protein assay dye reagent	Bio-Rad, München, Germany

2.1.4. Chemicals

All chemicals and other substances used were of analytical grade (p.A.).

Table 5: Chemicals

Chemical	Company
Lactose	Roth, Karlsruhe, Germany
Glucose	Roth, Karlsruhe, Germany
Kanamycin	Sigma Aldrich, Darmstadt, Germany
Tryptone	Roth, Karlsruhe, Germany
Yeast-extract	Roth, Karlsruhe, Germany
NaCl	Sigma Aldrich, Darmstadt, Germany
Terrific-Broth Medium	Roth, Karlsruhe, Germany
Glycerine	Sigma Aldrich, Darmstadt, Germany
KCl	Sigma Aldrich, Darmstadt, Germany
Sodium acetate	Sigma Aldrich, Darmstadt, Germany
MgCl2	Roth, Karlsruhe, Germany
CaCl2	Roth, Karlsruhe, Germany
MOPS	Sigma Aldrich, Darmstadt, Germany
Agar	Roth, Karlsruhe, Germany
NaH_2PO_4	Sigma Aldrich, Darmstadt, Germany
Ni-NTA Superflow	Qiagen, Hilden, Germany
Imidazole	Roth, Karlsruhe, Germany
Tris	Roth, Karlsruhe, Germany
Acrylamide	Sigma Aldrich, Darmstadt, Germany
Tris-HCl	Roth, Karlsruhe, Germany
SDS	Roth, Karlsruhe, Germany
APS	Roth, Karlsruhe, Germany
TEMED	Roth, Karlsruhe, Germany
β-Mercaptoethanol	Sigma Aldrich, Darmstadt, Germany
Bromphenolblue	Sigma Aldrich, Darmstadt, Germany
Isopropanol	Roth, Karlsruhe, Germany
Acetic acid	Roth, Karlsruhe, Germany
Coomassie Brilliant Blue R250	Roth, Karlsruhe, Germany
Bovine serum albumin	Sigma Aldrich, Darmstadt, Germany
Sodium cacodylate	Roth, Karlsruhe, Germany
PEG 3000	Roth, Karlsruhe, Germany
MES	Roth, Karlsruhe, Germany
Ammonium sulphate	Sigma Aldrich, Darmstadt, Germany
Sodium formate	Roth, Karlsruhe, Germany
PGA-LM	Molecular Dimensions, Suffolk, United Kingdom
PEG 8000	Roth, Karlsruhe, Germany
CoCl2 x 6 H2O	Roth, Karlsruhe, Germany
1,6-Hexanediol	Sigma Aldrich, Darmstadt, Germany
PEG 6000	Roth, Karlsruhe, Germany
Tris base/HCl	Roth, Karlsruhe, Germany

2.1.5. Culture media

Each media composition was sterilized by autoclaving at least for 20 min at 121 °C. Lactose 2 % (w/v) and glucose 5 % (w/v) were autoclaved separately from the medium and

added afterwards. Sterile filtered kanamycin was added into media at room temperature to a final concentration of 25 µg/mL. If bacterial growth on LB-agar plates was necessary, 15 g/L agar was added to the above media.

LB-Medium (Sambrook, et al., 1989)

10	g	Tryptone
5	g	Yeast-extract
5	g	NaCl
Ad 1000	mL	ddH_2O

Auto-inducing medium (Studier, 2005)

50.8	g	Terrific-Broth Medium
4	mL	Glycerine
Ad 890	mL	ddH_2O

Following solutions were added after autoclaving

10	mL	Glucose 5 %
100	mL	Lactose 2 %

SOB-medium

20	g	Tryptone
5	g	Yeast extract
0.6	g	NaCl
0.2	g	KCl
		pH 6.8-7
Ad 1000	mL	ddH_2O

2.2. Molecular biology methods

2.2.1. Isolation of plasmid-DNA

A 10 mL overnight culture (37 °C, 130 rpm) of *Escherichia coli* DH5α cells chemically transformed with the respective plasmid was harvested (10 min, 4 °C, 20000 x g) and used. The bacterial plasmid DNA was isolated using the "innuPREP plasmid mini kit" (Analytik Jena, Jena, Germany) following the manufacturer´s protocol with an exception of the last step where 30 µL ddH_2O was used.

DNA concentration was measured using the NanoPhotometer™ (IMPLEN, München, Germany).

2.2.2. Transformation of bacterial cells with plasmid DNA

2.2.2.1. Preparation of chemically competent *E. coli* cells

A 10 mL preparatory culture in LB-media was incubated over night at 37 °C with continuous shaking at 130 rpm. The main culture (300 mL SOB-Media) was inoculated with cells from the overnight culture to an OD_{600} of 0.1 and incubated at 37 °C at 150 rpm until an OD_{600} of

0.3 – 0.4 was obtained. *E. coli* cells were transferred into 50 mL Falcon tubes and kept on ice for 15 min. The cells were centrifuged for 15 min at 4 °C and 3500 rpm (Eppendorf centrifuge 5804R). The supernatant was discarded and the pellet was carefully resuspended in 60 mL TFB1 buffer (30 mM Na-acetate, 50 mM $MgCl_2$, 100 mM NaCl, 10 mM $CaCl_2$, 15 % glycerin, pH 6) and incubated on ice for 15 min. The cell suspension was centrifuged (15 min, 4 °C, 3500 rpm), the cell pellet was resuspended in 12 mL TFB2 (10 mM MOPS, 75 mM $CaCl_2$, 10 mM NaCl, 15 % Glycerin, pH 7.0) buffer and incubated on ice for 15 min. Subsequently, 50 µL aliquots were frozen in liquid nitrogen and stored at -80 °C.

2.2.2.2. Chemical transformation of *E. coli* cells

1 µL DNA solution (table 3) was added to an aliquot of 50 µL chemically competent *E. coli* cells (2.6.1) and incubated on ice for 20 min. A heat shock was given at 42 °C for 90 s (Eppendorf thermomixer). Subsequently, 1 mL LB-medium was added and the culture was incubated at 37 °C for 3 h. A minimum of 150 µL of the culture was plated on selective LB-agar plates, which were incubated overnight at 37 °C.

2.3. Protein biochemistry methods

2.3.1. Heterologous expression of LOV proteins

Preparatory cultures containing LB-media with kanamycin fc. 25 µg/mL were inoculated with fresh competent *E. coli* BL21(DE3) cells (s. 2.6.2) and incubated overnight at 37 °C and 150 rpm in shaking flasks. The main culture was inoculated with cells from the preparatory culture to an OD_{600} of 0.05 in auto-inducing medium with kanamycin (25 µg/mL) and incubated for 24 h at 37 °C and 130 rpm. The cells were then harvested (45 min, 5000 x g, 10 °C) and aliquots of 5 g were either used for purification or stored at -20 °C for later application.

2.3.2. Purification of LOV proteins

A 5 g aliquot of cell pellet was resuspended in 150 mL lysis buffer (50 mM NaH_2PO_4, 300 mM NaCl, pH 8), homogenized using a tissue grinder (Milleville, NJ, USA) and lysed with a cell disruptor in three cycles at 4 °C and 1.7 bar. The cell solution was centrifuged to separate the cell debris from the soluble fraction (45 min, 28750 x g, 11 °C) and the supernatant was then transferred to a new vessel. 5 mL Ni-NTA Superflow (Qiagen, Hilden, Germany) was equilibrated with 5 CV lysis buffer. The cell free soluble fraction was applied to the column, followed by 5 CV lysis buffer and 10 CV washing buffer (50 mM NaH_2PO_4, 300 mM NaCl, 50 mM Imidazole, pH 8). The protein was eluted from the column with 10 CV elution buffer (50 mM NaH_2PO_4, 300 mM NaCl, 250 mM Imidazole, pH 8) and fractionated in 5 mL aliquots.

Protein containing fractions were identified using SDS-PAGE (2.7.3), pooled and the buffer was exchanged into storage buffer (10 mM Tris, 10 mM NaCl, pH 7) using PD10 columns (GE healthcare, Freiburg, Germany) following the manufacturer´s protocol. Subsequently, the protein concentration (2.8.1) and the chromophore load was determined (2.8.3).

2.3.3. Sodium dodecyl sulfate-polyacrylamide gel electrophoresis (SDS-PAGE)

The SDS-PAGE was used to separate proteins under denaturing conditions in the presence of SDS (Laemmli, 1970). Proteins were stacked in a 5 % gel and separated in a 15 % gel. For sample preparation, 30 µL protein samples were mixed with 10 µL 4X SDS-loading dye and denatured before application for 10 min at 95 °C. The electrophoresis was conducted for 45 min with 40 mA per gel in 1X SDS-buffer using an electrophoresis power supply EPS-1001 (GE healthcare, Freiburg, Germany). The unstained protein molecular weight marker (Thermo Scientific, Braunschweig, Germany) was used for determination of molecular weight. Afterwards, the gels were stained with pre-heated (60 °C) Coomassie-stain for 20 min, washed with cold water twice and three times with boiled water.

Table 6: Composition of gels, buffer, loading dye, and Coomassie-stain for running SDS-gels.

5 % stacking gel	**15 % separation gel**
16.8 % (v/v) Acrylamide 30 %	50 % (v/v) Acrylamide 30 %
125 mM Tris-HCl pH 6.8	375 mM Tris-HCl pH 8.8
0.1 % (w/v) SDS	0.1 % (w/v) SDS
0.1 % (v/v) APS 10 %	0.1 % (v/v) APS 10 %
0.1 % (v/v) TEMED	0.04 % (v/v) TEMED

1X SDS-buffer	**4X SDS-loading dye**
50 mM Tris-HCl	20 mM Tris-HCl pH 6.8
385 mM Glycerin	8 % (w/v) SDS
0.1 % (w/v) SDS	8 % (v/v) β-Mercaptoethanol
pH 8.3	40 % (v/v) Glycerin
	3 g/L Bromphenolblue

Coomassie stain
25 % Isopropanol
10 % Acetic acid
0.5 g/L Coomassie Brilliant Blue R250

2.3.4. Size exclusion chromatography

To achieve a higher protein purity, a size exclusion chromatography (SEC) step was performed using a Hiload 26/60 Superdex 200 prep grade column (GE healthcare, Solingen, Germany). The column was equilibrated with 1 CV water and 1 CV Storage buffer (10 mM Tris, 10 mM NaCl, pH 7) with a flow rate of 2.6 mL/min using the äkta pure system (GE healthcare,

Solingen, Germany). The protein solution was applied with a 5 mL loop, eluted with 1.5 CV storage buffer, and collected in 5 mL fractions. The protein containing fractions were pooled for further application.

2.4. Optical methods

2.4.1. Determination of protein concentration

The protein concentration in solution was determined using the Bio-Rad protein assay dye reagent concentrate in imitation of Bradford, 1976 (Bradford, 1976). The standard curve was made with bovine serum albumin. The samples for the standard curve were prepared by adding 800 µL sample to 200 µL dye reagent with a final concentration of 0 to 10 µg/mL protein in 1 mL total volume. After mixing thoroughly, the mixture was incubated for 5 min at room temperature. Protein samples were prepared similarly. The absorbance was measured at 595 nm using a PRIM Vis spectral photometer (SCHOTT instruments, Bath, United Kingdom) and the concentration was then calculated using the standard curve.

2.4.2. Determination of light and dark state spectra of LOV proteins

The spectroscopic work was conducted under dim red safety light. The respective protein was set to an OD_{450} of 0.1 – 0.2 in storage buffer (10 mM Tris, 10 mM NaCl, pH 7). To achieve the light state, the protein was illuminated for 30 s with a blue-light LED (λ=440 nm, 180 mW cm^{-2}, Luxeon Lumileds, Philips, Aachen, Germany). A spectrum of the UV/vis region 250 nm – 600 nm was recorded for the dark state first and after exposure of the sample to light. The temperature of the sample holder inside the spectrometer was set to 20 °C.

2.4.3. Determination of kinetic recovery of LOV proteins

The respective protein was set to an OD_{450nm} of 0.2 in storage buffer (10 mM Tris, 10 mM NaCl, pH 7). To achieve the light state, the protein was illuminated for 30 s with a blue-light LED (λ=440 nm, 180mW cm^{-2}, Luxeon Lumileds, Philips, Aachen, Germany). The dark recovery was then recorded at 485 nm in triplicate. The data were analyzed using a single-exponential regression. The exponential function thereby fits the following equation:

$$y(t) = e^{-\frac{t}{\tau}}$$

t = time
τ = time constant

2.4.4. Determination of the cofactor loading (Endres, 2013)

The protein was diluted to approximately 0.5 mg/mL in storage buffer (10 mM Tris, 10 mM NaCl, pH 7) and measured at 280 nm and 450 nm with a UV/Vis –spectrophotometer UV-18000 (Shimadzu, Duisburg, Germany). The extinction coefficients of the LOV proteins at 280 nm and 450 nm were determined, and subsequently the concentrations of loaded protein and cofactor were calculated using the Lambert-Beer law. The ratio of both concentrations corresponds to the ratio of holoprotein in relation to the total protein amount.

$$E_\lambda = \varepsilon_\lambda \times c \times d$$

E_λ = Extinction
ε_λ = extinction coefficient
c = concentration
d = thickness of cuvette

2.4.5. Single crystal microspectrometry

A dark-grown single crystal of the respective protein was used to measure an absorbance spectrum in the wavelength range 350 – 700 nm. The crystal was placed in the cavity of a glass slide, 5 µL reservoir solution was added to cover the crystal and a cover slip was put above. The dark state spectrum was recorded at 25 °C using an UV/Vis microscope with a 100-W Hg lamp (Efremov, et al., 2006). The light state spectrum was recorded after illumination of the crystal with blue light (λ_{max}=460 nm; ± 10 nm half-width; 1.3 mW/cm^{-2}) for 15 min minimum. Additionally, some spectra were also recorded at the cryobench laboratory ID29S at ESRF (Grenoble, France; de Sanctis et al., 2012) at 100 K using a HR2000 (OceanOptics) on an microspectrophotometer.

2.5. X-ray crystallography

2.5.1. Crystallization

The purified protein solution was concentrated after purification to a certain concentration (table 7) using a Vivaspin 20 (Sartorius, Göttingen, Germany). Different crystallization screens were used initially gaining an overview of crystallization conditions which were refined afterwards (Table 7 and 8). Crystallization setups were performed using vapor diffusion method with sitting drops (1 µL protein + 1 µL reservoir solution) at 19 °C. The vapor diffusion method contains an aqueous drop with a mixture of protein solution and reservoir with the ratio 1:1 which is kept on plateau relative to the reservoir well filled with the crystallization solution. On basis of the equilibration between the drop and the reservoir solution the concentration of the molecules inside the drop increase, resulting in the nucleation and formation of a crystal. After

two weeks first observations were done to monitor the crystallization progress. Observed crystals were tested at the ESRF (Grenoble, France) and the diffraction quality was tested. If improvement was necessary, the protein solution was applied in fine screens using the original crystallization conditions with minor changes in the buffer pH value or concentrations of precipitant or salt. The final composition of the reservoir solution for successful crystallization differed for each protein (table 7).

Table 7: Concentration, crystallization conditions and required time for crystal growth for the different LOV proteins.

Protein	Concentration [mg/mL]	Reservoir condition	Required time for crystal growth
PpSB1-LOV	100	0.1 M Sodium-cacodylate pH 6.5 10 % PEG 3000 0.2 M $MgCl_2$	4 weeks
PpSB1-LOV-C53A	104	0.05 $CoCl_2$ x $6H_2O$ 1.2 M 1,6-Hexanediol 0.1 M Sodium acetate x $3H_2O$ pH 4.6	4 weeks
PpSB1-LOV-R61H/R66I	80	0.2 $MgCl_2$ 0.1 M MES pH 6.6 15 % (w/v) PEG 4000	2 weeks
DsLOV-M49I	30	0.1 M Na-acetate pH 5 0.1 M Ammonium sulfate 0.3 M Sodium formate 3 % PGA-LM 5 % (w/v) PEG 8000	1 year
DsLOV-M49S	30	0.1 M Tris-HCl pH 8 30 % PEG 6000	1 week
DsLOV-C72A	20	0.1 M Tris base /HCl pH 8.5 0.2 M $MgCl_2$ 20 % PEG 8000	6 months

The setups were either exposed to continuous white light or kept in the dark to trap the respective state of the LOV protein. Unfortunately, crystals under continuous light conditions failed to crystallize. The required time for crystal growth varied for each protein and is listed in table 7. The dark crystals chosen for data collection were prepared and frozen under red light conditions. Prior to cryo-cooling, the crystals were soaked either with original reservoir solution added with increasing concentration of glycerin in steps of 5 % (v/v) or directly with a 30 % (v/v) glycerin solution if not already present in the reservoir solution.

Table 8: Overview of crystallization screens used in this thesis.

Screen	Company
PEG Screen I	Hampton Research, Aliso Viejo, USA
PEG Screen II	Hampton Research, Aliso Viejo, USA
Crystal Screen I/II	Hampton Research, Aliso Viejo, USA
PEG/Ion Screen	Hampton Research, Aliso Viejo, USA
PGA-LM Screen	Molecular Dimensions, Suffolk, United Kingdom
JCSG I	Qiagen, Hilden, Germany
JCSG II	Qiagen, Hilden, Germany
JCSG III	Qiagen, Hilden, Germany
JCSG IV	Qiagen, Hilden, Germany
$AmSO_4$ Screen	Qiagen, Hilden, Germany
Anions Screen	Qiagen, Hilden, Germany
Additive Screen	Hampton Research, Aliso Viejo, USA
Wizard I/II	Rigaku, Ettlingen, Germany

2.5.2. Data collection

The X-ray diffraction data were collected at different beamlines of the European Synchrotron Radiation Facility (ESRF, Grenoble, France) and are listed in table 9. As each data set was recorded at 100 K, radiation damage was taken into account based on calculations using the program BEST (Bourenkov, et al., 2010). In case of illuminated data, dark grown crystals were illuminated with blue light by interrupting the cryostream of the beamline for 1s after completion of data collection of the dark state.

Table 9: Beamline and further information about data collection for the different proteins.

Protein	Beamline	Detector	Wavelength [Å]	Reference
PpSB1-LOV	ID29	Pilatus-6M	0.979	(de Sanctis, et al., 2012)
PpSB1-LOV-C53A	ID29	Pilatus-6M	0.979	(de Sanctis, et al., 2012)
PpSB1-LOV-R61H/R66I	ID29	Pilatus-6M	0.979	(de Sanctis, et al., 2012)
DsLOV-M49S	ID14-4	Q315-2x	0.979	(McCarthy, et al., 2009)
DsLOV-M49I	ID29	Pilatus-6M	0.979	(deSanctis, et al., 2012)
DsLOV-C72A	ID23-2	Pilatus-2M	0.873	(Flot, et al., 2010)

2.5.3. Model building and refinement

A detailed overview about the complete process beginning with the crystallization of a protein to the final structure is displayed in a flow scheme in figure 8.

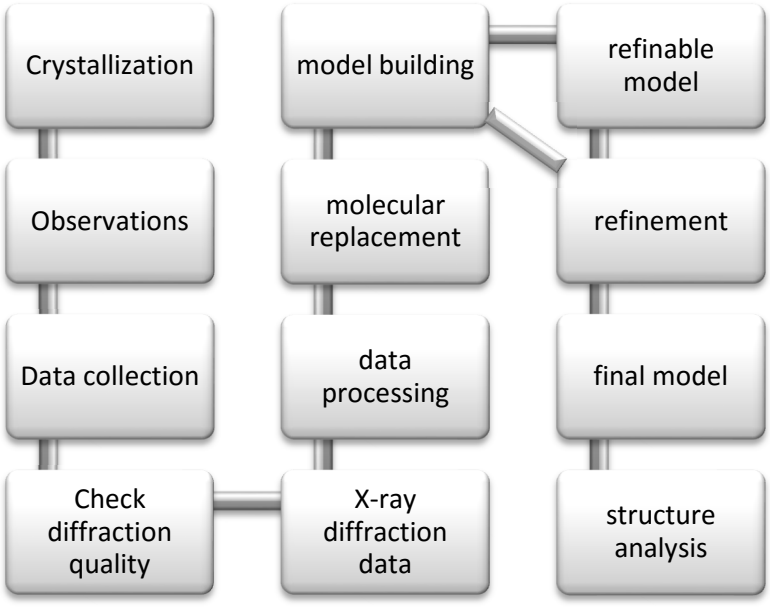

Figure 8: Process of structure determination using X-ray crystallography.

After successful collection of high quality data sets at ESRF (Grenoble, France) the data for the respective LOV proteins are processed with XDS (Kabsch, 2010). The program XDS combines eight subroutines that in summary, identify strong detection spots, determine the orientation and symmetry of the crystal lattice, recognize untrusted spots and determines the intensities of single reflection spots. The last step in XDS is the correction of intensities, followed by the

refinement of the unit cell. In the end, XDS generates a file with integrated intensities which is then applied in the program POINTLESS to score all possible Laue groups and select a space group (Evans, 2006; Evans, 2011). Observations of reflections are scaled and combined in an average intensity using the program AIMLESS (Kabsch, 1988; Evans, 2006; Evans, 2011; Evans, et al., 2013) and the number of molecules inside the asymmetric unit is determined using MATTHEWS_COEF of the CCP4 package which is necessary for the molecular replacement described in the following (Matthews, 1968; Kantardjieff, et al., 2003; Winn, et al., 2011). The resolution for the structure of PpSB1-LOV in dark state and all subsequent structures described in this thesis were determined as a compromise between cc ½, R_{merge}, Mean I/σ(I) and the completeness to generate the most reliable structure. The next step in data processing is the establishing of an initial starting model for refinement using molecular replacement. This method is one possibility to solve the phase problem, where the phase problem describes the loss of information for the electron density as solely the intensity can be recorded but not the phase of the diffracting wave. On basis of the rapid ascent of available protein structures the frequency of applying the method of molecular replacement strongly increases as it requires solely a structure of homology (~30 %) to the regarded protein or even parts of it. The starting model was generated using the program MOLREP (Vagin, et al., 1997). For PpSB1-LOV the light state structure was already determined and thus one molecule of this structure was used as a starting model for the molecular replacement for the data sets of dark state PpSB1-LOV, illuminated PpSB1-LOV, dark and illuminated state of PpSB1-LOV-C53A and the dark state of PpSB1-LOV-R61H/R66I. Molecular replacement was used likewise for the dark state data sets of DsLOV-M49S, DsLOV-M49I and DsLOV-C72A where the dark state structure of the wildtype DsLOV was used as a starting model. The primary refinement of the model was conducted using the program REFMAC and for every following refinement the PHENIX software program was used (Adams, et al., 2002). The first refinement steps were conducted applying secondary structure and Ramachandran restraints with rigid body, real space refinement and a temperature of T = 5000 K for the simulated annealing process. After each refinement cycle the model was manually rebuilt with COOT, a program for visualization and manipulation of macromolecules (Emsley, et al., 2004). Single atoms and amino acid side chains are deleted if no significant density is observed in the $2mF_O - F_C$ map ($\sigma_A = 0.8$) to reduce misinterpretation. The final model was analysed with comprehensive validation in PHENIX, presenting geometry restraints outlier, Ramachandran and rotamer outlier, all atom contacts, and the real-space correlation (Chen, et al., 2010). A subsequent POLYGON analysis compares the final model with similar available structures in the PDB (Urzhumtseva, et al.,

2009). Data collection and refinement statistics are combined with PHENIX and listed in the respective result section. Inter- and intramolecular contacts and interaction were calculated using CONTACT (Collaborative Computational Project, 2011). Imprinted figures were generated with MOLSCRIPT (Kraulis, 1991) and RASTER3D (Merritt, et al., 1997) and DSSP (Kabsch, et al., 1983) for secondary structure assignments.

2.6. Small angle X-ray scattering (SAXS)

2.6.1. Sample preparation

Table 10: Overview on samples of different LOV proteins measured in SAXS experiments. All proteins were stored and measured in 10 mM Tris, 10 mM NaCl, pH 7.

Protein	Static or kinetic	Concentration [mg/mL]	Temperature [°C]	Measured in
PpSB1-LOV	Static	2.8 5.7 7.9	10	DESY, Hamburg
		1.8 2.5 6.3	10	ESRF, Grenoble, France
PpSB1-LOV-C53A	Static	2.2 5.7 15.5	10	DESY, Hamburg
PpSB1-LOV-R66I	Static	1.1 2.5 6.1	10	ESRF, Grenoble, France
	kinetic	1.1 1.5	20	ESRF, Grenoble, France DESY, Hamburg
PpSB1-LOV-R61H/R66I	Static	0.9 1.6 6.3	10	ESRF, Grenoble, France
		3.5 5.8 10.1	10	DESY, Hamburg
	kinetic	0.9 1.6	20 10	ESRF, Grenoble, France DESY, Hamburg
DsLOV-M49S	static	1.6 3.0 7.4	10	ESRF, Grenoble, France
		4.7 8.5 15.4	10	DESY, Hamburg
DsLOV-M49I	static	1.9 3.1 8.5	10	ESRF, Grenoble, France
	kinetic	1.9	4	ESRF, Grenoble, France

For SAXS measurements only proteins which were applied on SEC (2.7.4), were used in order to avoid the presence of any aggregates. The protein solution in storage buffer (10mM Tris, 10 mM NaCl, pH 7) was concentrated using a Vivaspin 20 (Sartorius, Göttingen, Germany). A minimum of three different concentrations between 1-10 mg/mL were prepared. The filtrate was collected and used as control during SAXS measurements.

2.6.2. Data collection

Small angle X-Ray scattering data were recorded at the beamline BM29 at ESRF (European Synchrotron Radiation Facility, Grenoble, France) (Pernot , et al., 2013) using a wavelength of 0.992 Å and at the EMBL beamline P12 at DESY (Deutsches Elektronen-Synchrotron, Hamburg, Germany) using a wavelength of 1.240 Å. SAXS-measurement comprised 10 frames with an exposure time of 1s at ESRF and 18 frames with an exposure time of 0.1 s at DESY each in dark and light states at a certain temperature (table 10). Recording of the buffer was done prior to and after the protein samples. The detectors used were PILATUS 1M 2D detector in Grenoble and PILATUS 2M 2D detector in Hamburg. Light state data of the protein was measured after illumination of the sample for 30 s minimum with a blue light (λ = 450 nm) LED LUXEON STAR HL-LED (plentino; Schwarmstedt, Deutschland). Dark state measurements were conducted under red light conditions.

2.6.3. Data analysis and *ab initio* model building

SAXS data analysis was conducted using the ATSAS suite version 2.5.2 (Petoukhov, et al., 2012). Initially, the recorded frames were analysed for radiation damage by the X-ray beam which might produce aggregation during the measurement making a reasonable analysis impossible. Subsequently, the frames are averaged and the buffer was subtracted from the protein solution frames with the program PRIMUS (Konarev, et al., 2003). The individual data sets for the different concentrations were merged by using data of high concentration samples for high *q*-values and data of low concentrations for small *q*-values (figure 9) (table 11). Additionally, the distance distribution function p(r), Radius of gyration, Porod volume were determined with GNOM (Svergun, 1992) and AUTORG (Petoukhov, et al., 2007). The scattering data were compared with the respective structure using CRYSOL (Svergun, et al., 1995) by fitting a calculated scattering curve based on the respective structure reported in this thesis to the experimental scattering curve.

In the case of PpSB1-LOV-R66I the crystal structures were not available, and thus the structures of wildtype PpSB1-LOV in dark and light state were used. Accounting for the missing residues of each crystal structure due to a higher flexibility at the N- and C-terminal regions, dummy atoms were introduced to account for this flexibility using CORAL (Petoukhov, et al., 2012).

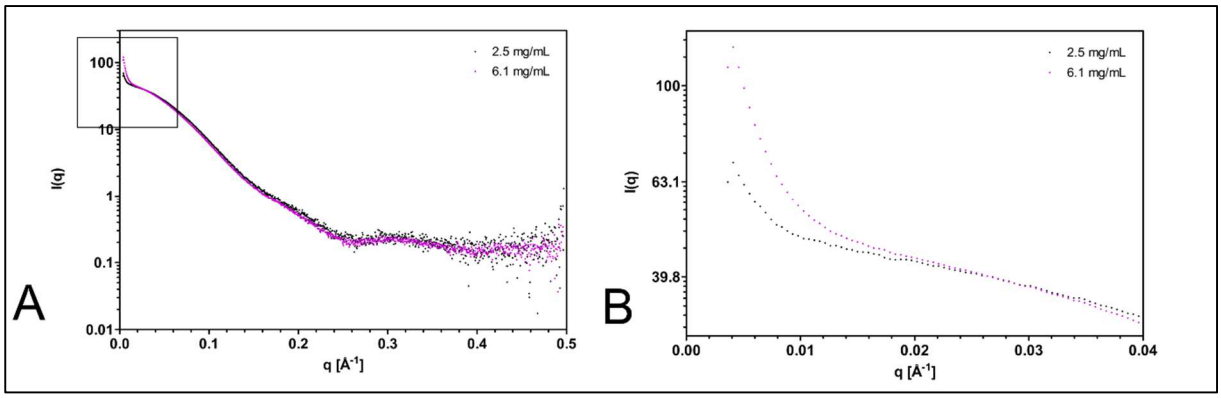

Figure 9: Example for averaging of scattering data of PpSB1-LOV-R66I. (A) Scattering data for PpSB1-LOV dark state for two different concentrations; (B) enlarged black box of panel (A) with observed aggregation at lower scattering vectors. For the sample with concentration of 6.1 mg/mL a low signal-to-noise ratio is observed at higher q-values, but at lower q-values radiation damage caused the protein to aggregate and therefore the first data should not be included in the scattering curve. The sample with lower concentration, although exhibiting a high signal-to-noise ratio at higher q-values, shows less aggregation. Therefore, the curves are merged by using the first data points at q-values up to 0.03 $Å^{-1}$ of the lower concentrated sample and the data points above q = 0.03 $Å^{-1}$ of the higher concentrated sample.

Ab initio modelling of twenty different models was conducted with (1) DAMMIN restoring low resolution shapes of randomly oriented molecules in solution (Svergun, 1999), (2) DAMMIF which basically resembles the functions of DAMMIN but uses a new algorithm accelerating the required processing time (Franke, et al., 2009) or (3)GASBOR where an average of residue densities constitute the protein structure in comparison to DAMMIN and DAMMIF where dummy atoms are used (Svergun, et al., 2001; Petoukhov, et al., 2012). The three methods were used with and without symmetry restraints. The models were averaged and filtered with DAMAVER (Volkov, et al., 2003). The envelope function is visualized and figures in this thesis are prepared with the SITUS package and the program CHIMERA (Pettersen, et al., 2004; Wriggers, 2010).

Table 11: Overview of merged data accounting for the radiation damage. DsLOV-M49I is the only protein, that does not require merging, as the radiation damage appears to be low at high concentration.

Protein	Dark/light	Concentration 1 [mg/mL]	Concentration 2 [mg/mL]
PpSB1-LOV	dark	1.8	7.7
PpSB1-LOV-C53A	dark	1.1	10.9
PpSB1-LOV-R66I	dark	2.0	6.1
	light	2.0	6.1
PpSB1-LOV-R61H/R66I	dark	1.95	9.6
DsLOV-M49I	dark	8.5	-

3. Results

3.1. PpSB1LOV

3.1.1. Dark state crystal structure of PpSB1-LOV determined with X-ray crystallography

After crystal structure determination PpSB1-LOV in light state (Circolone, et al., 2012), effort was put in the crystallization and data acquisition of the dark state. Vapor diffusion method using sparse matrix initially resulted in hexagonal and monoclinic crystals, that failed to diffract to higher resolutions than 4 Å. In order to overcome this problem, the screening for optimal crystallization conditions was repeated. The expression and purification was conducted as described in the materials and methods section (2.3.1 and 2.3.2). The utilized screens comprised for example PEG I Suite (Qiagen, Hilden, Germany) and Crystal I and II screens (Hampton Research, Aliso Viejo, USA). This effort finally resulted in the successful crystallization of PpSB1-LOV in dark state in monoclinic crystal form using the conditions 0.1 M Sodium-cacodylate pH 6.5, 10 % PEG 3000, and 0.2 M $MgCl_2$. Subsequently, the data acquisition was done at beamline ID29 at ESRF (Grenoble, France). The resolution limit was chosen as a compromise between the highest resolution and acceptable values for the completeness and mean I/sigma(I) and R_{merge} as described in the material and methods section 2.5.3. The asymmetric unit comprised four molecules forming two dimers. The number of molecules was determined using the program MATTHEWS_COEFF of the CCP4 package (Matthews, 1968) (Winn, et al., 2011) as also for each following data set.

The data were processed using XDS (Kabsch, 2010) and the final structure was determined with molecular replacement using the program MOLREP (Vagin, et al., 1997) of the CCP4 package (Winn, et al., 2011) by using chain A of PpSB1-LOV in light state (PDB-entry: 3SW1) as a search model. Details on data acquisition and refinement statistics can be found in table 12. The PpSB1-LOV crystal belonged to space group C2 and diffracted to a resolution of 2.55 Å. The secondary structure arrangements determined with the secondary structure analysis using DSSP (Kabsch, et al., 1983) did not show differences in comparison to the light state structure. PpSB1-LOV exhibits an antiparallel β-sheet formed by 5 β-strands Aβ (res. 17-24), Bβ (res. 27-33), Gβ (res. 79-86), Hβ (res. 92-103), and Iβ (res. 110-118) (figure 10A). These β-strands are flanked by four α-helices Cα (res. 35-41), Dα (res. 45-48), Eα (res. 53-56) and Fα (res. 64-75). This folding motif - the canonical α/β-PAS fold - was already described in the introduction (Nambu, et al., 1991; Pellequer, et al., 1998). Two additional secondary structure elements protruding away from the core are flanking the core domain A'α (res. 4-12) at the N-terminus and (res. 120-132) at the C-terminus Jα.

Table 12: Data collection and refinement statistics on PpSB1-LOV crystals.

X-ray data	**PpSB1-LOV dark state**	**PpSB1-LOV illuminated state**
Beamline	ID29, ESRF (Grenoble, France)	ID29, ESRF (Grenoble, France)
Detector	DECTRIS PILATUS 6M-F	DECTRIS PILATUS 6M-F
Wavelength [Å]	λ=0.97	λ=0.97
Monochromator	Silicon (1 1 1) channel-cut	Silicon (1 1 1) channel-cut
Resolution range [Å]	48.94 – 2.55 (2.66 – 2.55)[x1]	45.68 – 2.67 (2.8 – 2.67)[x1]
Space group	C 1 2 1	C 1 2 1
Unit cell a, b, c [Å]; β	102.38, 71.09, 91.26; 91.08	102.41, 71.08, 91.37; 91.02
Total reflections	106566	104162
Unique reflections	21326 (2561)[x1]	18700 (2461) [x1]
Multiplicity	5.0 (4.9) [x1]	5.6 (5.4) [x1]
Completeness [%]	99.2 (98.9) [x1]	99.5 (99.2) [x1]
Mean I/sigma(I)	14.7 (1.5) [x1]	17.9 (1.7) [x1]
Wilson B-factor [Å^2]	75.2	82.4
R_{merge}	0.049 (0.911) [x1]	0.048 (1.044) [x1]
R_{meas}	0.055 (1.018) [x1]	0.053 (1.157) [x1]
Refinement		
Resolution range [Å]	45 – 2.55 (2.641 – 2.55)[x1]	45.7 – 2.67 (2.766 – 2.67) [x1]
R_{work}	0.20 (0.30) [x1]	0.19 (0.27) [x1]
R_{free}	0.26 (0.44) [x1]	0.26 (0.32) [x1]
Coordinate error (max.-likelihood based)	0.44	0.42
Number of non-hydrogen atoms	4194	4159
Macromolecules	4070	4035
Ligands	124	124
Water	0	0
Protein residues	539	535
RMS (bonds)	0.012	0.009
RMS (angles)	1.66	1.38
Ramachandran favored [%]	98	97
Ramachandran outliers [%]	0	0
Clashscore	10.14	7.02
Average B-factor [Å^2]	106.5	113.4
Macromolecules [Å^2]	106.4	113.0
Ligands [Å^2]	109.2	126.5
Solvent [Å^2]	0	0

[x1] Statistics for the highest-resolution shell are shown in parentheses

The heterologously expressed PpSB1-LOV forms a dimer in solution, which was previously shown by analytical HPLC-based size-exclusion chromatography (Jentzsch, et al., 2009). Each molecule consists of 162 residues. The first 20 N-terminal residues comprise the His_6 tag and a thrombin cleavage site which can be ascribed to the properties of the pET28a(+) vector used for expression in this work. In the crystal structure, electron density was not visible for the first 20 residues N-terminally for all four chains and 9 and 8 residues C-terminally in chain A and chain B, C, D, respectively. This observation indicates that these parts are flexible.

Residues located on the β-scaffold and the surrounding α-helices coordinate the FMN chromophore as described below. The poor electron density for the FMN molecule in chain B was ascribed to an incomplete load of the protein with FMN. In addition, for the ligand a high B-factor of 109.2 Å^2 was found. The B-factor accounts for the spatial displacement of an atom around its position and partly describe dynamic motion inside a crystal. Nevertheless, HPLC analysis previously confirmed that PpSB1-LOV majorly accepts FMN as a chromophore

compared to other LOV-proteins like PpSB2-LOV, for example which accepts FMN and RBF at a ratio of 70:30 (Jentzsch, et al., 2009).

3.1.1.1.The dimer interface of PpSB1-LOV crystal structure in dark state

The dimer interface is mainly constituted by hydrogen bonds between both molecules accompanied by several hydrophobic interactions (figure 10A). In detail the hydrogen bonds are formed between the N-terminal α-helix A'α and the loop between Hβ and Iβ, and the loop between A'α and Aβ and the β-sheet (table 13) (figure 10C and D).

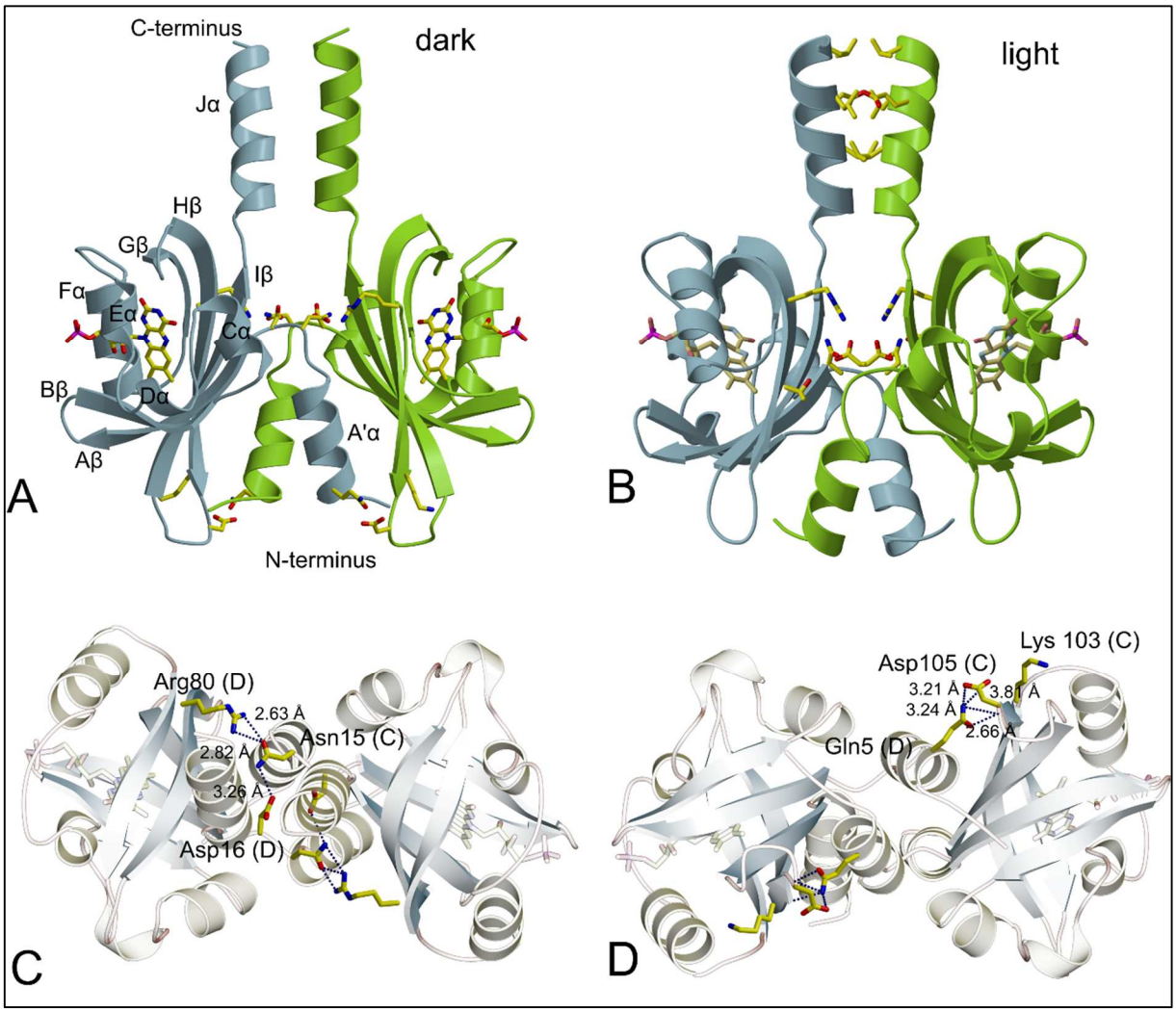

Figure 10: Dimer interface of PpSB1-LOV. Ribbon representation of the dark and light state crystal structures of PpSB1-LOV. Residues constituting the interface are represented in stick model with carbon atoms highlighted in standard color code. The ribbon representation of the dimer in 10C and 10D is kept transparent for clarity; (A) The dimer interface of PpSB1-LOV in dark state, chain C is colored in blue, chain D in green. (B) The dimer interface of PpSB1-LOV in light state, chain A is colored in blue, chain B in green (A); (C) View from the C-terminus along the Jα-helix towards the core domain of the dimer of PpSB1-LOV dark state; (D) View from the N-terminus along the A'α helices towards the core domain of the dimer of PpSB1-LOV dark state.

Hydrophobic interactions are mainly found between the N-terminal helix A'α (Leu6, Met10, Val11) or the loop between A'α and Aβ (Ala13) and the β-strands Aβ (Ile18, Val20), Bβ (Ile31, Tyr32) and Iβ (Ile115) or between the two C-terminal Jα-helices on both molecules (Leu125, Leu129, Leu132).

Table 13: Hydrogen bond interaction contributing to the dimer interface of PpSB1-LOV in dark state. The analysis was conducted with CONTACT from the CCP4 package (Collaborative Computational Project, 2011) with a cutoff of 3.35 Å.

Chain	Secondary structure element	Residue	Atom	Distance [Å]	Atom	Residue	Secondary structure element	Chain
C	A'α	Gln5	OE1	2.68	N	Asp105	Hβ-Iβ loop	D
C	A'α	Gln5	NE2	2.98	O	Lys103	Hβ	D
C	A'α	Gln5	NE2	3.24	N	Asp105	Hβ-Iβ loop	D
C	A'α	Gln5	NE2	2.97	OD2	Asp105	Hβ-Iβ loop	D
C	A'α-Aβ loop	Asn15	OD1	3.20	NH2	Arg80	Gβ	D
C	A'α-Aβ loop	Asn15	ND2	3.26	OD2	Asp16	A'α-Aβ loop	D
C	Gβ	Arg80	NH1	2.82	OD1	Asn15	A'α-Aβ loop	D
C	Gβ	Arg80	NH2	2.63	OD1	Asn15	A'α-Aβ loop	D
C	Hβ	Lys103	O	3.32	NE2	Gln5	A'α	D
C	Hβ-Iβ loop	Asp105	N	2.91	OE1	Gln5	A'α	D
C	Hβ-Iβ loop	Asp105	OD2	3.21	NE2	Gln5	A'α	D
C	Hβ-Iβ loop	Asp105	N	2.91	OE1	Gln5	A'α	D
C	Hβ-Iβ loop	Asn105	OD2	3.21	NE2	Gln5	A'α	D

3.1.1.2.FMN binding pocket

The dark adapted FMN chromophore which was found in the cavity of the core domain is non-covalently linked to the protein and mainly coordinated by several hydrogen bonds (figure 11A). The photoactive Cys53-Sγ is located on the helix Eα close to the FMN-C4a atom, the interaction partner upon formation of the covalent bond with a distance of 3.57 – 4.1 Å depending on the respective chain. Several amino acid side chains mainly coordinate the chromophore located on the loop between Dα and Eα, Eα, Eα-Fα loop, Fα, Gβ, Hβ (figure 11A) (table 14).

Table 14: Residues of PpSB1-LOV in dark state coordinating the FMN chromophore via hydrogen bonds. The analysis was conducted with CONTACT from the CCP4 package (Collaborative Computational Project, 2011) and the cutoff was set to 3.35 Å.

Secondary structure element	Residue	Atom	Distance [Å]	FMN-Atom
Dα-Eα loop	Asp52	OD1	2.82	O2'
Eα	Arg54	NE	3.07	O2P
Eα	Arg54	NH2	2.96	O1P
Eα- Fα loop	Gln57	NE2	2.77	O4'
Eα- Fα loop	Gln57	NE2	3.35	O2
Eα- Fα loop	Arg61	NH1	3.15	O2P
Eα- Fα loop	Arg61	NH2	2.96	O2P
Fα	Arg66	NE	2.94	O3P
Fα	Arg66	NH2	3.13	O3P
Fα	Arg70	NH1	2.48	O3P
Gβ	Asn85	OD1	2.71	N3
Gβ	Asn85	ND2	2.89	O2
Hβ	Asn95	ND2	3.19	O4

As already described previously for the light state structure a set of four arginines is found in PpSB1-LOV tightly coordinating the phosphate group of the FMN which is unique amongst the LOV proteins (figure 11B) (Circolone, et al., 2012). Similar interactions are present in the dark state structure (figure 11A, 12A).

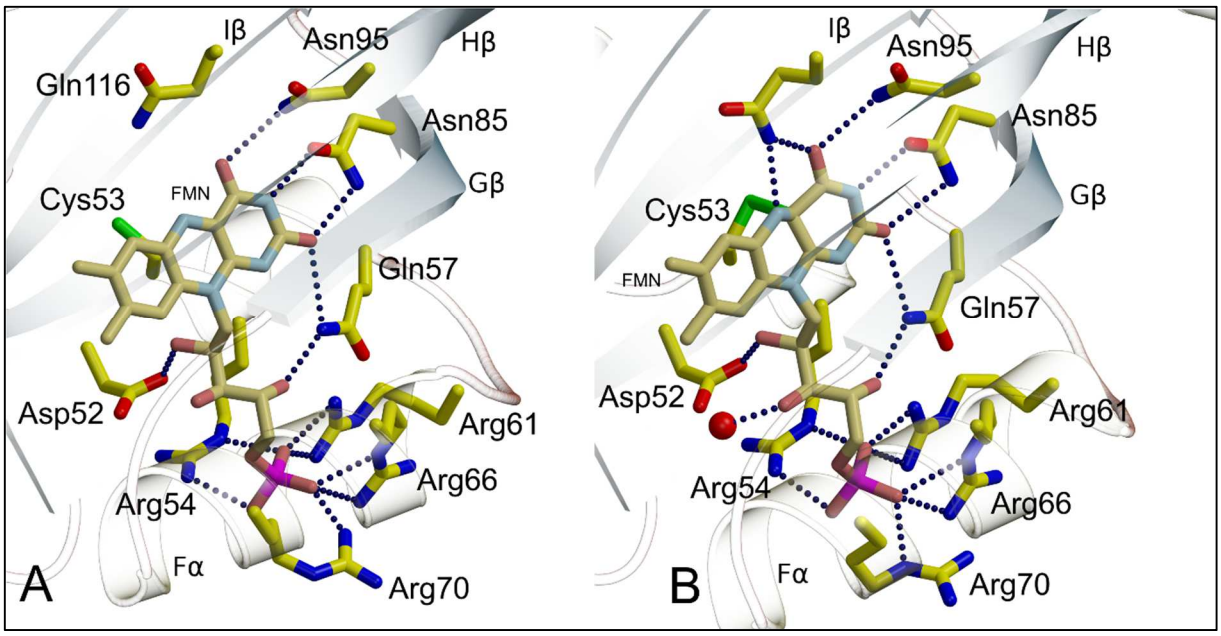

Figure 11: Active site of PpSB1-LOV in dark (A) and light (B) states. Amino acid side chains and FMN are represented in stick model and standard colors are used for the different atoms. Hydrogen bonds are represented in dark blue, dotted lines. For a better discrimination between chromophore and protein the FMN is kept in pale colors. (A) Hydrogen bonds between FMN atoms and protein residues. As expected for the dark state the photoactive Cys53 does not show any covalent interactions with the chromophore located inside the LOV-core. (B) As already defined for the true light state in (Circolone, et al., 2012) the Sγ atom of Cys53 and the C4a atom of the FMN chromophore within a distance of 2.35 Å.

3.1.2. Comparison of the dark state crystal structure with the true light state structure of PpSB1-LOV

A comparison between dark and light state structures of PpSB1-LOV is indispensable as it might present further information about the reception, the primary events after illumination in the protein and the signal propagation to receptor domains fused or unfused to one of the terminal extensions. The dimer interface of the light state is mainly defined by hydrophobic interactions. In detail, these interactions are found in three main regions: (1) between the N-terminal caps of both the molecules in the dimer, (2) between the N-terminal cap and the β-sheet of the other subunit, and (3) between the C-terminal extension Jα of both the subunits. Additionally, the dimer is constituted by several hydrogen bonds between the loop between A'α and Aβ and the β-sheet (Asp16-OD2…*OG-Ser98,* 2.64 Å; T100-OG1…*N-Asn15,* 2.97 Å; Arg80-NH1/NH2…*OD2-Asp16,* 3.30 Å) and a salt bridge (Glu128-OE2…*NH2-Arg133*, 2.81 Å) (residues in italics refer to those from the other molecule) (Circolone, et al., 2012). The

overall dimer interface in the dark state remains similar to the light state. However, a buried surface area of 3732 Å^2 in the light state compared to 2756 Å^2 in the dark state clearly indicates a different composition of the dimer interface which is highly likely evoked by the illumination. The buried surface areas were determined by PISA analysis (Krissinel, et al., 2007). Although some interactions remain in both states like interactions of residues Arg80, Leu125, Leu129 and Leu132, entirely new interactions between the two molecules are observed and the salt bridge is completely missing in the dark state interface. These new interactions include the formation of a hydrogen bond between Arg80 and Asp16 instead of Asn15 as observed in the light state.

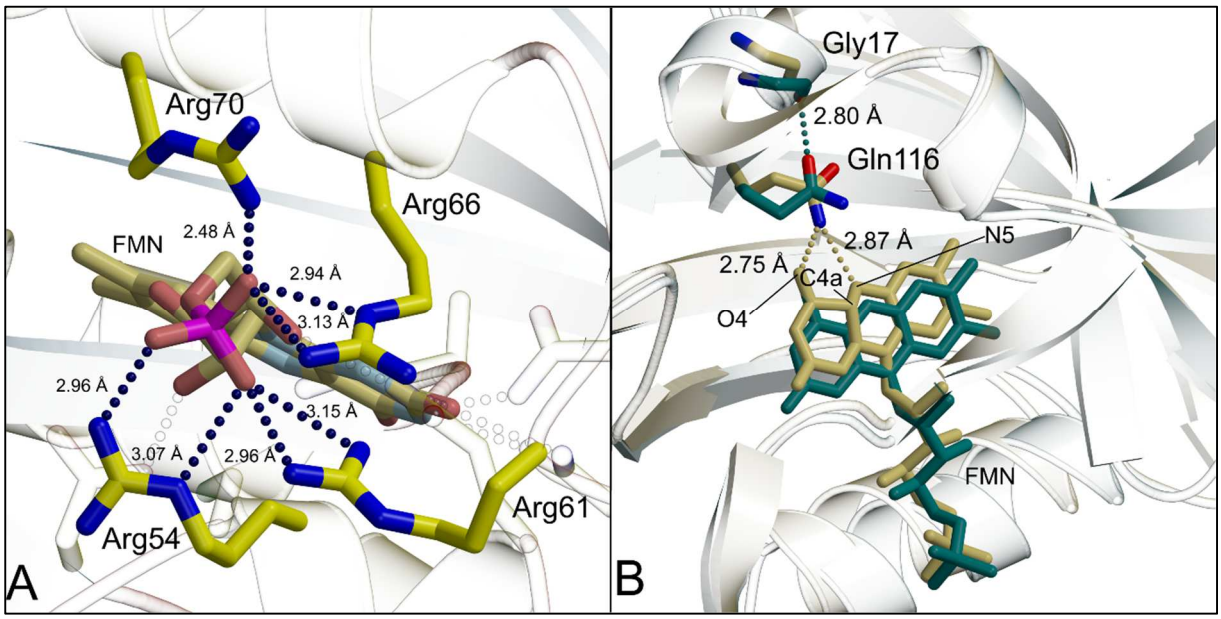

Figure 12: Coordination of the phosphate moiety of the FMN in PpSB1-LOV dark state (A) and superposition of the core domain of PpSB1-LOV in dark (petrol) and light (gold) state (B). (A) Representation of the previously described arginine cluster coordinating the FMN by several hydrogen bonds (Circolone, et al., 2012). (B) The amino group of residue Gln116 in light state forms hydrogen bridges with the O4 and N5 atom of FMN. In contrast, in the dark state the Gln116 undergoes a conformational reorientation in the dark state which leads to loss of interaction between the glutamine and the FMN. Instead it interacts with the backbone oxygen of Gly17 (strand Aβ).

As mentioned in the introduction, the first reaction step in the LOV protein after illumination with blue light is the formation of a covalent bond between the FMN and the protein. It is thus important to compare the chromophore coordination of the light state and the dark state. The comparison of both structures in light and dark state basically revealed the same chromophore coordination (figure 11). The only major difference besides the close distance of the Cys53 with the FMN (Cys-Sγ…C4a-FMN, 2.35 Å) can be found in the orientation of the Gln116 side chain (figure 12B). The Gln116 is highly conserved and has been proposed previously to play a key role in signal propagation in LOV proteins (Federov, et al., 2003; Nozaki, et al., 2004; Möglich, et al., 2007; Zoltowski, et al., 2007; Circolone, et al., 2012; Conrad, et al., 2012;

Bocola, et al., 2015). In the light state two hydrogen bonds are formed between the NE2 atom of Gln116 and the O4 and N5 atom of the FMN, close to the Cys53 in the core cavity beneath. In contrast, no interactions between the Gln116 and the FMN are found in the dark state structure. The glutamine undergoes a side chain reorientation and forms a new hydrogen bond with the carbonyl oxygen of Gly17 on the Aβ-strand (figure 12B).

A striking difference between light and dark states in PpSB1-LOV is a major reorientation in the C-terminal Jα-helix. A superposition of chains A to D of the dark state on chain A of the light state reveals a distance of 6.3 – 11.8 Å between the Cα atoms of residues Ala134 (figure 13) (table 15). As chain A of the dark state structure is missing residue 134, the distance is determined between the Cα atom of residue Arg133 and determined to 4.58 Å (table 15).

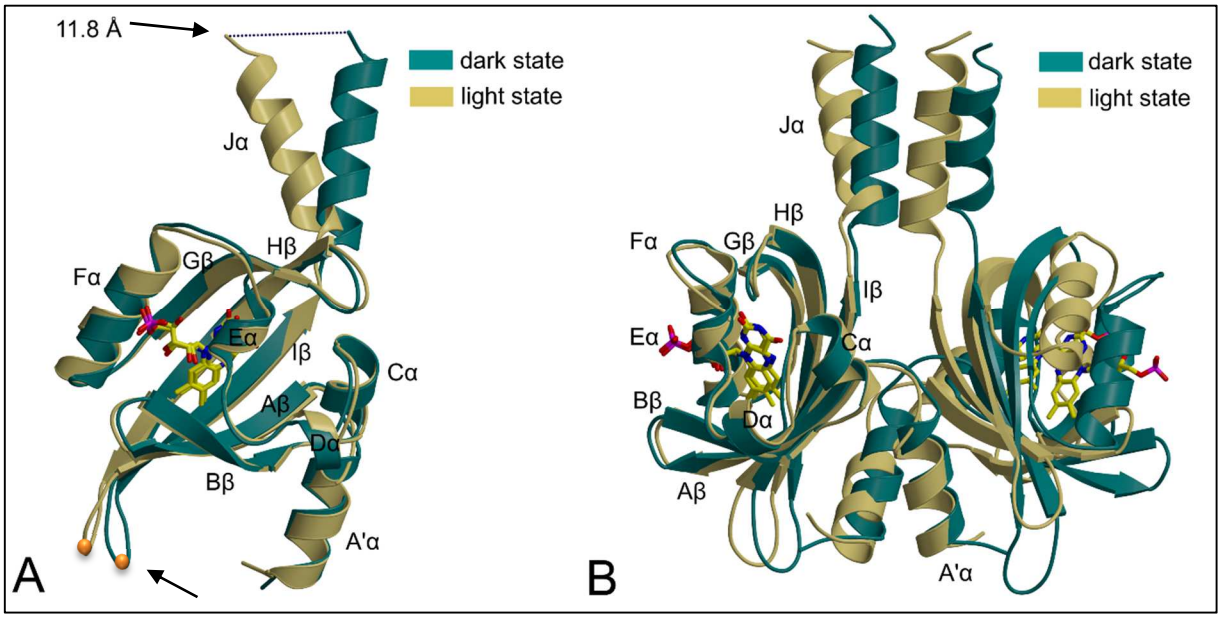

Figure 13: Superposition of PpSB1-LOV crystal structure in dark (petrol) and light (yellow) state. (A) The superposition of the monomers demonstrates the movement of the Jα helix between the dark and light state structures. (B) The superposition of the dimer with the focus on chain C (residues 1-119), chains in left, illustrates the differences between the dark state and the light state crystal structures. The arrow marks the difference in the Hβ-Iβ loop. The orange dots highlight the position of Phe106.

The overall structure of the core domain (residues 17-118) does not show significant differences besides the Hβ-Iβ loop (residues 104-109, figure 13A black arrow) (table 16). Differences of 3.04 – 5.10 Å were found between the Cα atoms of residue Phe106 (orange dots, figure 13A) in each chain of the dark state structure and chain A of the light state structure. The dimeric structure of PpSB1-LOV is shown in figure 13B. The dark state dimer was superposed on the light state dimer using chain C (chain in left) as reference with the program COOT (Emsley, et al., 2004; Krissinel, et al., 2004). The superposition of both structures show a reasonably good overlap for the chains C as shown in figure 13A, but the second chain D of both dimers show major differences and a poor overlap.

Table 15: Distances between Cα-atoms of C-terminal residues 133 and 134 upon superposition of all chains on each other of PpsB1-LOV in dark and light states. Chain A is missing residue 134 in dark state, therefor residue 133 was used for comparison.

		PpSB1-LOV in dark state			
		chain A Arg133	chain B Ala134	chain C Ala134	chain D Ala134
PpSB1-LOV light state	chain A Arg133	4.58 Å	-	-	-
	chain A Ala134	-	11.8 Å	8.0 Å	6.3 Å

Table 16: Distances between Cα-atoms of Phe106 in the Hβ-Iβ loop upon superposition of all chains on each other of PpSB1-LOV in dark and light states.

		PpSB1-LOV in dark state			
		chain A Phe106	chain B Phe106	chain C Phe106	chain D Phe106
PpSB1-LOV light state	chain A Phe106	4.2 Å	4.4 Å	3.0 Å	5.1 Å

The rotation of chain D relative to chain C is required, and was determined in two steps (figure 14). First, both dimers were superposed as described above. Based on this arrangement a second superposition was performed but now using the chain D of the light state as reference. This movement resulted in a rotation angle of ~ 29°. This observed difference in the dimer formation is also reflected in the unequal contribution of residue constituting the dimer interface as described above.

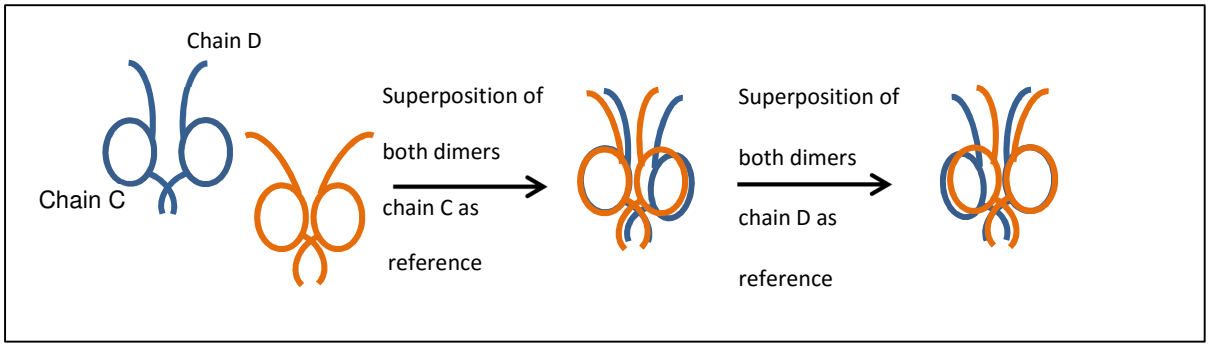

Figure 14: Cartoon showing how the superposition of Dimer of PpSB1LOV in dark and light states was done. The dark state dimer (orange) was superposed on the light state dimer (blue) using chain C (left) as reference with the program COOT (Emsley, et al., 2004) (Krissinel, et al., 2004). A second superposition was performed but now using the chain D of the light state as reference. Subsequently, rotation angle was determined to superpose chain D on its equivalent in light state.

3.1.3. Dark state crystal structure of PpSB1-LOV-C53A – active site mutant of PpSB1-LOV determined with X-ray crystallography

In recent years different LOV proteins were modified by exchange of the photoactive cysteine into an alanine preventing the photocycle in order to create fluorescence reporter proteins like iLOV (Chapman, et al., 2008), Pp2FbFP and BsFbFP (Drepper, et al., 2007), and miniSOG (Shu, et al., 2011). Similar approach was conducted for PpSB1-LOV. The expression and purification of PpSB1-LOV-C53A was executed equally to PpSB1-LOV and resulted in an

approximate yield of 250 mg/L. The pure protein solution was set to a concentration of 104 mg/mL and several screening conditions were tested. After four weeks of incubation at 20 °C in dark, monoclinic crystals grew in 0.05 M $CoCl_2$ x $6H_2O$, 1.2 M 1,6-Hexanediol, 0.1 M Sodium acetate x 3 H_2O pH 4.6, diffracting to a resolution of 2.6 Å with four chains per asymmetric unit. The collected data were processed as described for PpSB1-LOV in section 3.1.1. Details on data acquisition and refinement statistics are provided in table 17. The superposition of Cα-atoms of PpSB1-LOV and the mutant PpSB1-LOV-C53A resulted in a RMSD of 1.14 Å suggesting no significant change in the overall fold. In comparison to the dark state wildtype, the electron density around the FMN chromophore in each chain is improved.

Table 17: Data collection and refinement statistics on PpSB1-LOV-C53A mutant crystals.

X-ray data	**PpSB1-LOV-C53A dark state**	**PpSB1-LOV-C53A illuminated state**
Beamline	ID29, ESRF (Grenoble, France)	ID29, ESRF (Grenoble, France)
Detector	DECTRIS PILATUS 6M-F	DECTRIS PILATUS 6M-F
Wavelength [Å]	λ=0.97	λ=0.97
Monochromator	Silicon (1 1 1) channel-cut	Silicon (1 1 1) channel-cut
Resolution range [Å]	49.42 – 2.6 (2.72 – 2.6)[x1]	47.02 – 2.6 (2.72 – 2.6)[x1]
Space group	C 1 2 1	C 1 2 1
Unit cell a, b, c [Å]; β	99.14, 83.52, 94.5; 94.46°	99.21, 83.48, 94.45; 94.46°
Total reflections	108998 (13323)[x1]	85136 (10436)[x1]
Unique reflections	23590 (2840) [x1]	23578 (2846) [x1]
Multiplicity	4.6 (4.7) [x1]	3.6 (3.7) [x1]
Completeness [%]	99.3 (98.9) [x1]	99.3 (99.0) [x1]
Mean I/sigma(I)	9.5 (1.3) [x1]	10.8 (1.0) [x1]
Wilson B-factor [Å^2]	82.0	77.8
R_{merge}	0.075 (0.9829) [x1]	0.055 (1.117) [x1]
R_{meas}	0.085 (1.119) [x1]	0.065 (1.310) [x1]
Refinement		
Resolution range [Å]	47.1 – 2.6 (2.693 – 2.6) [x1]	47.08 – 2.6 (2.693 – 2.6) [x1]
R_{work}	0.20 (0.45) [x1]	0.18 (0.33) [x1]
R_{free}	0.27 (0.53) [x1]	0.25 (0.41) [x1]
Coordinate error (max.-likelihood based)	0.52	0.41
Number of non-hydrogen atoms	4157	4220
Macromolecules	4033	4096
Ligands	124	124
Protein residues	535	536
RMS (bonds)	0.009	0.009
RMS (angles)	1.25	1.31
Ramachandran favored [%]	100	100
Ramachandran outliers [%]	0	0
Clashscore	9.42	7.01
Average B-factor [Å^2]	104.1	97.7
Macromolecules [Å^2]	104.3	98.2
Ligands [Å^2]	95.5	82.6

[x1] Statistics for the highest-resolution shell are shown in parentheses

The dark state crystal structures of PpSB1-LOV and PpSB1-LOV-C53A do not reveal clear differences in the dimer interface and chromophore binding. A minor difference however is the presence of the salt bridge between the NZ atom of Lys117 and OD1 of Asp16. These interactions were observed in the light state but not in the dark state of PpSB1-LOV.

3.1.4. Crystal structures of PpSB1-LOV and PpSB1-LOV-C53A after illumination of the dark grown crystals

Several crystal structures of LOV proteins are available in light and dark states but most of the published light state crystals were not grown under light conditions (Möglich, et al., 2007; Vaidya, et al., 2011; Mitra , et al., 2012; Conrad, et al., 2013; Endres, et al., 2015). Usually, dark-grown crystals were illuminated prior to cryo-cooling. Although this method provides information about the structural changes in light conditions, large conformational changes expected to happen during the photocycle cannot take place due to the crystal packing. PpSB1-LOV was the first full-length short LOV protein structure published in true light state where the crystal grew under continuous light conditions. Now, it is of interest to see to what extent the illuminated structure provides information in comparison to the true light state. The crystal which was already used for the dark state structure of PpSB1-LOV was thawed to room temperature and illuminated for 2 secs with blue light and cooled down to 100K. The collected data were processed as described for the dark state and refined to a resolution of 2.6 Å. Details on data acquisition and refinement statistics can be found in table 12 and 17. As each data set was recorded at 100 K, radiation damage was taken into account based on calculations using the program BEST (Bourenkov, et al., 2010).

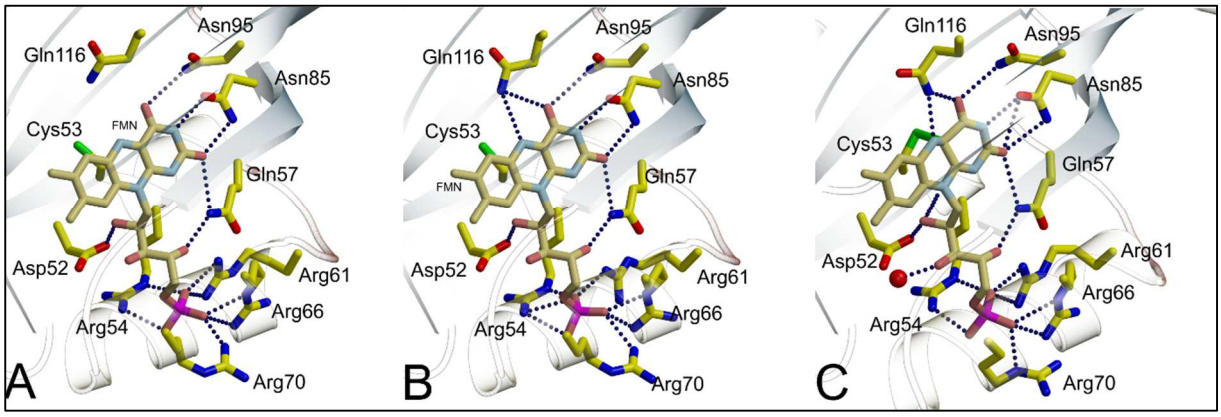

Figure 15: Active site and chromophore coordination of PpSB1-LOV in (A) dark, (B) illuminated and (C) light state. The FMN chromophore forms several hydrogen bonds with several amino acid side chains on Eα (Cys53, Arg54), the loop between Eα and Fα (Gln57, Arg61), Fα (Arg66, Arg70), Gβ (Asn85), Hβ (Asn95), and Iβ (Gln116). In all three states the coordination maintains as found in the dark state. A difference seen for Gln116 is that it forms hydrogen bonds with the O4 and N5 atom of the FMN in light and illuminated states but possesses a different rotamer orientation in the dark state.

Superposition of the dark state with the illuminated state structures yields a RMSD value of 0.42 Å, the tertiary structure does not reveal structural changes most likely due to the crystal packing. Nevertheless, differences between the dark, light and illuminated structures of PpSB1-LOV are found in some residues coordinating the chromophore (figure 15).

The Sγ atom of the photoactive Cys53 is in a distance of 2.35 Å with the sp^3 hybridized C4a atom of the FMN chromophore in the light state (figure 15C). A thioether covalent bond

was not observed but the authors still concluded a light state structure based on the growth of the crystal under continuous light and the electron density indicating a non-planar ring as observed in different light state structures. This bond is released during the dark recovery and as a result the chromophore is only coordinated by a number of hydrophobic interactions and hydrogen bonds in the dark state (figure 15A). The distance between the sulfur atom and the C4a atom adds up to 4.08 Å which is a non-covalent distance. In the illuminated state, a slight movement is observed for the cysteine as represented by a smaller distance of 3.90 Å. Nevertheless, these changes might arise due to the low resolution of the overall structure and should be treated with some caution. The Sγ atom of the Cys53 still remains in a non-bonding distance to the C4a atom of the FMN. An additional deviation was found for the amino acid Gln116. In the light state, the Gln116 does form two hydrogen bonds with the FMN chromophore, whereas in the dark structure the Gln116 did undergo a conformational change and now binds to the carbonyl oxygen of Gly17. On the contrary, in the illuminated state, which is based on the dark state crystal as already explained, the Gln116 again forms two weak hydrogen bonds with the O4 and N5 atom of FMN. In conclusion, the coordination of the chromophore in the illuminated state remains closer to the light state than to the dark state although no covalent bond was observed between C4a of FMN and Cys53 of the protein. A similar result was observed in the core domain of the illuminated crystal structure of PpSB1-LOV-C53A. The overall fold of the illuminated structure of PpSB1-LOV-C53A does not reveal clear conformational differences in comparison to the dark state structure. But a comparison of the electron density of the FMN chromophore reveals a spreading of electron density which is further discussed in the following section.

3.1.5. Photoreduction of PpSB1LOV-C53A investigated using single-crystal spectrometry

One of the observations in PpSB1-LOV-C53A illuminated crystal structures was spreading of electron density for the chromophore molecule. A possible explanation can be a higher flexibility in the ring system of the FMN chromophore. This flexibility can be achieved by a loss of double bonds which keep the isoalloxazine ring in the rigid conformation (figure 16). The reduction of oxidized FMN to FMN-semiquinone has previously been described for LOV1-C57S and LOV2-C250S of the LOV domains of the green alga *Chlamydomonas reinhardtii* by (Song, et al., 2007). In this study, the absorption spectra of wildtype phot LOV domains and serine mutants were investigated in aqueous solution under aerobic conditions. The authors reported the photoexcitation induced formation of a reversible FMN-C4a-cysteinyl adduct in the wildtype LOV1 and LOV2 domains. For this reaction a high quantum efficiency

was observed. In comparison, after excitation of the mutants LOV1-C57S and LOV2-C250S under aerobic conditions a reduction of the FMN to FMNH° semiquinone was observed. A continued excitation of the mutants with light additionally produced a reversible and fully reduced state of FMN. Based on observed differences in the kinetics for both mutants, the authors suggested different reaction mechanisms. The response to light of LOV1-C57S occurs time-delayed implicating necessary modifications of the FMN binding pocket prior to the photo-reduction of the FMN. For LOV2-C250S no time-delay was observed and the one-electron transfer starts immediately.

The reduction of FMN to FMNH° was not observed for the wildtype forms of LOV1 and LOV2. The high quantum efficiency of the covalent adduct formation most likely restrains this conversion. Both mutants LOV1-C57S and LOV2-C250S cannot form the covalent bond between chromophore and protein due to the missing photoactive cysteine. Thus, the primary and more favored event after excitation with light is the conversion of the oxidized FMN to the FMN-semiquinone.

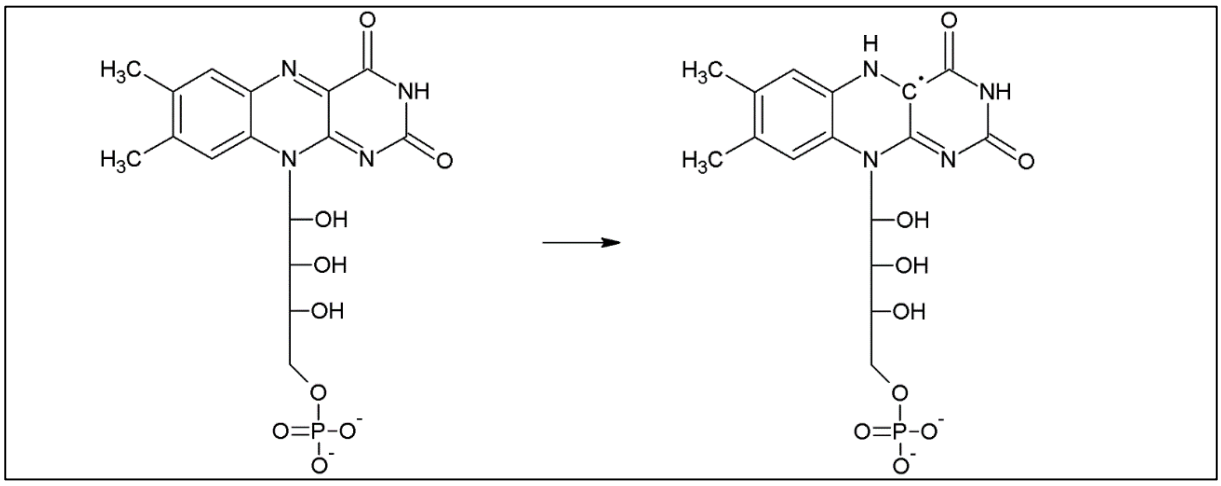

Figure 16: Reduction of FMN to FMNH° (FMN-semiquinone).

In the case of PpSB1-LOV-C53A, the photoactive cysteine is substituted by an alanine residue. In order to investigate if the reduction of FMN to FMN-semiquinone in this mutant occurs, a crystal showing the typical dark state spectrum (figure 17A, black line) was illuminated with blue light at room temperature with different exposure times and spectra were recorded between 400 nm and 600 nm.

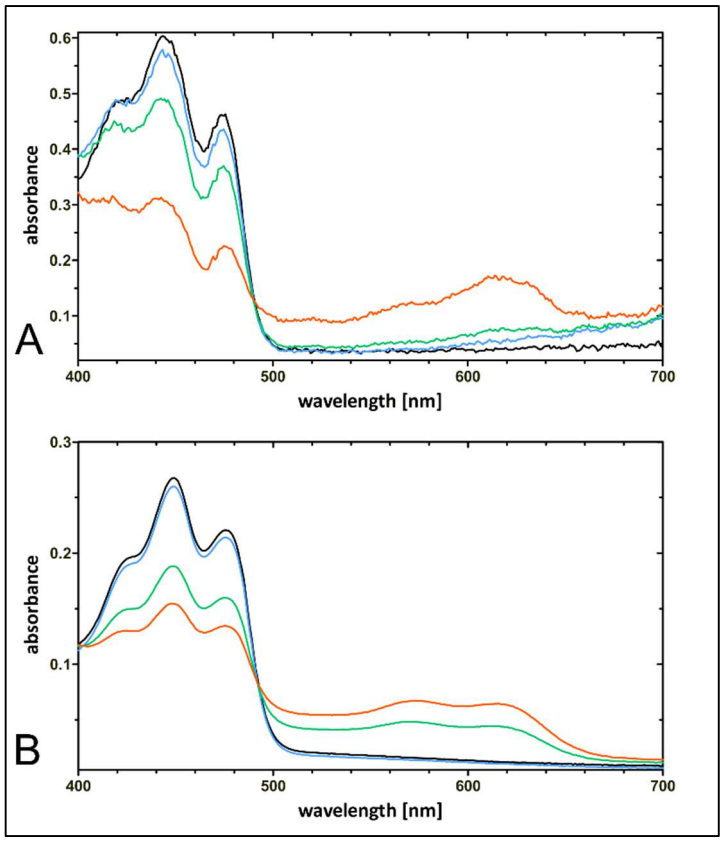

Figure 17: Single crystal microspectrometry of dark-adapted PpSB1-LOV-C53A. (A) Spectra of a dark-grown crystal of PpSB1-LOV-C53A was recorded before illuminating the crystal (black line) and after illumination for 1 min (blue line), 5 min (green line), and 15 min (orange line) with blue light. A typical dark spectrum for oxidized FMN in LOV proteins is observed with a maximum at 447 nm and a shoulder at 420 nm. After illumination, a loss of absorption in the blue region of the spectrum is observed, accompanied by a rise of a new spectral species with a maximum at 605 nm and a broad unstructured absorbance band between 500 nm and 600 nm. (B) The same experiment was performed with PpSB1-LOV-C53A protein in solution. Prior to illumination with the same ligth source as used for the crystal, the solution was degassed. For a better comparison, the color code used here is same as in panel (A). These measurements were done in collaboration with Dr. Ulrich Krauss from the Institute of Molecular Enzymetechnology, FZ Jülich, Germany.

The dark spectrum (black line) shows a maximum at 447 nm and a pronounced vibrational fine structure that is typical for LOV proteins (Kottke, et al., 2003). With an increase in the illumination time, this λ = 447 nm maximum decreases and another prominent species occurs around 605 nm (figure 17A) which can best be observed after 15 min of exposure to blue light (orange line). This species most likely can be attributed to the neutral radical, reduced FMN-semiquinone (Kottke, et al., 2003; Song, et al., 2007). The same experiment was repeated with the PpSB1-LOV-C53A mutant protein in solution which has been described for the mutated phot-LOV1 domain from *Chlamydomonas reinhardtii* (Kottke, et al., 2003). Initially, the protein was dissolved in 10 mM Tris, 10 mM NaCl, pH 7 and spectra were recorded after prolonged illumination. Unfortunately, no time-dependent changes were observed as found in the crystal. After degassing the solution, the same spectral behavior in crystal and solution were observed to be similar (figure 17B). Additionally, the conversion to the single electron-reduced FMN in solution is even faster than in the crystal as the new prominent species at 600 nm arises

after 5 min instead of 15 min. Comparison of the results observed in solution and in the crystal reveals a similar behavior of the protein towards the excitation with blue light (figure 17A and B). The double bond between the N5 and C4a atoms is lost in the FMN semiquinone state resulting in an unpaired electron at the N5 atom. As a result, the flexibility of the isoalloxazine ring is increased accounting for the observed spreading of the electron density in the crystal structure of PpSB1-LOV-C53A.

3.1.6. Dark state crystal structure of PpSB1-LOV-R61H/R66I mutant determined with X-ray crystallography

Prior to the identification of PpSB1-LOV in the proteo-bacterium *Pseudomonas putida*, another LOV protein was identified termed PpSB2-LOV. Both proteins possess 66 % identical amino acid positions (Jentzsch, et al., 2009). Nevertheless, they differ in their photochemical properties. The dark recovery constant of PpSB2-LOV (τ_{REC} = 137 ± 11 s, at 20 °C) is accelerated by a factor of 10^3 in comparison with the respective PpSB1-LOV recovery (τ_{REC} = 2471 ± 22 min, at 20 °C). Their high identities in primary structure and their significant differences in the photochemical properties make them an interesting set of LOV proteins for further investigations. Circolone et al. reported a high coordination of the FMN-phosphate by four surrounding arginines in PpSB1-LOV. Two of them, Arg61 and Arg66, are found to be a histidine and an isoleucine in PpSB2-LOV, observed as the most prominent difference between both proteins. Based on this observation the double mutant PpSB1-LOV-R61H/R66I was generated (compare 1.2). The resulting mutant exhibits a 270-fold acceleration in dark recovery (τ_{REC} = 9 min, at 20 °C) compared to the wildtype. Structural comparison of mutant and wildtype structures is expected to provide information on impact of arginine cluster-FMN coordination with regard to the dark recovery.

The pure protein solution was set to a concentration of 80 mg/mL and several screening conditions were tested. After four weeks of incubation at 20 °C in dark, monoclinic crystals grew in 0.2 $MgCl_2$, 0.1 M MES pH 6.6, 15 % (w/v) PEG 4000. The collected data were processed as described for the wildtype in section 3.1.1. Details on data acquisition and refinement statistics can be found in table 18. Overall the structure of the double mutant does not reveal new characteristics with respect to the wild type dark state structure (RMSD upon superposition taken all residues into account: 0.68 Å).

Table 18: Data collection and refinement statistics on PpSB1-LOV-R61H/R66I mutant crystal.

X-ray data	**PpSB1-LOV-R61H/R66I dark state**
Beamline	ID29, ESRF (Grenoble, France)
Detector	DECTRIS PILATUS 6M-F
Wavelength [Å]	λ=0.98
Monochromator	Silicon (1 1 1) channel-cut
Resolution range [Å]	48.45 – 2.04 (2.10 – 2.04)[x1]
Space group	C 1 2 1
Unit cell a, b, c [Å]; β	102.7, 76.51, 51.28; 106.23°
Total reflections	172136 (13667)[x1]
Unique reflections	39334 (3076) [x1]
Multiplicity	4.4 (4.4) [x1]
Completeness [%]	99.5 (99.7) [x1]
Mean I/sigma(I)	11.2 (1.7) [x1]
Wilson B-factor [Å^2]	37.5
R_{merge}	0.069 (0.914) [x1]
R_{meas}	0.078 (1.037) [x1]
Refinement	
Resolution range [Å]	44.68 – 2.04 (2.11 – 2.04) [x1]
R_{work}	0.20 (0.31) [x1]
R_{free}	0.24 –(0.36) [x1]
Coordinate error (max.-likelihood based)	0.29
Number of non-hydrogen atoms	4380
Macromolecules	4143
Ligands	124
Water	113
Protein residues	541
RMS (bonds)	0.008
RMS (angles)	0.94
Ramachandran favored [%]	100
Ramachandran outliers [%]	0
Clashscore	4.0
Average B-factor [Å^2]	56.5
Macromolecules [Å^2]	57
Ligands [Å^2]	50.0
Solvent [Å^2]	46.7
Number of TLS groups	33

[x1] Statistics for the highest-resolution shell are shown in parentheses

Unfortunately, crystallization trials failed under continuous light conditions, but upon comparison with the light state structure of PpSB1-LOV, the differences in the Jα helix which were already explained in section 3.1.2 were found also for the double mutant. Residues involved in the dimer interface are same as described in the dark state structure of PpSB1-LOV. The coordination of the chromophore did not change generally in the mutant in comparison to the dark state structure of PpSB1-LOV. As expected, the interactions between the mutated residues of protein and the phosphate moiety are missing due to the substitution of two arginines Arg61 and Arg66. Residues Arg54 and Arg70 are conserved in the LOV-protein family (Federov, et al., 2003; Möglich, et al., 2007; Zoltowski, et al., 2007; Circolone, et al., 2012; Conrad, et al., 2012). In the mutant structure they adapt the same conformation as observed in the wildtype dark state structure where Arg54 forms two hydrogen bonds and Arg70 forms one hydrogen bond with the phosphate (figure 18A and B). The Ile66, as an aliphatic amino acid, does not form a salt bridge with the phosphate but remains in the same rotamer in all four chains of the crystal structure. Although the imidazole ring of the histidine at position 61 is capable of

forming a hydrogen bond with the phosphate, the actual closest distance between the His-ND1/NE2 and the O1P-FMN atom is in the range 3.47 – 7.17 Å (chain B does not exhibit any electron density therefore His61 was truncated to the Cβ atom).

A comparison of all four chains in the crystal structure of PpSB1-LOV-R61H/R66I and in particular the residues Arg54, His61, Ile66 and Arg70 and the equivalent residues in the wildtype in dark state is represented in figure 18B. Residue Arg54 changed neither its conformation nor its interactions with the phosphate. The same was found for Arg70.

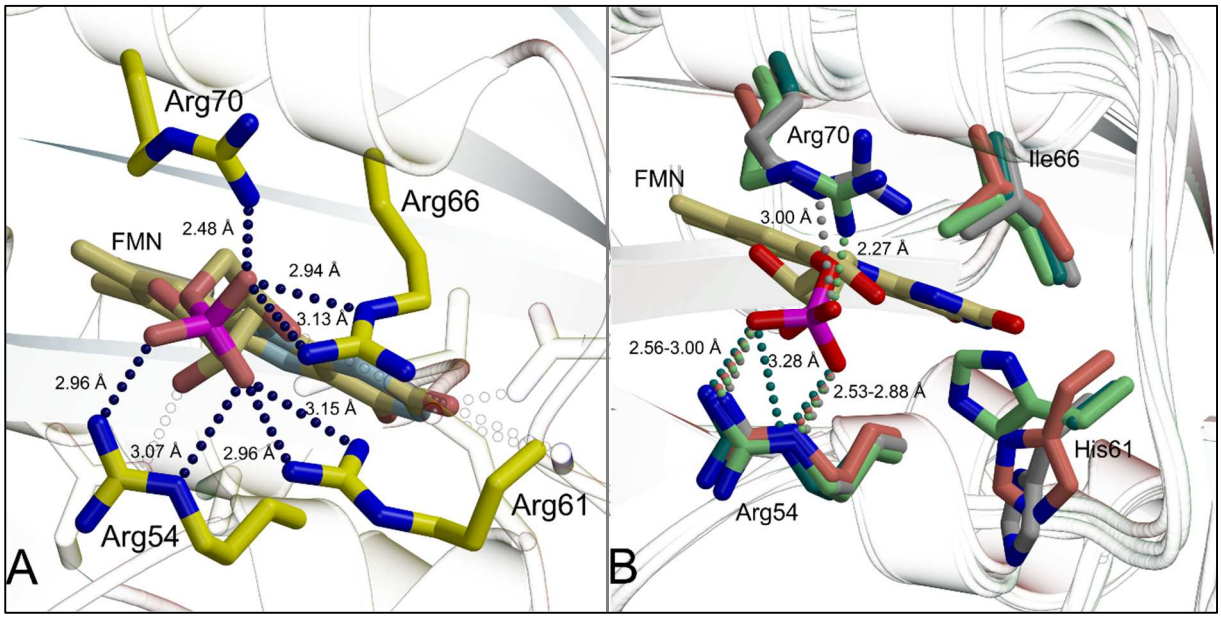

Figure 18: Coordination of the FMN phosphate moiety in PpSB1-LOV dark state (A) and PpSB1-LOV-R61H/R66I (B). (A) The phosphate is coordinated via hydrogen bonds by a cluster of four arginines (Arg54, Arg61, Arg66, and Arg70) which is unique amongst LOV proteins as previously reported (Circolone, et al., 2012). In the wildtype dark structure each arginine interacts with the PO_4^{2-}group of FMN. (B) In the dark state crystal structure of PpSB1-LOV-R61H/R66I four chains were found in the asymmetric unit. For the sake of completeness, the residues of each chain are pictured by different color coding. The exchange of two arginines (R61H, R66I) results in a loss of interactions between protein and chromophore.

3.1.7. Recovery kinetics of PpSB1-LOV and its mutants

The formation of the photoadduct in LOV proteins can be observed in the absorption spectra by the loss of absorption maxima at 449 nm and 485 nm which is typical for the dark state and an increasing absorption at 390 nm only present in the light state. In order to prove that LOV proteins not only undergo the photocycle in solution but also in crystals, spectra of solution and crystals of PpSB1-LOV and the respective mutants PpSB1-LOV-R66I and PpSB1-LOV-R61H/R66I were measured and are depicted in figure 19. For the spectra of PpSB1-LOV (figure 19B), PpSB1-LOV-R66I (figure 19D) and PpSB1-LOV-R61H/R66I (figure 19F) in solution clearly the above described differences between dark and light state can be observed. In comparison, for the respective crystal spectra of PpSB1-LOV (figure 19A) and

PpSB1-LOV-R61H/R66I (figure 19E) the differences between light and dark state appear not as obvious. Only PpSB1-LOV-R66I exhibits similar spectra profiles inside the crystal and in solution for light and dark state (figure 19C). However, the results clearly show that the described LOV proteins can undergo the photocycle inside the crystal.

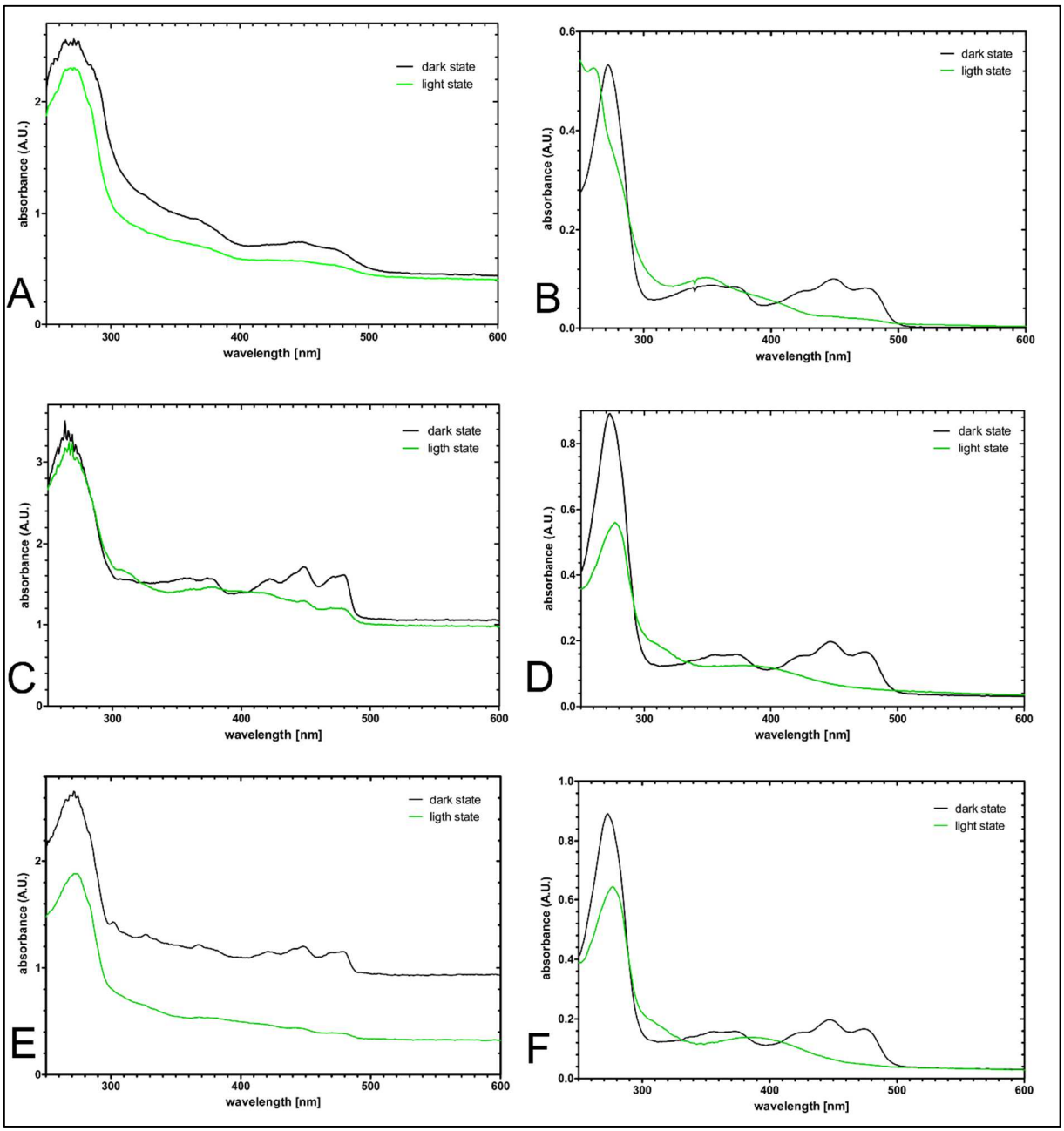

Figure 19: Absorption spectra of PpSB1-LOV and mutants. For each protein spectra in dark (black lines) and light state (green lights) were recorded inside a crystal (left) and in solution (right). (A)+(B) PpSB1-LOV, (C)+(D) PpSB1-LOV-R66I, (E)+(F) PpSB1-LOV-R61H/R66I

3.1.8. Small angle X-ray scattering of the short LOV protein PpSB1-LOV and its mutants in solution

3.1.8.1. SAXS analysis of PpSB1-LOV and its mutants in dark state

Although the crystal structures that were determined in this work provided a lot of information about the reaction of PpSB1-LOV to blue light, it is equally important to look at the behavior of the proteins in solution without any restrains of a crystal lattice in dark state and light state. For this, small angle X-ray scattering (SAXS) was used.

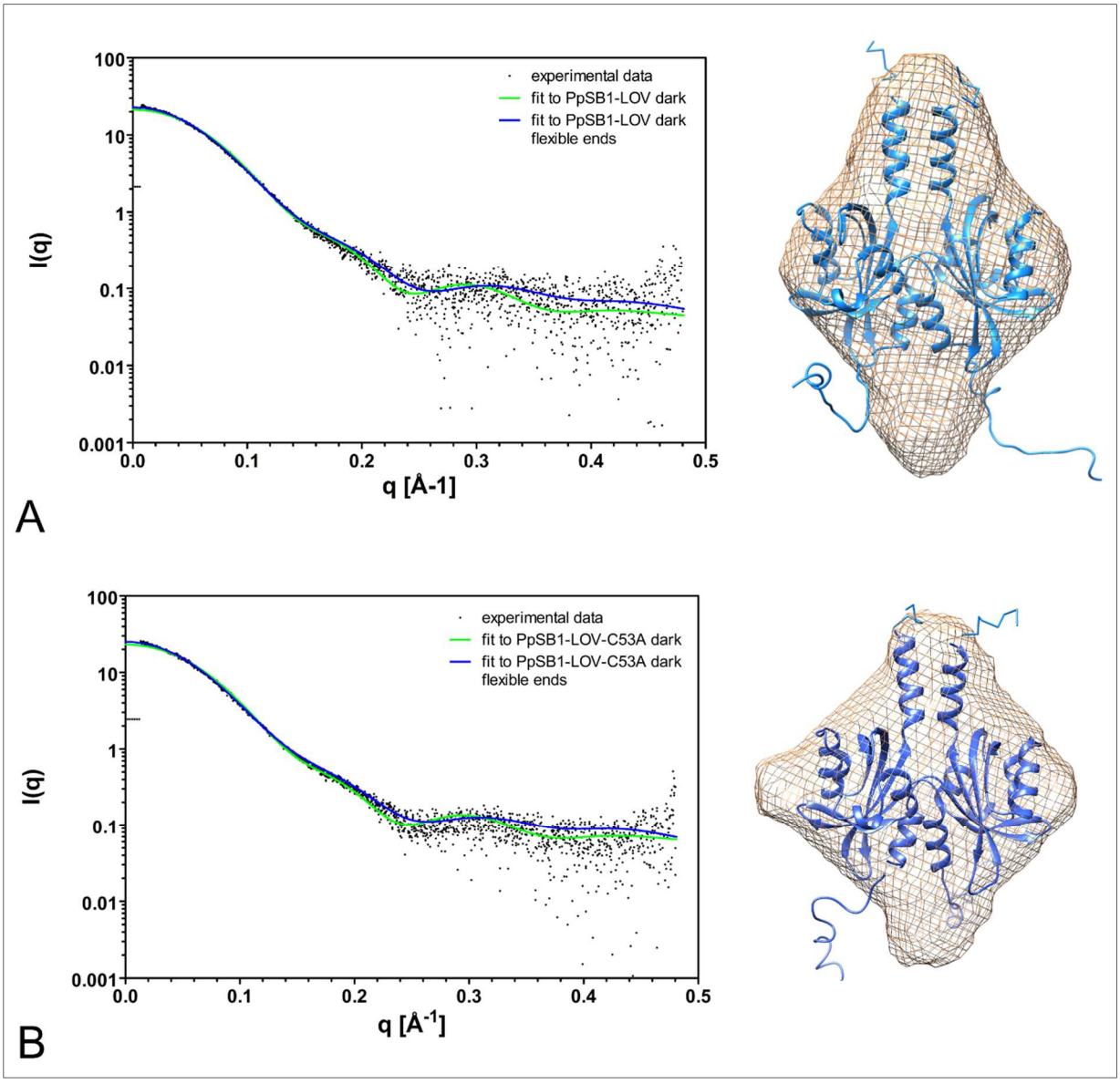

Figure 20: Small angle X-ray scattering of dark state PpSB1-LOV (A), PpSB1-LOV-C53A (B). The calculated curves of the respective dark state crystal structures (green) are fitted to the experimental SAXS data (black dots). In the crystal structure a decent number of C- and N-terminal amino acid residues are missing as no electron density was observed. These amino acids still contribute to the solution scattering data and therefore dummy atoms were modeled N- and C-terminally to the crystal structure using the program CORAL (Petoukhov, et al., 2012). Subsequently, calculated curves of the crystal structures with the introduced flexible ends (blue) were equally fitted to the experimental data. Additionally, the *ab initio* models (orange shown in mesh) of each structure are aligned with the crystal structures including the flexible ends (blue ribbon representation).

Biological macromolecules of variable molecular weight in a range from 5 kDa to 100 MDa can be investigated and information on the size and shape of the molecule can be collected. SAXS is an alternative to determine structural aspects of LOV proteins independently from the crystal structure. Results obtained from the protein in solution can complement the already obtained crystal structures explained above. The sample was illuminated inside the sample holder which was the fastest way to start with the measurement directly after illumination. The data are shown in figure 20 and 21, each scattering curve is fitted with a calculated scattering curve based on the crystal structure without and with flexible ends generated by the program CORAL (Petoukhov, et al., 2012). The oligomerization state of PpSB1-LOV, PpSB1-LOV-C53A and PpSB1-LOV-R61H/R66I has already been determined as dimer with SEC and was observed in the crystal structures. Hence, the ribbon representations of the LOV proteins are kept in dimer organization. The flexible ends account for the missing N- and C-terminal atoms of the heterologous expressed protein which cannot be modelled in the structure due to missing electron density. During data fitting with CORAL the positions of the flexible ends were allowed to vary until a structure was found, which best describes the measured SAXS curves.

A typical scattering curve is shown in figure 20A for PpSB1-LOV in dark state with a plot of the intensity I(q) against the scattering angle q [$Å^{-1}$]. Smaller q-values are more sensitive to molecular mass and global shape of the protein; the region of bigger q-values are more sensitive to the tertiary structure of a protein. Especially the region of lower q-values is sensitive to aggregation which is often caused by radiation damage and can be diminished by measuring different concentrations and subsequent merging of the obtained scattering curves as explained in detail in section 2.6.3. A general rule is the higher the concentration, the higher a possible aggregation in low q-range and the lower the signal-to-noise ratio in the higher q-range. In principle, besides the *ab initio* models and structural information, SAXS provides information about the molecular weight and oligomerization state of proteins. In the above described plot, I(0) is proportional to the molecular weight of the molecule in solution assumed that the concentration is well known. The oligomerization state can thus be calculated. In addition, a calculated scattering curve for the crystal structures are fitted to the experimental data. The quality of these fits was judged statistically by the χ-values which represent the discrepancy between experimental data and calculated curve calculated with the following formula.

$$x^2 = \frac{1}{N}\sum_q \left(\frac{I(q)_{experimental} - I(q)_{theoretical}}{\sigma}\right)^2$$

$$x = \sqrt{\frac{1}{N}\sum_{q}\left(\frac{I(q)_{experimental} - I(q)_{theoretical}}{\sigma}\right)^2}$$

N = number of experimental data points
q = scattering vector $Å^{-1}$
σ = error
I(q) = Intensity

Figure 20B shows the calculated scattering curve for the crystal structure of PpSB1-LOV-C53A fitted to the experimental scattering data in combination with the *ab initio* model. The χ-value of 1.11 improves when the calculated curve of the crystal structure plus flexible ends is fitted to the experimental data to 0.84.

A fourth protein is introduced in this section: PpSB1-LOV-R66I. In addition to PpSB1-LOVR61H/R66I this mutant exhibited interesting recovery kinetics. Solely the substitution of the Arg66 to an isoleucine decelerated the dark recovery by a factor of 100 to τ_{REC} = 23 ± 1 min. Effort was equally put into the crystallization and measurements to collect appropriate X-ray diffraction data. Unfortunately, it was not possible to collect X-ray diffraction data to determine the structure. Although crystals of PpSB1-LOV-R66I were observed in different conditions, the crystals did not diffract to an appropriate resolution. Nevertheless, PpSB1-LOV-R66I showed a decent behavior during SAXS measurement which is described in this section and the following (3.1.8.2). The calculated scattering curve of the wildtype PpSB1-LOV crystal structure was fitted to the scattering data of PpSB1-LOV-R66I (figure 21A). For the double mutant PpSB1-LOV-R61H/R66I the calculated scattering curve of the crystal structure determined in this thesis was fitted to the scattering data (figure 21B).

Overall, the theoretical curves of the crystal structures without flexible ends gave poor fits for every single protein, see figure 20 and 21 but increased significantly when the flexible ends were included. The quality of the fits was judged statistically by the χ-values which represent the discrepancy between experimental data and calculated curve, see table 19. The lower the χ-value, the better is the fit.

Table 19: Discrepancy between experimental data and calculated curve of the crystal structures of PpSB1-LOV and its mutants represented as χ-values determined by CRYSOL (Svergun, et al., 1995). In case of PpSB1-LOV-R66I the wildtype structure was used for the fit. The χ-value represents the discrepancy between experimental data and calculated curve with low χ-values (around χ = 1) represents a good fit.

Protein	χ-value (fit with respective crystal structure)	χ-value (fit with respective crystal structure plus the flexible ends)
PpSB1-LOV	1.19	0.84
PpSB1-LOV-C53A	1.11	0.84
PpSB1-LOV-R66I	3.14	1.33
PpSB1-LOV-R61H/R66I	2.93	0.82

Inclusion of the flexible ends resulted in clearly smaller χ-values between 0.82 and 0.84. Only PpSB1-LOV-R66I still remains with a higher χ-value of 1.33 which can be expected as the SAXS data are fitted to the structure of PpSB1-LOV and the error bars of the SAXS curve are smaller than in other curves, which increased the χ. The discrepancies are due to the different beamlines used for data collection. PpSB1-LOV-R66I was recorded at ESRF (Grenoble, France) and every other scattering data was measured at DESY (Hamburg, Germany).

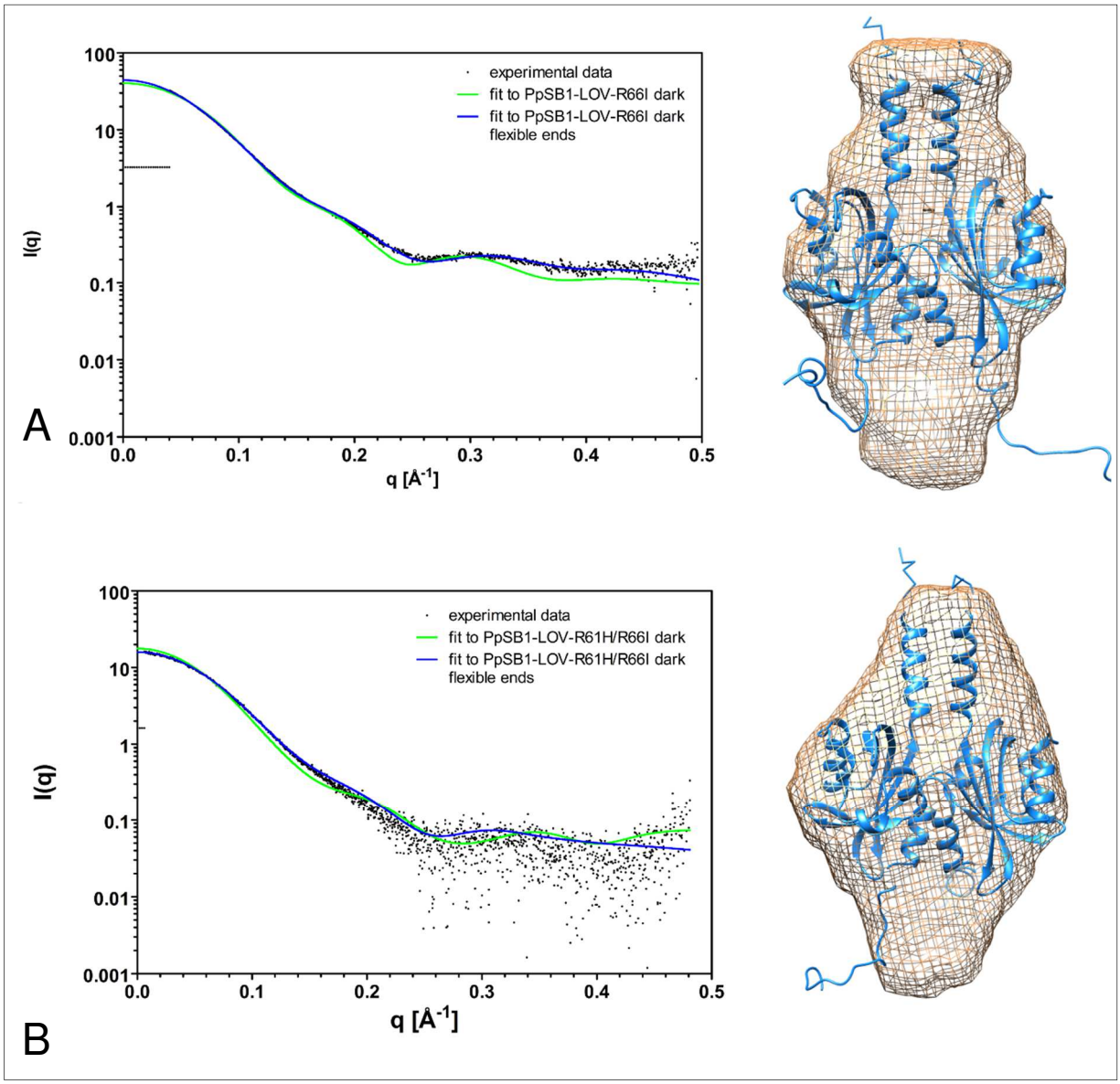

Figure 21: Small angle X-ray scattering of dark state PpSB1-LOV-R66I (A), PpSB1-LOV-R61H/R66I (B). The calculated curves of the respective dark state crystal structures (green) are fitted to the experimental SAXS data (black dots). In the crystal structure a decent number of C- and N-terminal amino acid residues are missing as no electron density was observed. These amino acids still contribute to the solution scattering data and therefore dummy atoms were modeled C- and N-terminally to the crystal structure using the program CORAL (Petoukhov, et al., 2012). Subsequently, calculated curves of the crystal structures with the introduced flexible ends (blue) were equally fitted to the experimental data. Additionally, the *ab initio* models (orange shown in mesh) of each structure are aligned with the crystal structures including the flexible ends (blue ribbon representation).

Independent from the above reported modelling, other values can be estimated from the results obtained. Especially, the values for the radius of gyration estimated from the Guinier plot using the program PRIMUS (Konarev, et al., 2003) and determined from the theoretical scattering curve calculated with the program CRYSOL (Svergun, et al., 1995) provides evidence for a qualitative fit between crystal structure and experimental values. In table 20, these values are listed for the proteins PpSB1-LOV, PpSB1-LOV-C53A, PpSB1-LOV-R66I, and PpSB1-LOV-R61H/R66I.

The maximum inter-atomic distances (D_{max}) of all structures are close to each other accounting for high similarity in the overall shape of the proteins in the dark state. The Rg values (electron density-weighted average radius of the molecules) of the structures taking the flexible ends into account are clearly more in agreement with those determined from the experimental scattering curve. This observation provides further evidence for the better agreement between the SAXS data and the crystal structures improved with dummy atoms independent from the model building.

Table 20: Structural parameters of the SAXS measurements for PpSB1-LOV and its mutants. D_{max} is the maximum inter-atomic distance of the model, the molecular mass can be determined from the I_0 in the Guinier plot. The radius of gyration is the electron density-weighted average radius of the molecule, determined from the solution experimental data and from the calculated scattering curve from the crystal structure without and with flexible ends.

Protein	D_{max}	R_g (determined from the experimental data)	R_g (calculated from the crystal structure)	R_g (calculated from crystal structure with flexible ends)
PpSB1-LOV	8.93	25.52	22.79	24.88
PpSB1-LOV-C53A	8.99	25.70	22.45	24.68
PpSB1-LOV-R66I	8.79	25.65	22.86	24.42
PpSB1-LOV-R61H/R66I	8.59	24.56	22.15	24.80

3.1.8.2.Differences between dark and light states of PpSB1-LOV-R66I in solution

SAXS data might provide additional insights into differences upon excitation of LOV proteins and primary structural events. Based on the resolution limit of the experiment itself especially large conformational changes are suspected to be observed.

For this reason, samples of PpSB1-LOV, PpSB1-LOV-R66I and PpSB1-LOV-R61H/R66I were measured under continuous red light conditions to account for the dark state and after illumination with blue light. Unfortunately, the excitation appeared to be the bottle neck of the experimental setting as the time delay between illumination and X-ray exposure was in the order of several minutes. Although the light samples of each protein were treated identically, differences in the light and dark state scattering was only observed for the mutant PpSB1-LOV-R66I at scattering vector range of q = 0.1 – 0.2 $Å^{-1}$ (figure 22). Smaller q-values are more sensitive to molecular mass and global shape of the protein; the region of bigger

q-values are more sensitive to the tertiary structure of a protein which indicates a difference in the tertiary structure of the LOV protein after illumination.

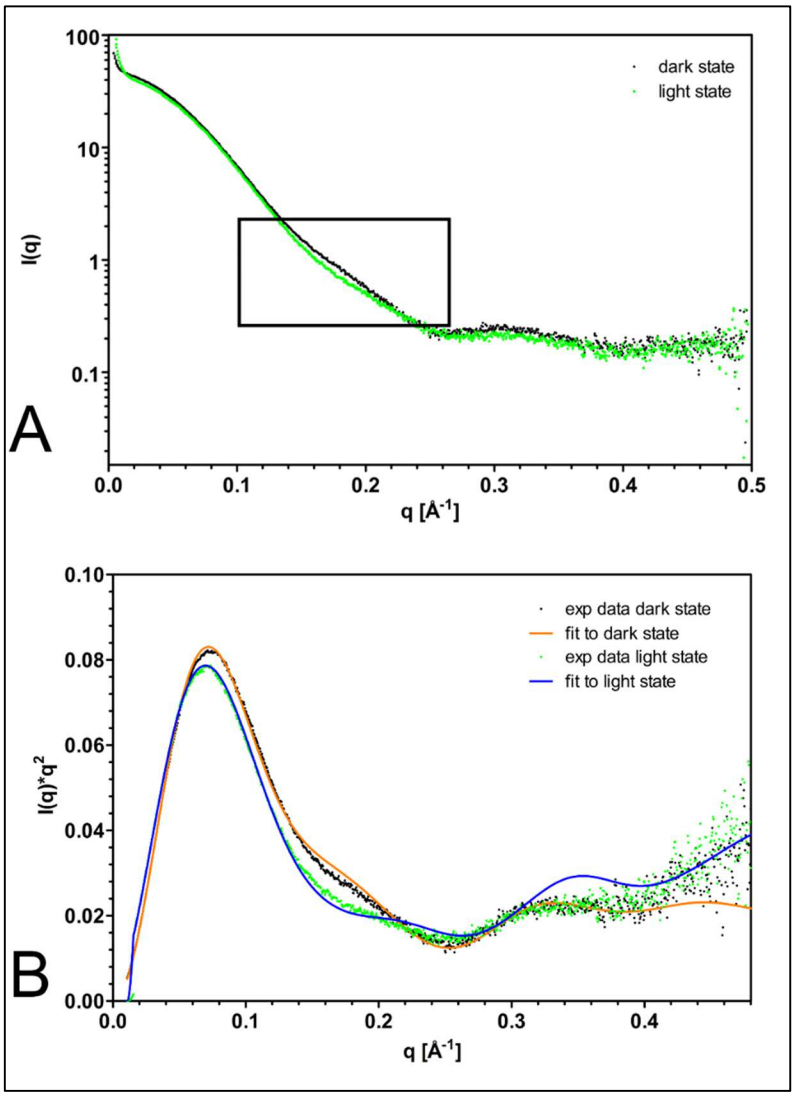

Figure 22: Small angle X-ray scattering data of PpSB1-LOV-R66I in dark (black) and light state (green line). (A) The black box indicates the light-induced difference in both scattering curves. The upturn at smallest q-values is related to the amount of aggregated protein. (B) the same scattering data are shown in a Kratky plot.

As already explained in section 3.1.8.1 the theoretical scattering curves of the crystal structure of PpSB1-LOV in dark state with and without flexible ends were calculated and fitted to the original scattering data of the mutant. These fits are depicted in figure 23A in combination with the envelope of PpSB1-LOV-R66I (orange mesh) determined by *ab initio* modelling using the program DAMMIN (Svergun, 1999) aligned with the dark state crystal structures of PpSB1-LOV in ribbon representation. The fit with the original crystal structure is poor with a χ-value of 3.14 which is highly improved by fitting the data with the flexible ends crystal structure resulting in an improved fit with a χ-value of 1.33 (table 21).

The same analysis was conducted for the light state SAXS data in combination with the light state crystal structure of PpSB1-LOV. In agreement with the dark state data an improvement of the X-value from 6.43 to 1.83 was observed (table 21). The calculated curve of the crystal structure and the SAXS data fits are shown in figure 23B. The envelope of PpSB1-LOV-R66I in light state was determined by ab initio modelling using the program DAMMIN (Svergun, 1999) and is shown in mesh in combination with the light state crystal structure of PpSB1-LOV in ribbon representation (blue, figure 23 B). The Rg-values for PpSB1-LOV-R66I is 25.65 in dark state and 25.58 in light state.

Table 21: χ-value of CRYSOL fits of measured SAXS data with the respective crystal structure of PpSB1-LOV-R66I. As the crystal structure for PpSB1-LOV-R66I is not available, the fit was conducted with the dark and light state crystal structures of PpSB1-LOV.

Protein	**χ-value (fit with respective crystal structure)**	**χ-value (fit with respective crystal structure plus the flexible ends**
PpSB1-LOV-R66I dark	3.14	1.33
PpSB1-LOV-R66I light	6.43	1.84

In both envelopes of light and dark state the dimer of PpSB1-LOV does fit really well. Nevertheless, the non-filled parts are most likely occupied by the missing residues in the crystal which can be observed in figure 23A and 23B.

A comparison of the light and dark state envelope reveals a slight difference in shape. The light state *ab initio* model appears more tight and compact then the dark state envelope, especially in regard to the region occupied by the C-terminal Jα helix. The modelled flexible ends in the crystal structures of PpSB1-LOV, PpSB1-LOV-C53A and PpSB1-LOV-R61H/R66I in dark state show no common preference in orientation and are most likely disordered (figure 23C). But in the case of the light state data the modelled dummy atoms appear as a prolongation of the C-terminal helical element which explains the narrower appearance of the upper part of the *ab initio* model (figure 23D).

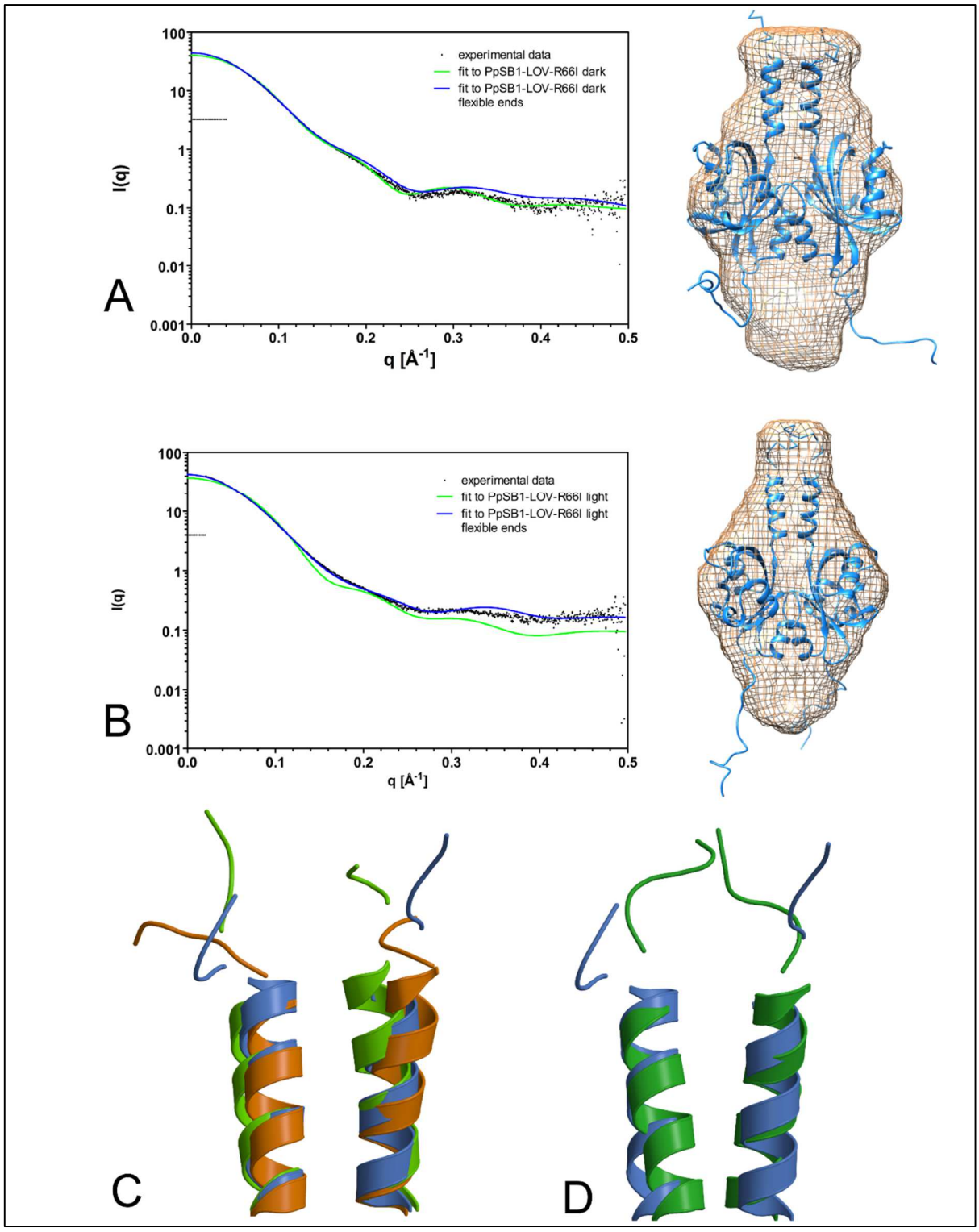

Figure 23: Differences between dark and light state of PpSB1-LOV-R66I. (A) The experimental data of PpSB1-LOV-R66I in dark state (filled dots) are shown in combination with the calculated curve of the crystal structure of PpSB1-LOV (green line) and with the calculated curve of the crystal structure of PpSB1-LOV with flexible ends (blue line) and the *ab initio* models (blue in ribbon representation, shown in orange mesh) of each structure are aligned with the crystal structure of PpSB1-LOV dark state including the flexible ends. The same results are shown in (B) for the light state structure. (C) The C-terminal Jα-helix of PpSB1-LOV (blue), PpSB1-LOV-C53A (orange), and PpSB1-LOV-R61H/R66I (green) including the modelled flexible ends in dark state. The flexible ends account for the amino acid residues in the crystal structure without electron density. The Jα-helices of all the PpSB1-LOV-C53A (rmsd = 1.14) and PpSB1-LOV-R61H/R66I (rmsd = 0.68) structures are nearly identical when superposed on the crystal structure of PpSB1-LOV, but the dummy atoms appear highly flexible and do not exhibit a secondary structure like element. (D) The C-terminal Jα-helix of PpSB1-LOV in dark state (blue) and light state (green) including the flexible ends.

In order to gain further information of structural changes during the photocycle based on the observed differences in the static measurements, time resolved kinetic measurements were performed. The sample was illuminated in the beginning and subsequently scattering curves were recorded in defined time steps of 3 and 6 min respectively for 63 minutes (figure 24). The dark recovery of LOV proteins can be described by an exponential decay function. The period of time was thus chosen based on the following formula using the time constant PpSB1-LOV-R66I τ_{REC} = 23 min.

$$y(t) = e^{-\frac{t}{\tau}}$$

t = time
τ = time constant

Applied in the equation it turns out, that after 63 min only 6-7 % of the protein population still remains in the light state. This was chosen as an appropriate value to distinguish possible differences between light and dark state data. For each time step of the kinetic measurements a specific amount of protein was taken out of the same batch of protein in order to compare the data with each other. As observed for the static measurements a difference was expected at a scattering angle of q = 0.1 – 0.2 $Å^{-1}$.

As shown in figure 24A, in this region the signal to noise ratio was poor in comparison to the static measurements (compare figure 22A). As a consequence, differences in the intensities evoked by large conformational changes of the protein are not found. Further analysis of the kinetic data is represented in figure 24B and C. The change of the scattering intensity at q = 0.18 $Å^{-1}$ as a function of time in combination with the values for the static dark and light state intensities are shown in figure 24B. Usually, one would expect a curve progression beginning in the range of the static light state towards the statistic dark state data points, but no clear trend in the experimental data is observed. The same result is found for the plot of the time-dependent change of the radius of gyration which is expected as the static Rg of PpSB1-LOV-R66I in dark and light state did not reveal significant differences (dark state: 25.65, light state: 25.58) (figure 24C).

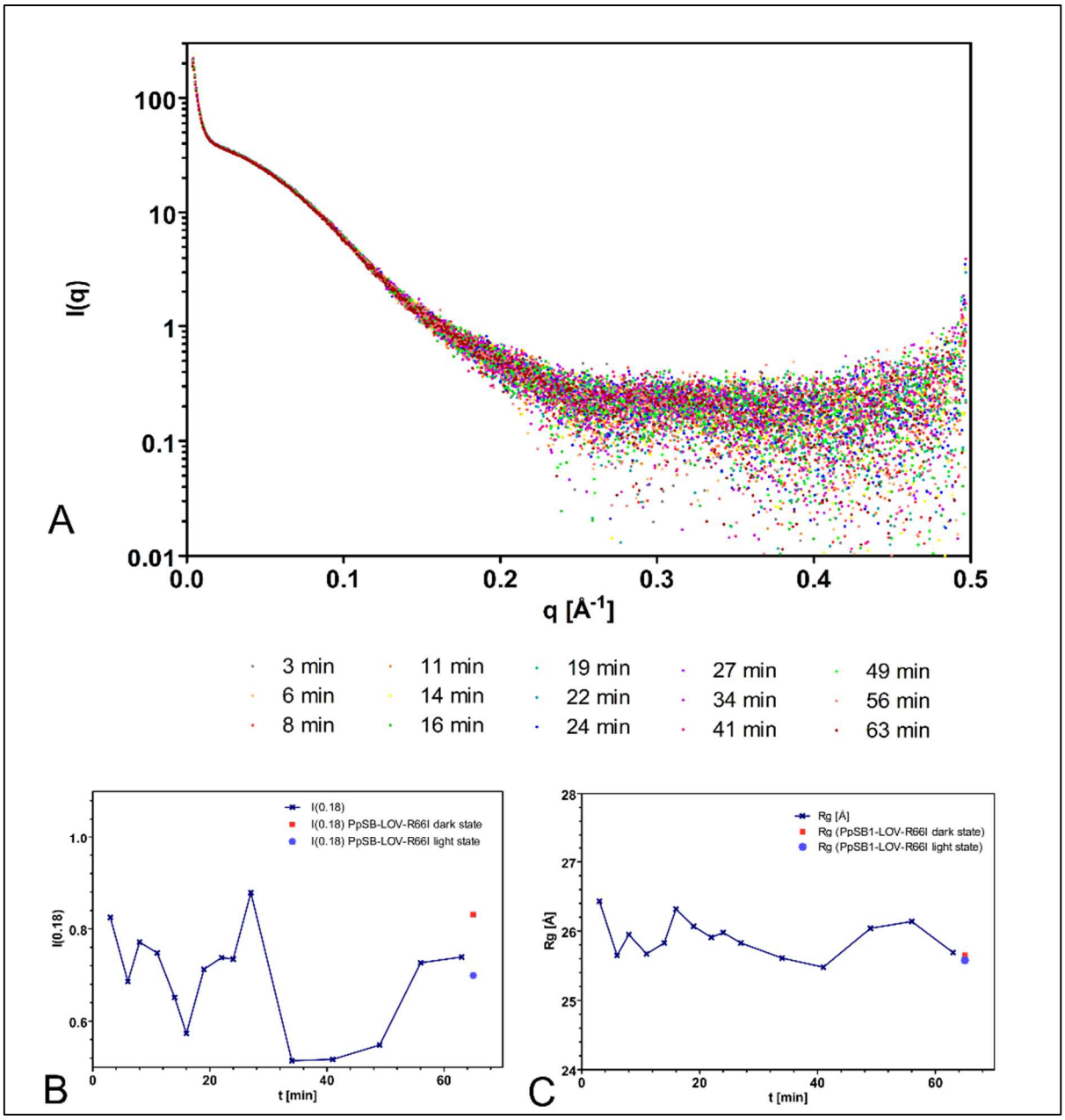

Figure 24: Kinetic SAXS measurements of PpSB1-LOV-R66I. (A) Scattering curves at different time points during dark recovery of PpSB1-LOV-R66I; (B) Time-dependent changes of the scattering intensity at q = 0.18 Å^{-1}, where the differences in the static measurements between dark and light state were observed, the intensities of the static dark and light state measurements are highlighted in pink and blue respectively; (C) Time-dependent changes of the radius of gyration during the dark recovery, the intensities of the static dark and light state measurements are highlighted in pink and blue respectively.

3.2. DsLOV

In addition to the structural studies on PpSB1-LOV, a second short-LOV protein DsLOV from the marine bacteria *Dinoroseobacter shibae* was focus of this thesis. Recently, the crystal structure of DsLOV was determined (Endres, et al., 2015). This protein shows an unusually fast dark recovery of τ_{REC} = 9.6 s and is involved in the synthesis of photopigment. The dark state crystal structure reveals the typical α/β-PAS fold and shows a N-cap derived dimerization. DsLOV might be an interesting candidate in the design of optogenetic tools based on its unique photophysical, structural, and regulatory properties.

3.2.1. Structure determination of DsLOV M49 mutant proteins with X-ray crystallography

Initial characterization of DsLOV was part of Stephan Endres PhD thesis in which he also characterized the two mutants, DsLOV-M49S and DsLOV-M49I (Endres, 2013). The rationale for design of these mutants is described in section 1.3 in the Introduction (page 12-13). The interesting result was the change in dark recovery time for the mutants compared to the wildtype protein. As shown in table 1 the dark recovery of the isoleucine mutant is decelerated by a factor of about 16. On the contrary, the serine mutant accelerated the recovery time by a factor of about 9. Crystal structure of DsLOV (Endres, et al., 2015) revealed two different rotamer orientations of the methionine at position 49, an indication of structural flexibility in the dark. The authors proposed that Met49 can flip into a different conformation as soon as the cysteine is released from the covalent interaction with the FMN to ease this particular movement.

The DsLOV-M49S mutant was heterologously expressed using *E. coli* BL21(DE3) with a C-terminal His_6 tag provided by the expression vector pRhotHi-2. After purification, the fractions containing the pure protein were concentrated to 30 mg/mL. Several crystallization screening conditions were prepared as explained in section 2.5.1 and the optimal composition for crystallization was determined. After two weeks of incubation at 20 °C in dark, monoclinic crystals grew in 0.1 M Tris-HCl, pH 8 and 30% PEG 6000, diffracting to a resolution of 1.7 Å with one chain per asymmetric unit. The collected data were processed as explained in the material and method section 2.5.3. Details on data acquisition and refinement statistics can be found in table 22.

The final structure comprised residues 20-139, where residues 1-19 and 140-146 (of the His_6 tag) could not be traced in the electron density, which might be due to a higher flexibility in these regions. Residues 36-139 revealed the typical α/β-PAS fold as observed in several other different LOV-proteins (Talyor, et al., 1999; Conrad, et al., 2013; Endres, et al., 2015).

Table 22: Data collection and refinement statistics for DsLOV-M49S.

X-ray data	**DsLOV-M49S dark state**
Beamline	ID14-4, ESRF (Grenoble, France)
Detector	ADSC Quantum Q135r
Wavelength [Å]	λ=0.98
Resolution range [Å]	45.19 – 1.96 (2.03 – 1.96)[x1]
Space group	C 1 2 1
Unit cell a, b, c [Å]; β(°)	89.88, 30.98, 49.48; 112.9°
Total reflections	37285 (1035)
Unique reflections	12222 (1187) [x1]
Multiplicity	1.7 [x1]
Completeness [%]	94.88 (93.69) [x1]
Mean I/sigma(I)	6.9 [x1]
Wilson B-factor [Å^2]	15.15
R_{merge}	0.12 (0.19) [x1]
R_{meas}	0.13 (0.26) [x1]
Refinement	
Resolution range [Å]	0.18 (0.22)[x1]
R_{work}	0.18 (0.22) [x1]
R_{free}	0.22 (0.28) [x1]
Coordinate error (max.-likelihood based)	0.19
Number of non-hydrogen atoms	1045
Macromolecules	947
Ligands	31
Water	67
Protein residues	120
RMS (bonds)	0.006
RMS (angles)	1.15
Ramachandran favored [%]	99
Ramachandran outliers [%]	0
Clashscore	6.2
Average B-factor [Å^2]	18.40
Macromolecules [Å^2]	18.30
Ligands [Å^2]	13.60
Solvent [Å^2]	22.10

[x1] Statistics for the highest-resolution shell are shown in parentheses

As described by Talyor, et al., 1999 five antiparallel β-strands Aβ (residues 36-40), Bβ (residues 49-52), Gβ (residues 98-105), Hβ (residues 111-122), and Iβ residues (residues 128-132) are flanked by four α-helices designated Cα (residues 24-27), Dα (64-67), Eα (residues 72-75), and Fα (residues 82-94). A non-canonical structural element is found at the N-terminus of the LOV domain built of a N-terminal turn motif (residues 20-23), a helix denoted as A'α (residues 24-27), and a loop (residues 28-36) linking the N-terminal cap region to the LOV core domain (figure 25A). Inside the LOV core the FMN chromophore is non-covalently bound to the protein. Several hydrogen bonds are formed between residues in several secondary structure elements of the core domain and the FMN (table 23).

A distance of 4.72 Å is observed between the Sγ atom of the photoactive Cys72 the C4a atom of FMN indicating a non-bonding distance between these two atoms characterizing the dark state of the protein. In figure 25B, the localization of the mutation of amino acid M49S is shown along with the FMN and the photoactive Cys72. Inside the core domain of the wildtype crystal structure a riboflavin molecule was found while the crystal structure of DsLOV-M49S exhibited an FMN molecule.

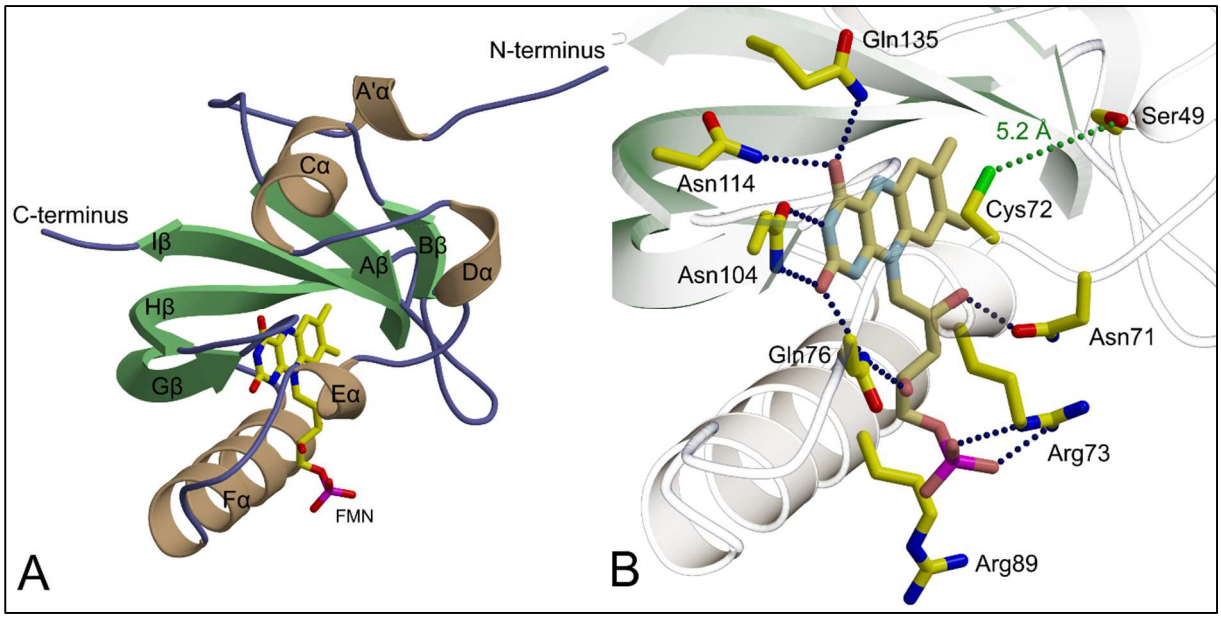

Figure 25: Dark state crystal structure and active site of DsLOV-M49S. (A) In this ribbon representation α-helices are highlighted in yellow, loops are highlighted in purple, and β-strands in green. The secondary structure elements are labelled in agreement with the previously described dark state structure of DsLOV (Endres, et al., 2015). (B) Amino acid side chains and FMN are represented in stick model and standard color code. Hydrogen bonds are represented in dark blue, dotted lines. The distance between Ser49-Oγ and Cys72-Sγ is shown in green, dotted line. The mutated position 49 can be found close to the FMN, pointing away from the Cys72 and the chromophore. For a better discrimination between chromophore and protein the FMN is kept in pale colors.

Endres at al. reported HPLC experiments that show DsLOV binds predominantly FMN (74.3 ± 0.2 %) over FAD (25.7 ± 0.2 %) whereas no riboflavin could be detected. The difference between riboflavin and FMN is the phosphate group and the authors ascribed its absence to hydrolysis of FMN in acidic conditions during the crystallization process. An effect of the RBF on the photocycle was not reported. This is most likely ascribed to the absence of RBF in aqueous protein solution which is required for the photokinetic measurement.

Table 23: Hydrogen bond interactions contributing to the chromophore coordination of DsLOV-M49S. The analysis was conducted with CONTACT from the CCP4 package (Collaborative Computational Project, 2011) with a cutoff of 3.35 Å.

Secondary structure element	Residue	Atom	Distance [Å]	FMN-Atom
Dα-Eα loop	Asn71	OD1	2.74	O2’
Eα	Arg73	NE	3.03	O3P
Eα	Arg73	NH2	3.00	O2P
Eα- Fα loop	Gln76	NE2	2.81	O4’
Eα- Fα loop	Gln76	NE2	3.06	O2
Gβ	Asn104	OD1	2.80	N3
Gβ	Asn104	ND2	2.98	O2
Hβ	Asn114	ND2	3.05	O4
Iβ	Gln135	NE2	3.03	O4

The previously described conserved arginines in DsLOV are Arg73 and Arg89. Arg73 forms hydrogen bonds with the ribityl chain in the dark state (Arg73-NH2…O5’-RBF), yet for Arg89 any interactions with the chromophore are absent which was described to the loss of the

phosphate disturbing the usual interaction. In DsLOV-M49S although FMN is present both the arginine residues adapt the same side chain orientation as found in the wildtype.

For the second mutant DsLOV-M49I the crystal structure was determined with a resolution of 1.8 Å with two chains per asymmetric unit (figure 26A). The crystal grew after approximately one year of incubation at 20 °C in dark. Unlike in case of DsLOV and DsLOV-M49S, tetragonal crystals grew in 0.1 M Na-acetate pH 5, 0.1 M Ammonium sulfate, 0.3 M Sodium formate, 3 % PGA-LM, and 5 % (w/v) PEG 8000. The data processing and structure refinement was conducted in accordance to DsLOV-M49S and details on data collection and refinement statistics can be found in table 24.

Table 24: Data collection and refinement statistics for DsLOV-M49I.

X-ray data	**DsLOV-M49I**
Beamline	ID-29, ESRF (Grenoble, France)
Detector	DECTRIS PILATUS 6M-F
Wavelength [Å]	λ = 0.97
Monochromator	Silicon (1 1 1) channel-out
Resolution range [Å]	45.89 – 1.86 (1.90 – 1.86)[x1]
Space group	$P4_1\,2_1\,2$
Unit cell a = b, c [Å]	56.67, 156.4
Total reflections	204668 (12467)
Unique reflections	22330 (1358) [x1]
Multiplicity	9.2 (9.2) [x1]
Completeness [%]	99.9 (100.0) [x1]
0Mean I/sigma(I)	23.2 (2.2) [x1]
Wilson B-factor [Å^2]	26.3
R_{merge}	0.06 (0.93) [x1]
R_{meas}	0.07 (0.99) [x1]
Refinement	
Resolution range [Å]	45.89 – 1.86 (1.926 – 1.86) [x1]
R_{work}	0.17 (0.24) [x1]
R_{free}	0.21 (0.26) [x1]
Coordinate error (max.-likelihood based)	0.16
Number of non-hydrogen atoms	1990
Macromolecules	1777
Ligands	75
Water	138
Protein residues	218
RMS (bonds)	0.007
RMS (angles)	1.02
Ramachandran favored [%]	98
Ramachandran outliers [%]	0
Clashscore	1.37
Average B-factor [Å^2]	35.5
Macromolecules [Å^2]	35.2
Ligands [Å^2]	33.9
Solvent [Å^2]	40.3

[x1] Statistics for the highest-resolution shell are shown in parentheses

Inside the core region FMN was found as a non-covalently bound chromophore typical for the dark state of LOV proteins. Several residues in the core region coordinate the FMN via hydrogen bonds with the isoalloxazine ring and the ribityl chain, hydrophobic interactions mainly with the isoalloxazine ring and salt bridges with the phosphate (table 25).

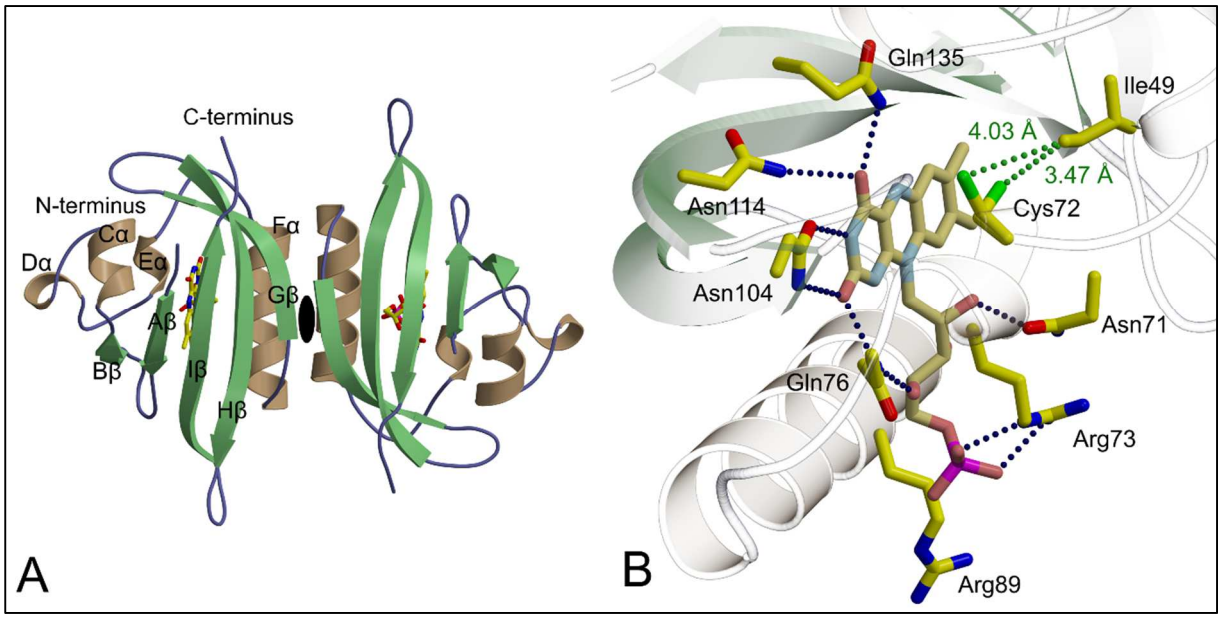

Figure 26: Dark state crystal structure and active site of DsLOV-M49I. (A) In this ribbon representation α-helices are highlighted in yellow, loops are highlighted in purple, and β-strands in green. The secondary structure elements are labelled in agreement with the previously described dark state structure of DsLOV (Endres, et al., 2015). The ellipse represents the two-fold axis. (B) Amino acid side chains and FMN are represented in stick model. Carbon atoms are represented in yellow, oxygen atoms in red, nitrogen atoms in blue and phosphate in pink. The mutated position 49 can be found close to the FMN, facing towards the Cys72 and the chromophore. In this mutant the Cys72 was found in two different orientations. One of these is similar to the wildtype structure and the other conformation is similar to that found in DsLOV-M49S.

The photoactive Cys72 in DsLOV-M49I exhibits two different rotamer conformations with distances of 3.73 Å and 4.51 Å between the Sγ and the FMN-C4a atom (figure 26B), whereas in the wildtype and the serine mutant only one of both are observed.

Table 25: Hydrogen bond interactions contributing to the chromophore coordination of DsLOV-M49I. The analysis was conducted with CONTACT from the CCP4 package (Collaborative Computational Project, 2011) with a cutoff of 3.35 Å.

Secondary structure element	Residue	Atom	Distance [Å]	FMN-Atom
Dα-Eα loop	Asn71	OD1	2.74	O2’
Eα	Arg73	NE	2.98	O2P
Eα	Arg73	NH2	2.99	O1P
Eα- Fα loop	Gln76	NE2	2.87	O4’
Eα- Fα loop	Gln76	NE2	2.96	O2
Gβ	Asn104	OD1	2.77	N3
Gβ	Asn104	ND2	3.00	O2
Hβ	Asn114	ND2	3.18	O4
Iβ	Gln135	NE2	2.98	O4

In the crystal a different dimer interface was observed than determined for the wildtype and DsLOV-M49S (compare figure 26A with figure 28). The formation of this dimer interface includes several hydrogen bond interactions listed in table 26. Additional hydrophobic interactions stabilizing the dimer are found on the secondary structure elements: Fα (His83, Ala94), the loop between Fα and Gβ (Thr96) and the strand Gβ (Phe98, Ile100). A detailed analysis of the dimer interface is described in section 3.2.3.

Table 26: Hydrogen bond interactions contributing to the dimer interface of DsLOV-M49I. The analysis was conducted with CONTACT from the CCP4 package (Collaborative Computational Project, 2011) with a cutoff of 3.35 Å.

Chain	Secondary structure element	Residue	Atom	Distance [Å]	Atom	Residue	Secondary structure element	Chain
A	Fα	His83	ND1	2.69	OE1	Gln90	Fα	B
A	Fα	Gln90	OE1	2.67	ND1	His83	Fα	B
A	Fα-Gβ-loop	Thr96	OG1	2.89	O	Asp101	Gβ	B
A	Fα-Gβ-loop	Arg97	O	3.07	N	Asp101	Gβ	B
A	Gβ	Thr99	N	2.83	O	Thr99	Gβ	B
A	Gβ	Thr99	O	2.81	N	Thr99	Gβ	B
A	Gβ	Asp101	N	3.13	O	Arg97	Fα-Gβ-loop	B
A	Gβ	Asp101	O	2.79	OG1	Thr96	Fα-Gβ-loop	B

3.2.2. Dark state crystal structure of DsLOV-C72A – active site mutant of DsLOV determined with X-ray crystallography

As reported for PpSB1-LOV in section 3.1.3, the exchange of the photoactive cysteine is a method to design decent fluorescence reporter proteins. Similar approach was conducted with DsLOV by substitution of the Cys72 into an alanine, designated DsFbFP. A deeper understanding on structural basis can provide further information in regard to design improved photosensor proteins.

The heterologous expression and purification was conducted as described for the Met49 mutants. The protein solution was set to a concentration of 20 mg/mL. Monoclinic crystals of the protein grew at 20 °C in dark with crystallization conditions of 0.1 M Tris base /HCl, pH 8.5, 0.2 M $MgCl_2$, 20 % PEG 8000 within six months.

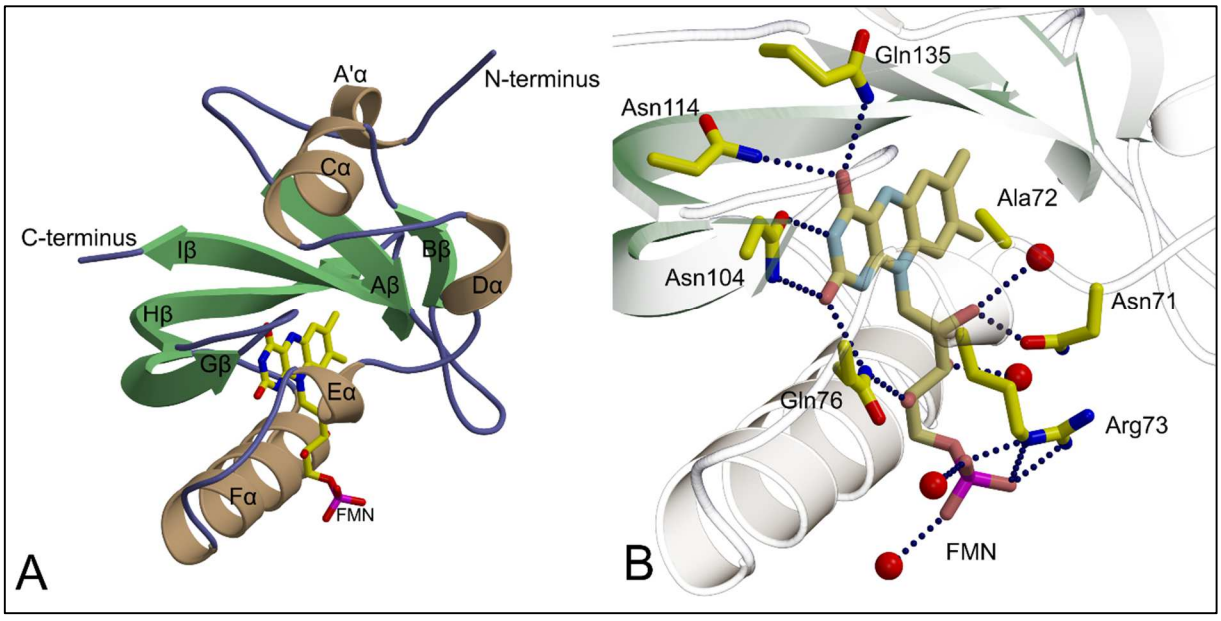

Figure 27: Dark state crystal structure and active site of DsLOV-C72A. In both panels the color code is in accordance with figure 24; (A) Ribbon representation of DsLOV-C72A. (B) Active site of DsLOV-C72A. The alanine does not interact with the FMN or surrounding residues.

The collected data were processed as described for DsLOV-M49S and details on data acquisition and refinement statistics can be found in table 27.

The final model comprises residues 21-138 (figure 27A). Secondary structure elements equivalent to DsLOV-M49S form the α/β-PAS fold consisting of five β-strands forming an antiparallel β-sheet with Aβ (residues 36-40), Bβ (residues 49-52), Gβ (residues 98-105), Hβ (residues 111-122), and Iβ residues (residues 128-132) flanked by four α-helices named Cα (residues 24-27), Dα (64-67), Eα (residues 72-75), and Fα (residues 82-94). A fifth α-helix A'α is part of the turn-helix-turn motif which was previously described by Endres et al., 2015.

Table 27: Data collection and refinement statistics for DsLOV-C72A.

X-ray data	**DsLOV-C72A**
Beamline	ID29, ESRF (Grenoble, France)
Detector	DECTRIS PILATUS 6M-F
Wavelength [Å]	λ = 0.97
Monochromator	Silicon (1 1 1) channel-cut
Resolution range [Å]	40.42 – 1.8 (1.84 – 1.8)[x1]
Space group	C 1 2 1
Unit cell a, b, c [Å],	91.48 28.22 48.03
α=γ=90°	119.40
Total reflections	65759
Unique reflections	10149 (598) [x1]
Multiplicity	6.2
Completeness [%]	99.8 (99.3) [x1]
Mean I/sigma(I)	11.1 (1.8) [x1]
Wilson B-factor [Å^2]	22.6
R_{merge}	0.10 (0.97) [x1]
R_{meas}	0.10 (1.06) [x1]
Refinement	
Resolution range [Å]	39.85 – 1.8 (1.864 – 1.8) [x1]
R_{work}	0.16 (0.27) [x1]
R_{free}	0.20 (0.35) [x1]
Coordinate error (max.-likelihood based)	0.22
Number of non-hydrogen atoms	1003
Macromolecules	924
Ligands	31
Water	48
Protein residues	119
RMS (bonds)	0.006
RMS (angles)	1.03
Ramachandran favored [%]	97
Ramachandran outliers [%]	0
Clashscore	1.07
Average B-factor [Å^2]	29.0
Macromolecules [Å^2]	28.8
Ligands [Å^2]	29.6
Solvent [Å^2]	32.6

[x1] Statistics for the highest-resolution shell are shown in parentheses

A Cα-based superposition of the crystal structures of DsLOV-M49S and DsLOV-C72A resulted in an RMSD of 0.9368 Å indicating high similarity between both structures. Additionally, chromophore coordination is similar in both the structures. The FMN is non-covalently bound inside the core domain forming interactions with surrounding secondary

structure elements (table 28) (figure 27B). The Ala72 does not interact with the FMN or surrounding residues.

Table 28: Hydrogen bond interactions contributing to the chromophore coordination in DsLOV-C72A. The analysis was conducted with CONTACT from the CCP4 package (Collaborative Computational Project, 2011) with a cutoff of 3.35 Å.

Secondary structure element	Residue	Atom	Distance [Å]	FMN-Atom
Dα-Eα loop	Asn71	OD1	2.58	O2'
Eα	Arg73	NE	3.28	O2P
Eα	Arg73	NE	2.55	O3P
Eα	Arg73	NH2	2.66	O2P
Eα- Fα loop	Gln76	NE2	2.75	O4'
Eα- Fα loop	Gln76	NE2	3.01	O2
Gβ	Asn104	OD1	2.78	N3
Gβ	Asn104	ND2	3.09	O2
Hβ	Asn114	ND2	3.28	O4
Iβ	Gln135	NE2	3.14	O4

3.2.3. Possible dimer formation for DsLOV-mutants

The DsLOV wildtype protein shows a dimer formation mediated by residues in the N-cap and the Hβ strand determined by X-ray crystallography, SEC and SAXS experiments (Endres, et al., 2015) (figure 28), designated N-cap-dimer in the following. The oligomerization state for above described mutants DsLOV-M49S and DsLOV-M49I was likewise proven to be a dimer (Endres, 2013).

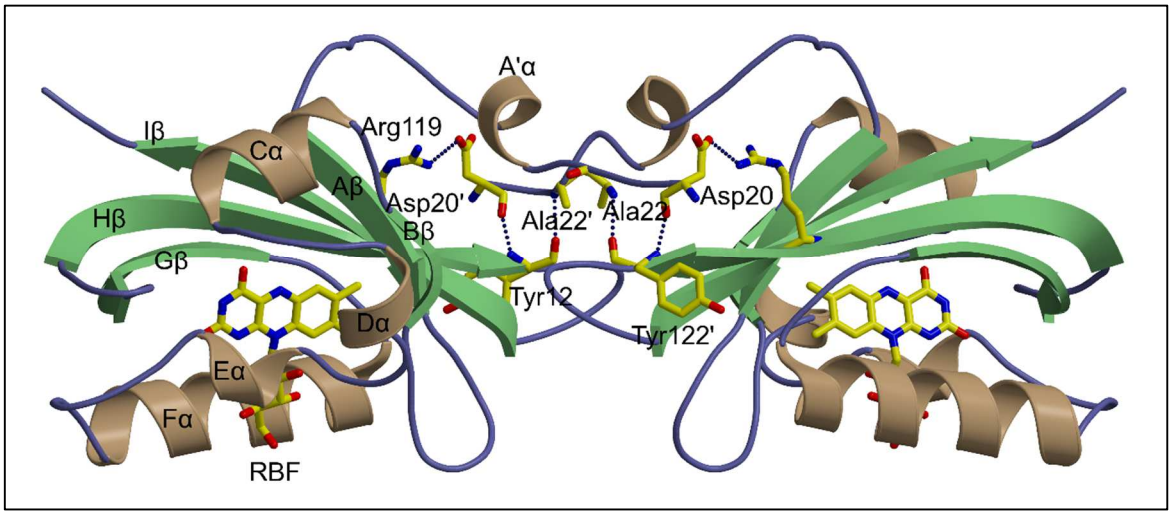

Figure 28: Dimer interface of DsLOV as previously described in Endres et al., 2015. Ribbon representation of the dark state crystal structure of DsLOV, with α-helices highlighted in yellow, loops in purple and β-strands in green. Residues constituting the interface are represented in stick model with carbon atoms highlighted in yellow, oxygen atoms in red, nitrogen atoms in blue and the phosphate atom in pink. Residues constituting the dimer interface by forming hydrogen bonds are found on the loop prior to A'α (Asp20, Ala22) and Hβ (Arg119, Tyr122).

The hydrogen bonds for the N-cap-dimers of all DsLOV proteins are listed in table 29. The interface interactions of the mutant dimer interfaces show significant differences in comparison to DsLOV.

Table 29: Distances between residues contributing to the N-cap dimers of DsLOV and its mutants.

Sec. structure element	Residue	Atom	Atom	Residue	Sec. structure element	Distance [Å] DsLOV	DsLOV -M49S	DsLOV-M49I	DsLOV-C72A
N-cap	Asp20	O	N	Tyr122	Hβ	2.7	2.84	-	-
N-cap	Asp20	OD2	NH1	Ag119	Hβ	3.4	-	-	-
N-cap	Ala22	N	O	Tyr122	Hβ	2.8	2.86	-	-
Aβ-Bβ-loop	Asp41	OD2	OD2	Asp41	Aβ-Bβ-loop	-	-	-	3.66
Aβ-Bβ-loop	Ser43	OG	NE2	Gln44	Aβ-Bβ-loop	-	-	-	3.45
Aβ-Bβ-loop	Gln44	NE2	OG	Ser43	Aβ-Bβ-loop	-	-	-	3.45
Bβ	Ile50	O	OE2	Glu125	Iβ	-	-	2.99	-
Hβ	Tyr122	O	N	Ala22	N-cap	-	2.84	-	-
Hβ	Tyr122	N	N	Ala22	N-cap	-	2.86	-	-
Iβ	Glu125	OE2	O	Ile50	N-cap	-	-	2.42	-

This particular dimer composition exhibits different buried surface areas and CSS values for all proteins (table 30) (figure 29). The CSS value rates the significance of the proposed interface, with a CSS value of 1 means representing 100 % of the interactions for the predicted assembly and therefor a high significance.

Surprisingly, DsLOV-M49I crystallized in a different space group and PISA analysis (Krissinel, et al., 2007) revealed a CSS = 0 for the N-cap-dimer. Inside the crystal a different dimer formation was observed constituted by interactions between residues in the Fα helix, the Fα-Gβ loop and the Gβ strand, designated β-sheet dimer in the following (table 30; figure 30). And for the second dimer interface the buried surface areas are similar to each other in all proteins but severe changes can be observed in the CSS values (table 30). Hydrogen bonds of the β-sheet-dimer interactions are listed in table 31.

Table 30: Statistics of the PISA analysis for DsLOV and its mutants (Krissinel, et al., 2007). The CSS value rates the significance of the proposed interface, with a CSS value of 1 means representing 100 % of the interactions for the predicted assembly and therefor a high significance.

Protein	Space group	Dimer form	Number of hydrogen bonds	Buried surface area [Å^2]	CSS
DsLOV	C2	N-cap dimer	3	948.2	0.54
		β-sheet-dimer	-	629.3	0.47
DsLOV-M49I	$P4_1\,2_1\,2$	N-cap dimer	2	437.9	0.00
		β-sheet-dimer	8	695.8	0.16
DsLOV-M49S	C2	N-cap dimer	4	953.2	0.44
		β-sheet-dimer	6	628.4	0.37
DsLOV-C72A	C2	N-cap dimer	3	846.9	0.50
		β-sheet-dimer	6	680.8	0.04

A superposition of the N-cap mediated dimer of DsLOV-M49S and DsLOV-C72A is shown in figure 29B with an RMSD value of 1.98 Å indicating a similarity between both dimer interfaces. This is supported by the CSS value of 0.50 Å for the N-cap dimer interface of DsLOV-C72A

with a buried surface area of 846.9 Å^2 comparable to those of DsLOV-M49S and DsLOV. For DsLOV-M49I the N-cap dimer was generated manually as it was observed differently in the crystal. A CSS of 0.16 and a buried surface area of 695.8 Å^2 suggests that it is unlikely that this mutant forms a N-cap-dimer.

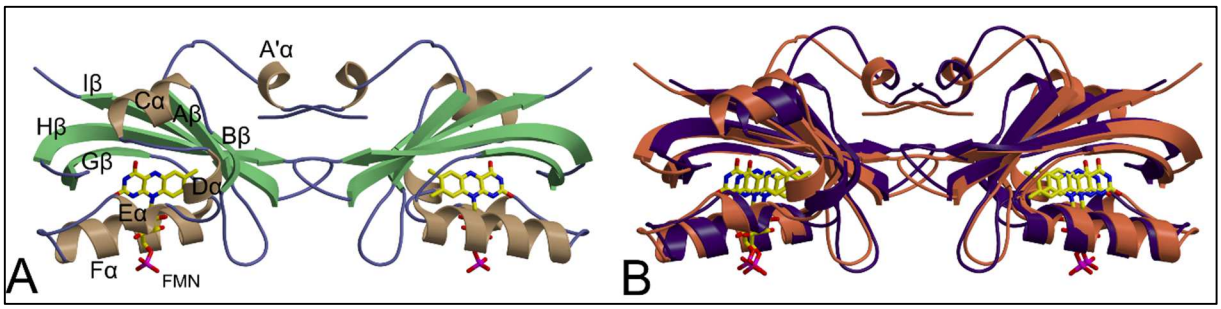

Figure 29: Dimer formation of DsLOV-variants as described for wildtype data (N-cap-dimer). (A) Dimer of DsLOV-M49S in ribbon representation. In this figure α-helices are highlighted in yellow, loops are highlighted in purple, and β-strands in green. The dimer was predicted by PISA analysis (Krissinel, et al., 2007). (B) Superposition of DsLOV-C72A (purple) on DsLOV-M49S (coral) resulting in an RMSD of 1.98 Å.

The same analysis was conducted with the β-sheet dimers of all proteins as found for DsLOV-M49I. The hydrogen bonds between both chains in the β-sheet dimer interfaces are listed in table 31. The residues involved in the dimer interface formation are similar in all proteins.

Table 31: Distances between residues contributing to the β-sheet dimer of DsLOV and its mutants.

Secondary structure element	Residue	Atom	Atom	Residue	Secondary structure element	Distance [Å]		
						DsLOV-M49S	DsLOV-M49I	DsLOV-C72A
Fα	His83	ND1	OE1	Gln90	Fα	-	2.69	-
Fα	Gln90	OE1	ND1	His83	Fα	-	2.67	-
Fα-Gβ loop	Thr96	OG1	O	Asp101	Gβ	2.74	2.89	2.74
Fα-Gβ loop	Arg97	O	N	Asp101	Gβ	3.07	3.07	3.07
Gβ	Thr99	N	O	Thr99	Gβ	2.79	2.83	2.79
Gβ	Thr99	O	N	Thr99	Gβ	2.79	2.81	-
Gβ	Thr99	O	OG1	Thr99	Gβ	-	-	2.62
Gβ	Asp101	N	O	Arg97	Fα-Gβ loop	3.07	3.13	3.07
Gβ	Asp101	O	OG1	Thr96	Fα-Gβ loop	2.74	2.79	2.74

The β-strand dimer of DsLOV-M49S with CSS of 0.37 and a buried surface area of 628.5 Å^2 and DsLOV-C72A with an CSS of 0.038 and a buried surface area of 680.8 Å^2 (table 30) was superposed on the dimer of DsLOV-M49I with RMSD value of 0.98 Å for DsLOV-M49S and 1.18 Å for DsLOV-C72A. The lower RMSD-value upon superposition of the β-strand dimer in comparison to the superposition of the N-cap dimers account for a higher possibility of dimer formation between residues in the core domain. In contrast the lower CSS values argue against the formation of the β-strand dimer (table 30) (figure 30).

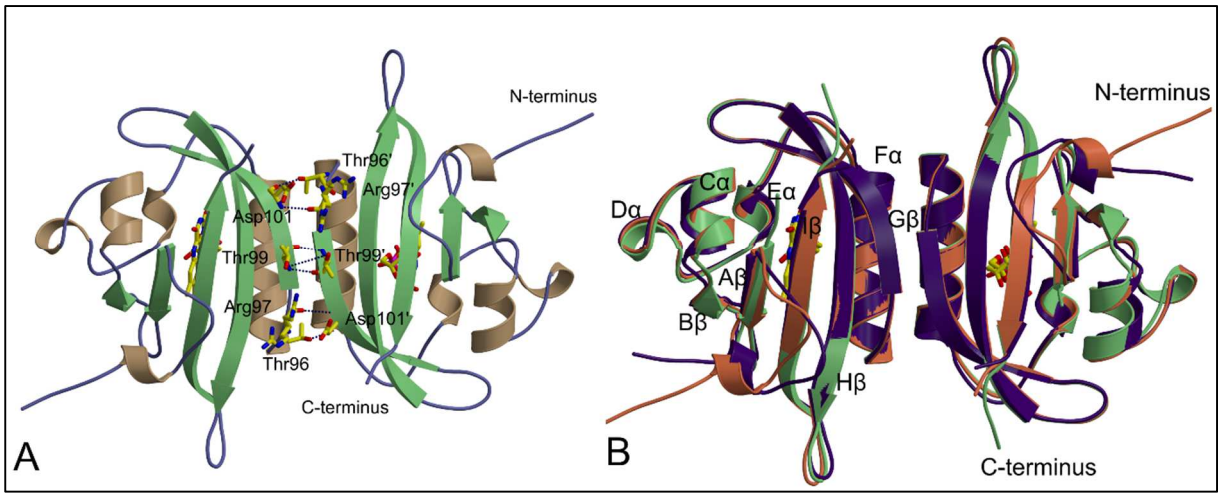

Figure 30: Dimer interface as found for DsLOV-M49I (β-sheet dimer). (A) Ribbon representation of the dark state crystal structure of DsLOV-M49S, with α-helices highlighted in beige, loops in purple and β-strands in green. Residues constituting the interface are represented in stick model with carbon atoms highlighted in yellow, oxygen atoms in red, nitrogen atoms in blue and the phosphate atom in pink. Residues constituting the dimer interface by forming hydrogen bonds are found on the loop between Fα and Gβ (Thr96, Arg97) and Gβ (Thr99, Asp101). (B) Superposition of the crystal structures of DsLOV-M49S (coral with an RMSD of 0.9681 Å) and DsLOV-C72A (purple with an RMSD of 1.1484 Å) on DsLOV-M49I (light green). The dimers were manually build by choosing a different chain generated by symmetry operation similar to the dimer formation of DsLOV-M49I.

3.2.4. Dark recovery inside the crystal of DSLOV-M49I and DsLOV-M49S

A typical absorption spectrum of a LOV protein in the dark state shows two maxima at 449 nm and 485 nm. After illumination of the protein these maxima decrease and simultaneously a new maximum appears at 390 nm characteristic for the light state of the protein.

In order to determine if DsLOV-M49S and DsLOV-M49I are still able to undergo the photocycle in crystal, absorption spectra of the dark state and of the light state were recorded. For the dark state spectrum, a crystal of each mutant was measured at 100 K in Grenoble (ID29S, ESRF, France) and illuminated subsequently with a blue light laser for 10 s at room temperature to record the light state spectrum. In parallel, the dark and light state spectra of aqueous protein solutions of both mutants were recorded in FZ Jülich.

The dark state spectrum of DsLOV-M49S in the crystal (figure 31A) clearly shows the absorption maxima at $\lambda = 449$ nm and $\lambda = 485$ nm. However, a decrease of these two maxima is expected, but not explicitly observed for the light state spectrum. They only show a decent decrease and the anticipated new absorption maxima at $\lambda = 390$ nm is not observed. This is probably explained by the fast dark recovery of DsLOV-M49S of $\tau_{REC} = 1.1$ s making it nearly impossible to measure the protein in the light state. For the aqueous protein solution of DsLOV-M49S a similar result was observed (figure 31B).

The mutant DsLOV-M49I exhibits a dark recovery of 153 s. This eases the measurement of the dark and light state absorption spectra. In figure 31C the typical dark state spectrum is shown

inside the crystal. The characteristic absorption maxima at λ = 449 nm and λ = 485 nm disappear after illumination with blue light resulting in a typical light state spectrum with a new prominent absorption maximum at λ = 390 nm. Single crystal microspectrometry experiments thus show that the protein exhibits characteristics that are similar to those in solution (figure 31D). These results show definitely that the protein is able to undergo photocycle in solution and in crystal.

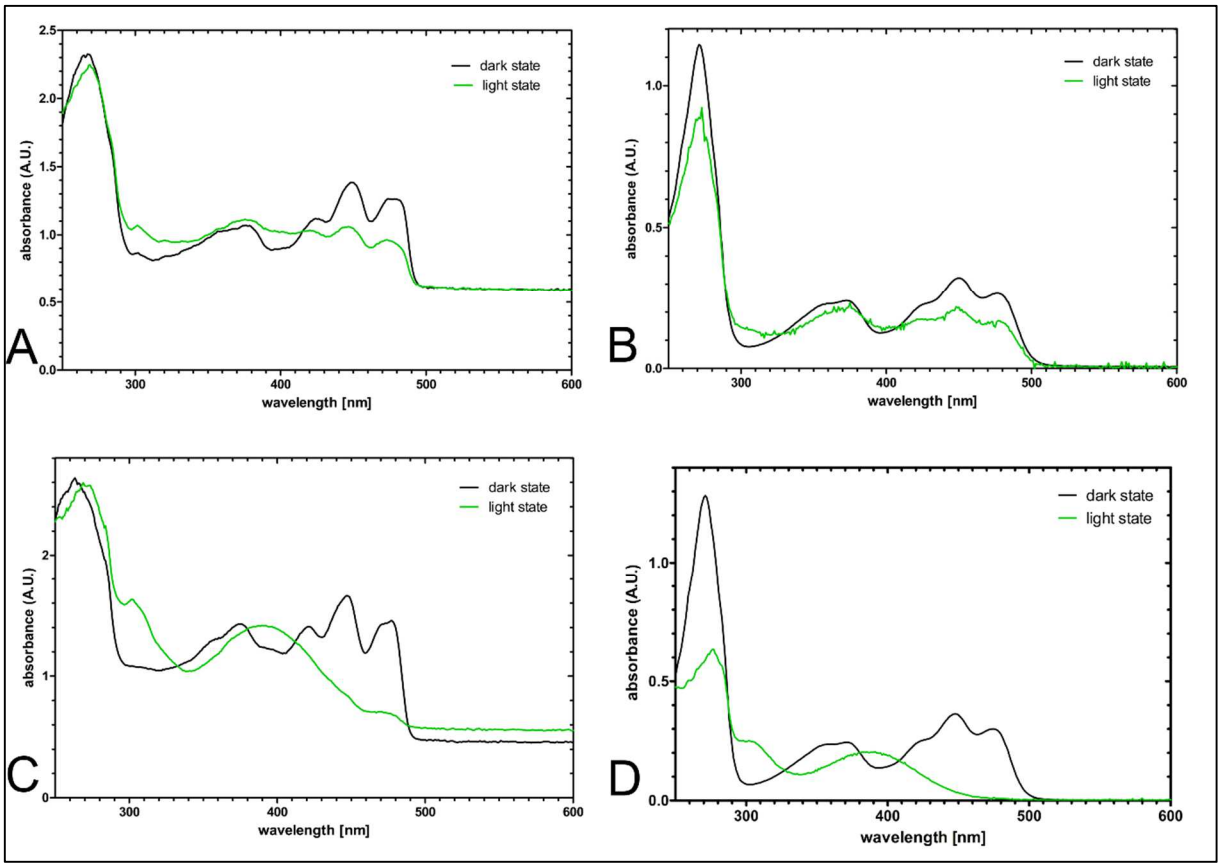

Figure 31: Absorption spectra of DsLOV mutants. (A) Dark and light state absorption spectrum of DsLOV-M49S inside the crystal; (B) Dark and light state absorption spectrum of DsLOV-M49S in solution; For the DsLOV-M49S mutant a typical light state spectrum was not observed most likely due to the fast dark recovery of τ_{REC} = 1.1 s; (C) Dark and light state absorption spectrum of DsLOV-M49I inside the crystal; (D) Dark and light state absorption spectrum of DsLOV-M49I in solution.

3.2.5. Recovery kinetics of DsLOV-M49S and DsLOV-M49I

As already explained in the introduction (page 5-6) LOV proteins undergo a photocycle after illumination with blue light. The required time to form the adduct light state is in the range of picoseconds and is conserved in the LOV protein family. The dark recovery however, is characteristic for each LOV protein and can vary from seconds to hours or even days. For the wildtype protein of DsLOV a fast dark recovery of 9.6 s was observed. The dark recovery constants for the mutants DsLOV-M49I and DsLOV-M49S were determined in this thesis to gather information about the influence of the methionine at position 49 in DsLOV. Sequence comparison with other LOV proteins revealed that this position usually is occupied by a leucine

or isoleucine. For DsLOV-M49S the dark recovery was observed to be 9-fold accelerated with τ_{REC} = 1.02 s while the dark recovery for DsLOV-M49I is decelerated 15-fold with τ_{REC} = 118.8 s (figure 32). These data are in accordance to the constants observed by Stephan Endres in his PhD-thesis, with DsLOV-M49S τ_{REC} = 1.1 s and DsLOV-M49I τ_{REC} = 153 s.

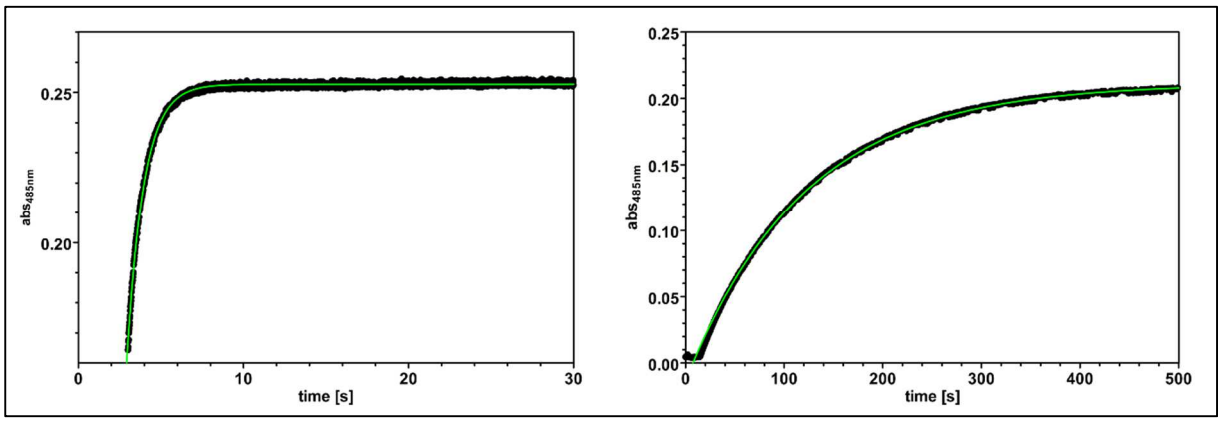

Figure 32: Determination of the photoadduct lifetime for DsLOV-M49S (A) and DsLOV-M49I (B). The absorption at λ = 485 nm was measured time-dependently after illumination of the sample with blue light. A non-linear regression was fitted to the obtained data. The observed dark recovery constants are DsLOV-M49S τ_{REC} = 1.02 s and DsLOV-M49I τ_{REC} = 118.8 s.

3.2.6. Small angle X-ray scattering of the short LOV protein DsLOV-M49I in solution

3.2.6.1. SAXS analysis of DsLOV-M49I in dark state

To determine which oligomerization states are present for the DsLOV mutants, SAXS measurements were conducted which analyse the biomolecular structure in solution (Jacques, et al., 2012). As explained in the material and methods section, a set of different concentrations of DsLOV-M49S, DsLOV-M49I and DsLOV-C72A in storage buffer (10 mM Tris, 10 mM NaCl, pH 7) were prepared in duplicate, using one set for the light state and the second set for the dark state. The data collection was conducted in ESRF (Grenoble, France) on the beamline BM29 and DESY (Hamburg, Germany) on the beamline P12. With the exception of DsLOV-M49I, all other samples showed aggregation which made further processing of the data impossible.

Using the program CRYSOL (Svergun, et al., 1995) calculated scattering curves of the crystal structure of the β-sheet dimer DsLOV-M49I were compared with the SAXS data shown in figure 33A. In that context it is important to consider that the crystal structure of DsLOV-M49I is missing 33 residues N-terminally and 5 residues C-terminally. In order to account for the missing atoms, dummy atoms were implemented in the crystal structures by a simulated annealing protocol using the program CORAL (Petoukhov, et al., 2012). Likewise, for the generated structure with flexible ends, a theoretical scattering curve was generated and fitted to

the experimental scattering data (figure 33A). The quality of these fits is expressed in the χ-value for the respective fit (table 32) as described in section 3.1.8. For the actual crystal structure, a χ-value of 16.0 was observed. In contrast, the structure with flexible ends produced a χ-value of 4.3 when fitted to the experimental SAXS-data.

Table 32: χ-value of CRYSOL fits of measured SAXS data with the respective crystal structure for DsLOV and DSLOV-M49I.

Protein	χ-value (fit with respective crystal structure)	χ-value (fit with respective crystal structure plus the flexible ends)
DsLOV-M49I N-cap dimer	21.3	6.3
DsLOV-M49I β-sheet dimer	16.0	4.3
DsLOV N-cap dimer	-	2.4*

* (Endres, et al., 2015)

Endres and coworkers recently reported the dimer interface of DsLOV formed by the N-terminal cap proven by PISA analysis and SAXS measurements (N-cap dimer). In the case of DsLOV-M49I the dimer interface is constituted of residues in the β-sheet and the surrounding helices (β-sheet dimer). In order to compare both possibilities, a N-cap dimer was generated for DsLOV-M49I with the program SUPCOMB (Kozin, et al., 2001). For this dimer a theoretical scattering curve was generated and fitted to the experimental data as already performed for the β-sheet dimer (figure 33C). The fit revealed a χ-value of 21.3. In addition, flexible ends were added C- and N-terminally to the structure likewise leading to an improved χ-value of 6.3 (table 32).

In summary, solely based on the statistics SAXS scattering data lead to the assumption that the β-strand dimer with flexible ends is the preferred dimer interface. *Ab initio* modelling was conducted to determine the envelope of DsLOV-M49I with the program DAMMIN (Svergun, 1999). The envelope is shown in figure 33B and D. The general shape overlaps with both of the dimer interfaces thus none of the dimer interface can be excluded which leaves the statistical evaluation as the only qualitative estimation. The non-filled parts of the envelope most probably correspond to the N- and C-terminal residues missing in the crystal structure.

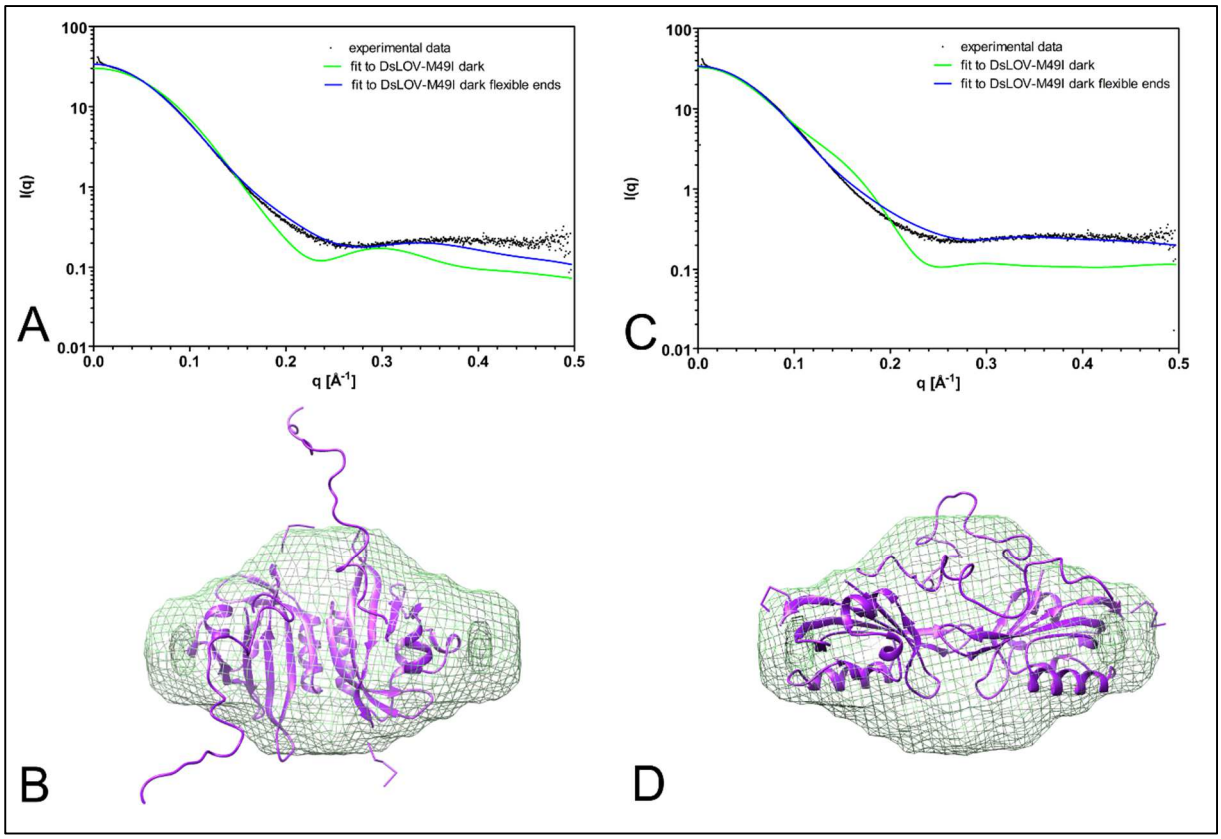

Figure 33: Small angle X-ray scattering of DsLOV-M49I dark state. (A)The experimental data (filled dots) are shown in combination with the calculated curve of the crystal structure of DsLOV-M49I β-sheet dimer (green line) and with the calculated curve of the crystal structure β-sheet dimer with flexible ends (blue lines). (B) The crystal structure of DsLOV-M49I (β-sheet dimer) in ribbon representation (purple) is aligned to the *ab initio* model in mesh(blue). (C)The experimental data (filled dots) are shown in combination with the calculated curve of the generated N-cap dimer structure of DsLOV-M49I (green line) and with the calculated curve of the equal dimer structure with flexible ends (blue lines). (D) The crystal structure of DsLOV-M49I (N-cap dimer) in ribbon representation (purple) is aligned to the *ab initio* model in mesh (blue).

In section 3.1.8.2, another approach of SAXS-measurements is explained where the scattering data are recorded in time-dependent manner. The expectation was to trap structural rearrangements during dark recovery and based on observed differences between dark and light state data of PpSB1-LOV-R66I. The sample was illuminated prior to the measurements for approximately 30 s and the scattering data were recorded in 3 and 7 min time steps, respectively (figure 34). The time span was determined as explained in section 3.1.8.2 to 72 min, with the additional assumption, that the dark recovery is decelerated at lower temperatures.

The measurement was conducted in accordance to the previously described kinetic experiment of PpSB1-LOV-R66I. The most significant difference between static light and dark state scattering data of PpSB1-LOV-R66I was observed at a scattering angle of q = 0.18 $Å^{-1}$. As shown in figure 34A in this region the signal-to-noise ratio is poor and differences are not observed. The same result is found regarding the time-resolved change of the intensity at a scattering angle of q = 0.18 $Å^{-1}$ (figure 34B) and the radius of gyration changes over the time (Figure 34C).

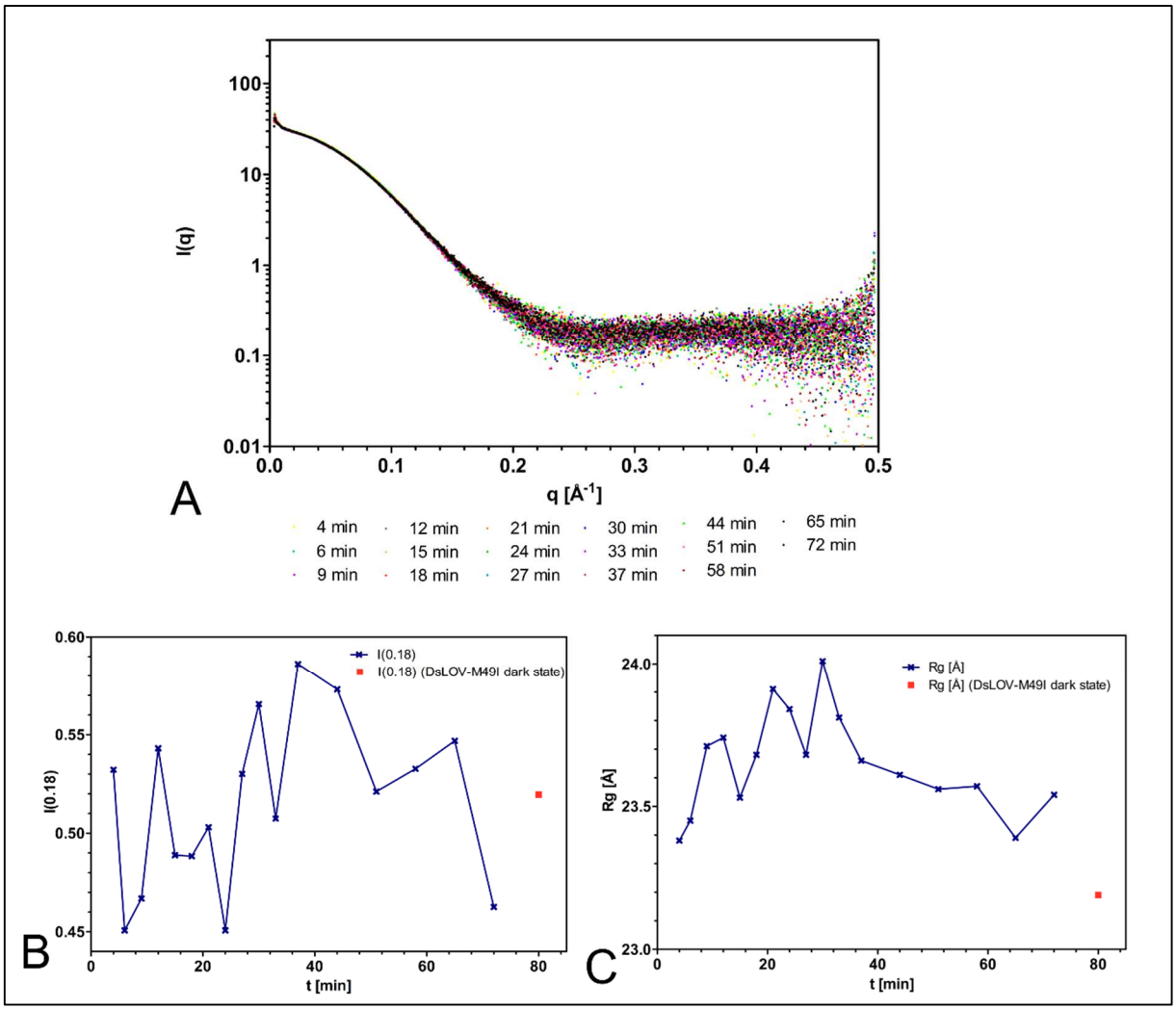

Figure 34: Kinetic SAXS measurements of DsLOV-M49I. (A) Scattering curves at different time points during dark recovery of DsLOV-M49I; (B) Time-dependent changes of the scattering intensity at q = 0.18 Å^{-1}, where the differences in the static measurements between dark and light state of PpSB1-LOV-R66I were observed, the intensities of the static dark state measurements of DsLOV-M49I are highlighted in pink; (C) Time-dependent changes of the radius of gyration during the dark recovery, the intensities of the static dark state measurements are highlighted in pink

4. Discussion

Understanding the photoreaction mechanism that a LOV protein undergoes after illumination is a major challenge in the area of LOV protein family. One of the objectives is to gather information about the actual processing and propagation of the signal, as most LOV proteins possess an effector domain fused N- or C-terminally. In case of PpSB1-LOV, the short LOV protein is predicted to interact with a free effector domain inside the cell (Circolone, et al., 2012). A reasonable approach to address this objective is comparison of the dark and light state proteins to look for the possible differences occurring at molecular level. This has been previously reported for various LOV proteins (Halavatny, et al., 2007; Möglich, et al., 2007; Endres, et al., 2015). The crystals taken for the data acquisition of the light state in these studies are not grown in permanent light conditions but were grown in the dark, which were illuminated prior to cryo-cooling. For a better discrimination in this thesis, crystal structures determined with this method are referred to as illuminated state instead of light state. A covalent bond between the chromophore and protein is, however, observed in several other structures (Möglich, et al., 2007; Zoltowski, et al., 2007). These minor differences observed in the chromophore binding region of the LOV core domain provides valuable information regarding the initiated events of photoactivation at molecular level. One of the problems of illuminated state is that the crystal lattice constraints do not allow larger conformational changes in the protein upon light absorption that are expected (Harper, et al., 2003; Möglich, et al., 2007).

Table 33: Overview of crystals obtained and structures determined in this thesis.

Protein		Obtained crystals	Determined structure
PpSB1-LOV	dark	yes	yes
	light	1)	1)
PpSB1-LOV-C53A	dark	yes	yes
	light	yes	no
PpSB1-LOV-R66I	dark	yes	no
	light	yes	no
PpSB1-LOV-R61H/R66I	dark	yes	yes
	light	no	no
DsLOV	dark	1)	1)
	light	yes	no
DsLOV-M49S	dark	yes	yes
	light	yes	no
DsLOV-M49I	dark	yes	yes
	light	no	no
DsLOV-C72A	dark	yes	yes
	light	yes	no

1) Structure already published

Currently, only two true light state structures are available, where crystals were grown in continuous light conditions: VVD from the fungus *Neurospora crassa* (Vaidya, et al., 2011) and PpSB1-LOV from the soil bacterium *Pseudomonas putida* (Circolone, et al., 2012). The

low number of published true light state structures reveal the challenging nature of these research aims.

In this work, crystallization attempts were done to obtain crystals of short LOV proteins in both, light and dark conditions. Several crystal structures were determined in dark and illuminated states. Under continuous light conditions, although crystals were obtained of DsLOV, DsLOV-M49I, DsLOV-M49S, DsLOV-C72A, PpSB1-LOV-C53A, and PpSB1-LOV-R66I proteins, they did not diffract and could not be improved (table 33).

4.1. PpSB1-LOV

4.1.1. Comparison of dark, light, and illuminated structures

In this work it was shown by single crystal microspectrometry that PpSB1-LOV proteins are able to undergo the photocycle inside a crystal. The differences in the characteristic maxima in dark state at λ = 449 nm and λ = 485 nm and in light state at λ = 390 nm indicates formation of the photoadduct. The coordination of the chromophore is conserved among the LOV protein family and several research groups have reported differences in dark and illuminated states (Möglich, et al., 2007; Nash, et al., 2008; Raffelberg, et al., 2011; Endres, et al., 2015).

The most prominent differences in PpSB1-LOV for light and illuminated states are found for the photoactive Cys53 on Eα and the Gln116 on the Iβ-strand. Generally, in the light state structures of LOV proteins, the formation of a covalent bond is observed between the Sγ atom of the cysteine and the C4a-atom of the FMN which is absent in the dark state structure. However, in PpSB1-LOV no covalent bond was observed, but the indication of a sp^3 hybridized FMN-C4a, a continuous density in the area where the covalent bond is assumed and the distance of 2.35 Å between Cys53-Sγ and FMN-C4a indicates the presence of the light state in the crystal. The loss of the covalent bond is most probably ascribed to radiation damage as previously reported (Federov, et al., 2003; Zoltowski, et al., 2007; Circolone, et al., 2012). The second major difference was found for the Gln116 forming two hydrogen bonds with the O4 and N5 atom of the FMN in light state. These interactions with the chromophore are lost in the dark state where the glutamine forms a new hydrogen bond with backbone residue Gly17 on the Aβ strand. In the illuminated state, which was determined with the same crystal as used for the dark state, weak hydrogen bonds between FMN and Gln116 are observed. Large conformational changes like Jα movement and rotational movement in dimer as observed upon comparison of dark and true light state (described in following section) were not observed in the illuminated state data. In conclusion, the illuminated structure is more similar to the light

state structure than to the dark state structure of PpSB1-LOV with regard to the chromophore coordination. Thus, illuminated structures provide detailed information in the chromophore binding pocket as expected for the light state, however, large conformational changes in secondary, tertiary and quaternary structural elements cannot be observed. Large conformational changes in response to light were proposed previously (Halavaty, et al., 2007; Zoltowski, et al., 2007; Möglich, et al., 2007; Nash, et al., 2011; Conrad, et al., 2012), which are possibly relevant to the transfer of signal to the effector domain. The illuminated structure of a LOV protein thus cannot replace the true light state structure, but can provide the information on the initial steps of photoactivation. This is especially useful for LOV proteins where crystallization trials under continuous light is not possible, for e.g. where the dark recovery is in the range of seconds time scale (Endres, et al., 2015).

4.1.2. Signal propagation and structural rearrangements of PpSB1-LOV after illumination

The photocycle in LOV proteins has been characterized in detail in the literature as described in the introduction (page 5-6). In contrast, the mechanism of signal propagation in LOV proteins still remains unclear. Much effort was made to postulate the structural basis of the signal propagation in LOV proteins evoked by excitation with blue light. Four types of conformational changes have been proposed till now for LOV proteins by Herrou and Crosson, 2012: (1) unfolding of the protein leading to loss of interactions between core domain and N- or C-terminal extensions, as observed in phot1LOV2 of *Arabidopsis thaliana* (Halavaty, et al., 2007) (figure 35A), (2) reorientation of the N-terminus and subsequent dimerization as in VVD from *Neurospora crassa* (Zoltowski, et al., 2007) (figure 35B), (3) conformational changes in the Jα helix, in particular tilting and rotation of this helix leading to a reorientation of the effector domain into an activated state as shown in YtvA-LOV of *Bacillus subtilis* (Möglich, et al., 2007) (figure 35C) and (4) unfolding of a compact LOV monomer followed by dimerization on DNA as observed for EL222 of *Erythrobacter litoralis* (Nash, et al., 2011) (figure 35D).

These mechanisms include a conserved reaction of the flavin-protein complex with surrounding amino acids and an additional response varying amongst the different LOV proteins. Recently, a fifth possible structural mechanism was proposed for the short LOV protein RsLOV from *Rhodobacter sphaeroides* (Conrad, et al., 2012). Based on derived SAXS and NMR results, the authors described a dimer under dark state conditions that dissociates into monomers. This monomerization is evoked by the partial unfolding of the Jα helix after illumination. The latter

then propagates the signal to the helix Kα. In addition, they suggested large conformational changes of the C-terminal helices Jα and Kα away from the core domain (figure 35E).

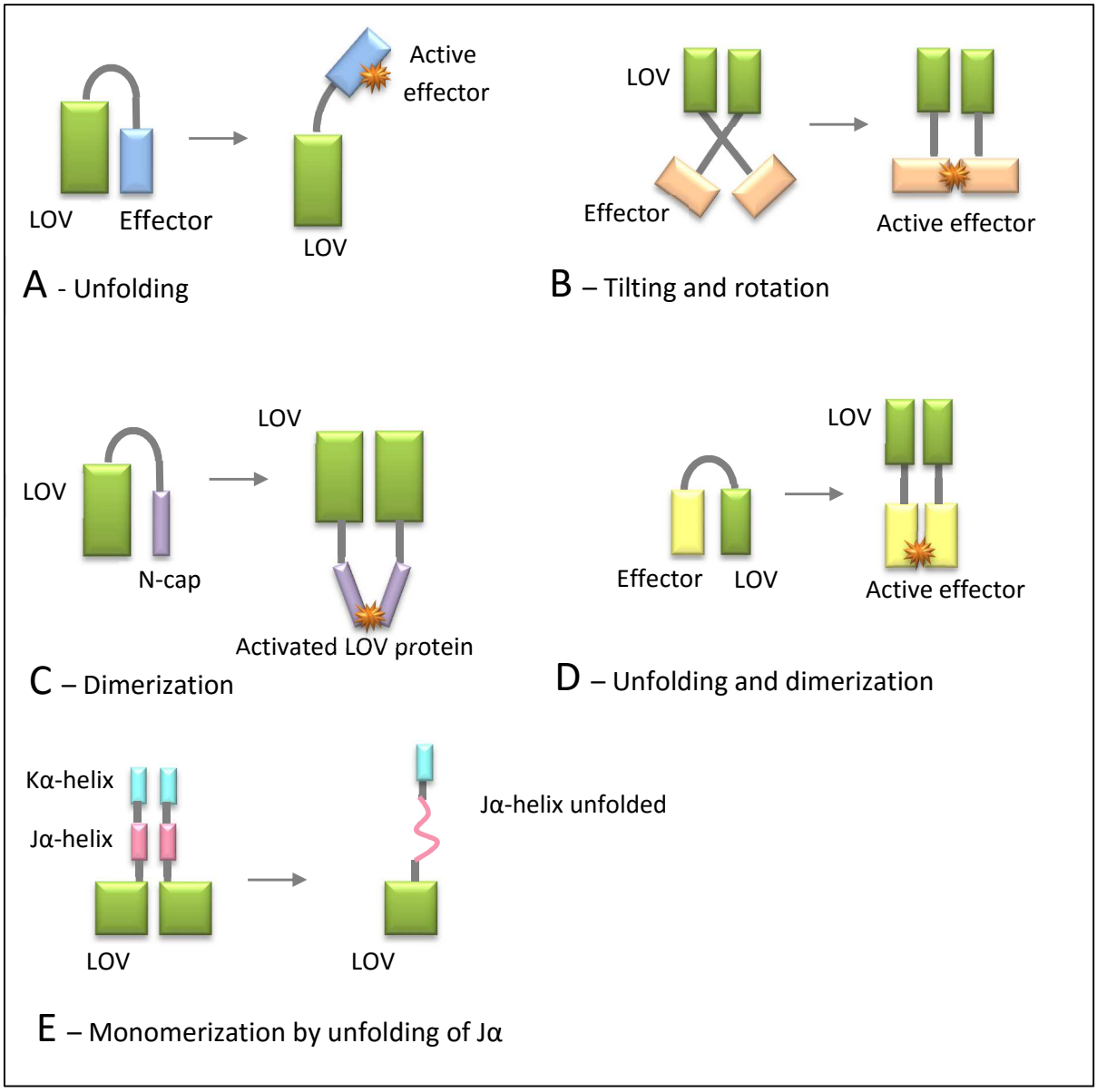

Figure 35: Structural rearrangements in LOV proteins after illumination. (A) unfolding of the LOV protein releases the effector domain from the LOV protein and thus the effector is activated; (B) Tilting and rotation of both domains result in a different arrangement and activates the effector domain; (C) Illumination induces the release of the N-cap from the LOV protein which then can form homodimers with a second molecule; (D) unfolding of monomeric effector domain from the LOV domain induces dimer formation and subsequent activation of the effector domain; (E) The dimeric state is disrupted by the unfolding of the C-terminal Jα helix and the signal thereby is propagated to the Kα helix; adapted from (Herrou, et al., 2012).

Structural comparison of PpSB1-LOV with other LOV proteins currently available on the PDB-server revealed the highest similarity, with the dark state YtvA-LOV (PDB-ID: 2PR5) of *Bacillus subtilis* and the protein NifL from *Azotobacter vinelandi* (PDB-ID: 2GJ3) (table 34) and does not include VVD, indicating a different mechanism in PpSB1-LOV. VVD is the only other protein where structure information is available in both, dark and true light states.

The LOV domain of the transferase NifL (PDB-entry: 2GJ3) present in *Azotobacter vinelandi*

consists of 119 amino acids with a FAD molecule inside the PAS-core domain. Although the core domains of PpSB1-LOV and NifL share the same fold, NifL is deficient of the C-terminal helix protruding away from the core domain found in PpSB1-LOV and YtvA-LOV, indicating a common signal propagation mechanism between NifL and the latter two proteins as improbable.

Table 34: Structural comparison of PpSB1-LOV in dark state with other LOV domains currently available on the PDB-server. The structural comparison was conducted using PDBeFold (Krissinel, et al., 2005). The quoted Q-value describes the identity of the different structures in comparison with PpSB1-LOV in dark state, with Q=1 for complete identity. N_{alg} describes the number of compared residues.

Protein	PDB-ID (As used on the PDB website)	Q-score	N_{alg}
PpSB1-LOV light	3SW1	0.71	129
YtvA-LOV dark	2PR5	0.66	116
YtvA-LOV illuminated	2PR6	0.65	116
NifL	2GJ3	0.64	111
EL346	4R38	0.59	102
Phot-LOV1 illuminated	LN9N	0.59	102
Phot-LOV1 dark state	LN9L	0.59	102

The highest Q-value was observed for YtvA-LOV domain (PDB-entry: 2PR5) of the YtvA protein of *Bacillus subtilis.* The full-length protein is composed of a N-terminal segment (residues 1-24), a core LOV domain (residues 25-126), and a C-terminal sulfate transporter and anti-σ factor antagonist (STAS) domain (residues 148-258) connected to the core domain via a helical linker (residues 127-147). Crystal structures of YtvA-LOV comprise the core domain and the linker region (residues 20-147). The isolated LOV domain possesses structural elements as described for PpSB1-LOV with a core domain, and N- and C-terminal helical extensions. In their work the authors compared the dark state crystal structure of YtvA (PDB-ID: 2PR5) with the illuminated state (PDB-ID: 2PR6) (Möglich, et al., 2007). Upon illumination, the two chains of the dimer undergo a scissor-like rotation relative to each other. The signaling mechanism was proposed to start with a rotation of both the monomers relative to each other, which is accompanied by a movement of the Jα-helices. Subsequently, the signal propagation takes place to the STAS domain at the C-terminus of YtvA.

The C-terminal Jα-helix of YtvA-LOV exhibits several interactions with symmetry-related chains inside the crystal. This is likely to influence the orientation of the Jα helices. Additionally, the published light state structure is an illuminated structure as the data was collected from a dark-grown crystal that was illuminated prior to cryo-cooling. Therefore, large conformational differences between the dark and illuminated structures are not likely to be observed due to the crystal packing.

For PpSB1-LOV, the true light state structure has been published (Circolone, et al., 2012) and

can be compared to the dark state structure described in this thesis. A comparison of both the structures reveals major structural rearrangements. The basic dimer organization of PpSB1-LOV resemble those of YtvA where the crystal structures in dark (PDB-ID: 2PR5) and illuminated state (PDB-ID: 2PR6) are available (Möglich, et al., 2007) The secondary structure elements in YtvA and PpSB1-LOV are termed identical. The authors describe a combined tilt like motion in YtvA of the Gβ-Hβ loop (residue 96-100; in PpSB1-LOV residue 87-91), the Eα-Fα loop (residue 66-71; in PpSB1-LOV residue 76-81) and the Jα helix (127-145; in PpSB1-LOV residue 128-132) away from the dimer interface (compare with sequence alignment in figure 2). Simultaneously, the Hβ-Iβ loop shifts towards the dimer interface resulting in a scissor like motion (Möglich, et al., 2007). However, the dark state is not compared with the true light state but with the illuminated crystal structure of YtvA and larger changes in the dimer interface remain unlikely due to the crystal packing. This means illumination with blue light evokes a slight change of the interactions between both monomers of YtvA, and thus it is most likely that these motions have an impact on the signal propagation of the LOV domain of YtvA to the effector domain.

In comparison, the interface of the light state structure of PpSB1-LOV described in Circolone et al., 2012 exhibits various hydrophobic interactions as well as hydrogen bond formation and a salt bridge between the β-sheets and Jα- helices. Hence, both monomers contribute to the dimer interface. The interface interactions of the here introduced dark state structure PpSB1-LOV appear to be different as described in the following. These differences include the observation of additional hydrogen bonds for Gln5 (A'α), Asn15 (loop between A'α and Aβ), and Asp105 (loop between Hβ and Iβ) which results in a different dimer interface (figure 10 and 13). A similar arrangement was observed for the mutant PpSB1-LOV-C53A which was expected as it cannot undergo the photocycle.

Excitation with blue light evokes a rotation of the conserved Gln116 towards the FMN, forming two hydrogen bonds with the N5 atom of the chromophore and induces the covalent bond between the sulfur atom of the Cys53 and the C4a atom of FMN (figure 11B). Consequently, a shift in Iβ strand is likely to affect the Hβ-Iβ conformation and its interaction with A'α helix of the opposite subunit. A change in dimer interface can cause re-orientation of the dimer, as seen in PpSB1-LOV crystal structures (figure 13). Additionally, as each of the subunit is bound to a FMN molecule, combined effects of blue-light illumination are expected to take place in the dimer of PpSB1-LOV protein. Large structural changes such as ~ 10 Å Jα movement and ~ 29° rotation of dimer subunits relative to each other as seen in PpSB1-LOV structure are remarkable, providing the experimental evidence of signaling mechanism in short LOV

proteins.

These results are also supported by the obtained SAXS data. For PpSB1-LOV only dark state scattering data were recorded with *ab initio* models and compared with the dark state crystal structure. Scattering data for both the dark state and light state of the mutant PpSB1-LOV-R66I were collected successfully. And severe differences between both structural arrangements are not expected. The calculated *ab initio* models reveal differences in the region of the C-terminal Jα-helix. The shape of the models is tighter and compacter in the light state and the dummy atoms (accounting for the missing residue in the crystal structure) are arranged in line with the Jα helix. This argues for a higher rigidity of PpSB1-LOV in light state. The rigidity of the light state structure in comparison to a "relaxed" dark state structure is also reflected by high B-factors of the dark state structure. The stable light conformation most likely ensures the signal propagation to the effector protein. A more flexible form for the dark state of the protein is highly likely and this flexibility is changed as soon as light hits the protein. The observed conformational changes might then be propagated via the C-terminal extension and requires a more stable conformation to ensure an appropriate signal transfer to the effector protein. Based on these results, kinetic SAXS measurements were recorded. The aim was to visualize the change in shape of time, but the time-dependent scattering curves did not show any differences. This is most likely due to the low concentration which was used, and the technical problems related to illuminating the sample. These measurements deserve further improvement.

In conclusion, the signal transduction pathway in PpSB1-LOV starts in the conserved LOV core region with the formation of the covalent bond between protein Cys53-Sγ and chromophore FMN-C4a atom and propagates via changes in the secondary (amino acid side chain reorientation of Gln116) and tertiary structure elements (Iβ) to the outer parts of the protein including the Jα helix movement and reorientation of the dimer. The described mechanism appears to be the most probable way to transfer the signal to a putative interaction partner inside the cell. Evidence for this kind of regulation has been previously reported for LOV proteins phot1LOV2 from *A. sativa* and phot2LOV2 from *A. thaliana* interacting with kinases via the C-terminal Jα helix (Harper, et al., 2003) (Harper, et al., 2004) (Eitoku, et al., 2005).

4.1.3. Accelerated dark recovery evoked by the substitution of two arginines coordinating the phosphate moiety

In addition to the structures of PpSB1-LOV and PpSB1-LOV-C53A in dark and illuminated states, this study also describes the dark state structure of PpSB1-LOV-R61H/R66I. In

PpSB1-LOV two additional arginines (Arg61 and Arg66) in the core LOV domain were found (Circolone, et al., 2012). These residues previously have been identified as key amino acids in the fast dark recovery of PpSB1-LOV τ_{REC} = 2471 min (Jentzsch, et al., 2009). The double substitution of Arg61 into a histidine and Arg66 into an isoleucine resulted in a ~ 270-fold acceleration of the dark recovery. A comparison on structural level might provide further information on influence of the arginine cluster with regard to the dark recovery. The overall structure of PpSB1-LOV-R61H/R66I does not reveal significant differences in comparison to the wildtype dark state crystal structure. In general, the chromophore is coordinated as in the wildtype. The lack of the two arginines is compensated by the conserved arginines Arg54 and Arg70 coordinating the phosphate moiety.

In conclusion, the only observed difference in the structures of PpSB1-LOV and PpSB1-LOV-R61H/R66I in dark state is the reduced coordination of the phosphate moiety by two remaining arginines. Crystal structure of PpSB1-LOV-R61H/R66I reveals that the mutations have no significant effect on the protein conformation. The accelerated dark recovery in the mutant is thus probably due to different molecular dynamics for which NMR spin relaxation methods can be applied here.

4.2. DsLOV

The second LOV protein DsLOV was found as the only short LOV protein in the marine bacterium *Dinoroseobacter shibae* (Endres, et al., 2015). Its fast dark recovery kinetics and the small size makes it an interesting candidate in the design of optogenetic tools. Stephan Endres characterized the wildtype protein biochemically, photochemically and structurally in his PhD thesis. He also observed interesting changes in the dark recovery upon substitution of a methionine into an isoleucine and a serine by site-directed mutagenesis (Endres, 2013). These changes enhanced the interest to analyze the mutants at molecular level using X-ray crystallography.

4.2.1. Amino acid position 49 has a strong influence on recovery time

Sequence alignment of different LOV proteins revealed a conserved aliphatic amino acid in the Bβ strand that is usually a leucine or isoleucine. In *Avena sativa* phot1LOV2, PCR-based random mutagenesis resulted in the substitution of the respective Ile16 into a valine. For this mutant an approximately 10-fold acceleration of the dark recovery was observed (Christie, et al., 2007). This major change in recovery time is of particular interest as it was caused by the deletion of a methyl group at amino acid position 16. Further information was expected by the exchange of Ile16 into a leucine. However, no major structural or electrostatic changes were observed and the determined dark recovery time was stated as 19 s. This is an approximate two-fold enhancement in comparison with the wildtype. For the mutant phot1LOV2-I16T with $\tau_{REC} < 2$ s an even faster dark recovery was observed. The authors concluded a strong influence of the isoleucine on the stabilization of the FMN-cysteinyl adduct supported by a progressive decrease of the size of the amino acid side chain followed by an increase in recovery time. The stated explanation refers to a loss of interactions between the photoactive Cys39 and the I16V based on the missing methyl group. The loss would provoke a movement of the cysteine side chain towards the valine to compensate for the missing interaction and thus a reorientation of the side chain away from the FMN-C4a atom would lead to a destabilization of the photo adduct accompanied by an accelerated dark recovery.

Similar results were observed for a short LOV protein in *Rhodobacter sphaeroides* designated RsLOV by the substitution of isoleucine at the corresponding position 32 into a valine resulting in an acceleration of approximately 14 fold in comparison with the wildtype RsLOV. The authors described substantial differences in the electron density of the helices Dα, Eα and Fα and their connecting loops upon comparison with the wildtype RsLOV structure. The electron density is more defined for residues in RsLOV-L32V than in the wildtype. However, similar to the argumentation for phot1LOV2, the changes are explained by an increase in conformational

freedom for the photoactive Cys55. The authors postulated a decreasing stability of the photoadduct in particular the covalent bond between chromophore and cysteine due to increased domain movements supported by a greater solvent accessibility of the N5 atom in FMN (Conrad, et al., 2012) leading to an accelerated dark recovery.

In sequence alignment of different LOV proteins, DsLOV reveals a methionine at position 49 that corresponds to phot1LOV2-Ile16 and RsLOV-Ile32 which is unique in the LOV protein family. Usually this position is occupied by an aliphatic amino acid like leucine and isoleucine. Recovery time of the short LOV protein DsLOV was determined as τ_{REC} = 9.6 s (Endres, 2013) which is comparably faster than other known LOV proteins like PpSB1LOV with τ_{REC} = 2471 ± 22 min, PpSB2-LOV with τ_{REC} = 137 ± 11 s (Jentzsch, et al., 2009), YtvA with τ_{REC} = 45 min (Losi, et al., 2003), and RsLOV with τ_{REC} = 2357 s (Conrad, et al., 2012). To evaluate the influence of the unique methionine on the dark recovery, the mutants M49S and M49I were generated based on the sequence alignment (figure 2). The remarkable 10-fold enhancement of the recovery time upon substitution into a serine can be expected based on previously discussed results involving amino acids with smaller side chains. Additionally, as revealed by measurements of solvent isotope effects, the shielding of the chromophore in DsLOV-M49S is reduced and therefore the recovery into the dark state is favored (Endres, 2013). In comparison, the exchange into an isoleucine resulted in a slower dark recovery of τ_{REC} = 153 s. Following the line of previous arguments this substitution was expected to accelerate the recovery time as the isoleucine occupies less volume than methionine. A possible explanation might be the presence of a sulfur atom in the methionine side chain which can further interact with the cysteine and thus destabilize the covalent bond of the photoadduct. Additionally, solvent isotope measurements revealed a reduced accessibility of the chromophore leading to a slower deprotonation (Endres, 2013). The crystal structures of DsLOV-M49S and DsLOV-M49I support this explanation. In DsLOV-M49S the cysteine does not interact with the serine. The large gap between both amino acid side chains mirrors the low shielding effect of the serine and the fast dark recovery observed for this mutant. The cysteine side chain in DsLOV-M49I exhibits two different rotamer forms one is bending towards the isoleucine with a distance of 3.47 Å between Ile49-Cδ and Cys53-Sγ indicating an interaction between both residues and thus accounting for the reduced accessibility of the chromophore. The second rotamer conformation of the cysteine exhibits a weaker interaction but still is in closer distance to the cysteine than the Oγ atom of Ser49 in the other mutant.

4.2.2. Conserved arginines coordinating the phosphate moiety of the FMN in DsLOV and its mutants

Sequence alignment of several LOV proteins reveal two highly conserved arginines suspected to coordinate the phosphate moiety of the flavin chromophore mainly to keep the chromophore in close contact to the photoactive cysteine (Möglich, et al., 2007; Nash, et al., 2011; Vaidya, et al., 2011; Conrad, et al., 2012; Circolone, et al., 2012; Rivera-Cancel, et al., 2014; Lokhandwala, et al., 2015). One of these arginines is also located in the conserved sequence motif ahead of the photoactive cysteine on the Eα helix and the side chain of this arginine remains in parallel orientation to the ribityl chain of the FMN. The second arginine residue is located in the Fα helix. In DsLOV, these arginines are Arg73 (Eα helix) and Arg89 (Fα helix). The structure of DsLOV in dark state was published in February 2015 and comprised a more detailed overview about the actual situation inside the core domain (Endres, et al., 2015). Surprisingly, the observed chromophore was RBF instead of FMN. The simple difference between both molecules is the phosphate group at the end of the ribityl chain which is present in FMN and deficient in RBF. The authors propose that presence of RBF instead of FMN is due to hydrolysis in acidic pH conditions in which protein was incubated during the crystallization. In the wildtype structure, the Arg73 interacts with the ribityl chain instead of the phosphate moiety. The second arginine is facing away from the ribityl chain which was hypothesized due to the loss of interactions with the missing phosphate moiety (Endres, et al., 2015). All mutant structures discussed in this thesis were not expected to change their chromophore binding specifications solely based on the amino acid substitution, DsLOV-M49S, DsLOV-M49I and DsLOV-C72A exhibited a FMN molecule inside the core domain of the crystal structure. In the crystal structures of DsLOV-M49S, DsLOV-M49I and DsLOV-C72A both arginines were found as in the wildtype, where the Arg73 forms hydrogen bonds with the phosphate instead of the ribityl chain and interacts with Asp46 on Dα indicating a tight coordination of the side chain. The second arginine Arg89 does not interact with the FMN. In the mutant DsLOV-C72A, the electron density for this particular residue was poorly defined indicating a higher flexibility of the side chain.

It is interesting that crystal structure of PpSB1-LOV revealed four arginines coordinating the FMN molecule, where PpSB1-LOV shows the slowest dark recovery kinetics τ_{REC} = 148000 s (Jentzsch, et al., 2009). In contrast, DsLOV shows a fast dark recovery τ_{REC} = 9.6 s (Endres, et al., 2015), where the FMN phosphate moiety coordination involves only one conserved arginine in the crystal structure. Even though role of arginine residues seems to be a common mechanism of coordination of the phosphate moiety of chromophore, each LOV protein with a fused

effector domain or as a short LOV protein probably adapts specific and individual mechanisms that control the stability of the photo adduct and therefore the dark recovery.

4.2.3. A different dimer interface was found for DsLOV-M49I formed mainly by residues in the β-sheet

For DsLOV a dimeric organization in aqueous solution was demonstrated in SEC in dark and light state (Endres, et al., 2015). The crystal structure revealed one chain in the asymmetric unit, thus the dimer was generated by choosing a symmetry equivalent molecule based on PISA analysis (Krissinel, et al., 2007). The dimer interface was proposed as a N-cap dimer (Endres, et al., 2015), based on the CSS score and the SAXS data. Additional structural comparison proved a high similarity to VVD. The dimer interface of VVD consists of a N-terminal extension (α-helix and β-strand). VVD forms monomers in dark state and dimerizes upon illumination with blue light. DsLOV exhibits a N-terminal extension composed of a linker region, a small helix designated A'α and a turn motif. The proposed dimer interface is mainly derived from hydrogen bonds between the N-terminal helix and its counterpart on the second chain, important to mention that no clues were found that DsLOV dimerizes upon excitation but remains as a dimer in both states.

Interestingly, DsLOV-M49I crystallizes in tetragonal space group with two chains in the asymmetric unit. These chains form a dimer that corresponds to the β-sheet dimer, which was the less favored type of dimer in other DsLOV proteins described above. In DsLOV-M49I missing electron density for amino acids 1-33 compared to 1-19 for the other three structures accounts for a higher flexibility in the N-terminal cap. It appears that this N-terminal flexibility is induced by a single substitution of the amino acid Met49 located inside the core domain into an isoleucine, which is a surprising result. It can be hypothesized that a loss in rigidity of the N-cap also diminishes role of this region in dimer formation. If the N-terminus exhibits a higher flexibility it is highly unlikely that it can form a stable dimer in DsLOV. Additionally, SAXS data supports the theory of a β-sheet mediated dimer for DsLOV-M49I. PISA analysis revealed the possibility of a β-sheet dimer also for the mutants DsLOV-C72A and DsLOV-M49S, although the CSS score is remarkably lower than for the N-cap dimer. Two possible explanations for the different dimer formation in DsLOV-M49I seem to be possible. First, a dimer formed by residues in secondary structure elements like α-helices and β-strands seems to be more stable. This is based on the fact that these elements are stabilized by mainly hydrogen bonds and therefore, a dimer constituted by residues in such elements seems to be energetically favored. The CSS value is theoretically calculated and not measure experimentally, and actual

biological factors such as temperature, pH and surrounding molecules are not taken into account in these calculations. CSS values should thus be treated carefully. Another explanation might be an enhanced flexibility of secondary structure elements caused by the substitution of the methionine into an isoleucine. A similar effect has already been observed in the helices Dα, Eα, Fα, and their connecting loops in RsLOV upon substitution of the Leu32, the equivalent position to Met49 (Conrad, et al., 2012). The present results do not account for one of the dimer interfaces to a full extent and further experimental evidence is necessary. A possible approach is the elimination of the N-terminal extension and subsequent analysis of the oligomeric state by SEC. A dimeric organization in that case would account for the formation of the β-sheet dimer. Additional crystallographic studies and small angle X-ray scattering experiments will provide further information in future.

4.3. Biological implications of the structural investigations

The LOV protein family gained interest in the usage as optogenetic tools based on their interesting characteristics in comparison to GFP and similar established optogenetic tools (Chalfie, et al., 1994; Drepper, et al., 2007; Chapman, et al., 2008; Shu, et al., 2011). The comparable smaller size of LOV proteins, its ability to react in anaerobic conditions and the usage of FMN as chromophore which is ubiquitous inside the cell makes it an interesting new optogenetic device. In comparison, GFP auto-catalyzes its chromophore under aerobic conditions and exhibits a bigger size (Drepper, et al., 2010). As already reported, LOV proteins exhibit fast folding kinetics and spontaneous incorporation of the chromophore leading to a fast fluorescence active conformation (Drepper, et al., 2010; Mukherjee, et al., 2013; Wingen, et al., 2014).

However, a full understanding of the structural mechanism of the LOV proteins is missing in order to generate variants with novel characteristics. Besides the biochemical characterization and the analysis of the optical properties, the structural investigations would assist in gathering information of intra- and intermolecular interactions (Zoltowski, et al., 2008; Pudasaini, et al., 2015). For this approach, the structures of true light state and dark states are important and required. Differences would lead to further information about conformational changes inside the protein. The design of LOV proteins would assist in blue light-driven protein-protein interactions, regulation of gene transcription activation and influencing enzyme activity (Shcherbakova, et al., 2015).

Random and site-directed mutational experiments of LOV proteins revealed many mutants with severe differences of their photochemistry (Jentzsch, et al., 2009; Endres, 2013;

Endres, et al., 2015). Sequence alignment as exemplary conducted in the introduction section revealed a low identity amongst LOV proteins. However, it can be observed that substitutions of conserved residues like the two arginines coordinating the phosphate in PpSB1LOV described in this thesis and the Met49 in DsLOV have a higher impact on the photochemistry than others (Jentzsch, et al., 2009). This impact is clearly observed in the altered dark recovery of the mutants PpSB1-LOV-R66I, PpSB1-LOV-R61H/R66I, DsLOV-M49I, and DsLOV-M49S. Structural analysis can contribute further information to this aspect. Intermolecular interactions can be observed and analyzed, especially the differences between wildtype proteins and mutants can be compared. The combination of photochemistry and structural analysis can serve as a basis to design new photosensors. Further detailed structure analysis will help designing new photosensors and reporters like the already mentioned FbFPs where the optimal properties can be attained such as monomeric proteins with higher solubility and higher quantum yields. LOV proteins are called FbFPs after exchange of their photoactive cysteine into an alanine for example preventing the formation of the photoadduct and are permanent fluorescent molecules. A possible way to achieve the above mentioned optimal properties in DsLOV might be the removal or replacement by a synthetic fragment of the flexible N-terminus.

5. Conclusion and Outlook

The results obtained in this thesis lead to the prediction of the proposed signal propagation mechanisms in the short-LOV protein PpSB1-LOV from *Pseudomonas putida*. This prediction is based on the obtained dark and light state crystal structures in combination with SAXS data. This combination is worth mentioning as high-resolution data derived from X-ray scattering of crystals are combined with low-resolution data derived from aqueous protein solution. These data cover most aspects of the structure and are therefore as close as possible to the biological appearance of proteins inside the cell. The obtained illuminated state data, although useful for proteins unable to crystallize in the light state, can provide only minor information on large structural changes based on the crystal restraints. The design of photoreceptor proteins with interesting characteristics still remains challenging, but for PpSB1-LOV a successful manipulation of the dark recovery kinetics was already observed for the mutant PpSB1-LOV-R61H/R66I. The structure of PpSB1-LOV reveals a tight coordination of the phosphate moiety of the chromophore by four arginines with two of them already known to be conserved. The substitution of two arginines (R61H and R66I) resulted in an accelerated dark recovery.

A similar result was observed for DsLOV with a fast dark recovery in comparison to other LOV proteins in which at position 49 a methionine was observed but sequence alignment with other LOV proteins revealed that usually a leucine or isoleucine occupy this position. Site-directed mutagenesis revealed a severe influence of the methionine on the fast dark recovery as the substitution into an isoleucine or serine changes the dark recovery constant significantly. Thus indicating this position as highly relevant in the photochemistry in DsLOV.

The dimer interface reported for DsLOV was similar for DsLOV-M49S and DsLOV-C72A. Crystal structure of DsLOV-M49I revealed an entirely different dimer interface - mediated by the β-sheet of the LOV core domain instead of the N-terminal cap region as reported for the wildtype. This finding is most likely ascribed to a high flexibility in the N-terminus hindering the formation of a stable N-cap mediated dimer and shifts the formation slightly towards the β-sheet dimer formation.

The reported results of this thesis take the investigation of short-LOV proteins one step further. Currently, only two LOV proteins with true light state crystal structures are available. In comparison, both exhibit a different structural composition and a different oligomerization behavior. To an extent, these properties explain differences in the reaction to blue light and the photomechanism. However, the data available is still limited, further effort has to be put in the determination of light state structures. One has to take into account that the crystal structures

can only provide information about a rigid conformation. Additional methods based on aqueous samples such as SAXS and NMR have to be performed with regard to protein dynamics as in part presented in this thesis.

In this thesis, it was shown how a single mutation in DsLOV-M49I resulted in a dimer (β-sheet mediated) different to the wildtype (N-cap mediated). Further site directed mutagenesis and high resolution data will facilitate in the design of optogenetic tools with novel physical as well as spectral properties.

6. Literature

Adams, P. D., et al. 2002. PHENIX: building new software for automated crystallographic structure determination. *Acta Crystallogr. D Biol. Crytsallogr.* 2002, Bd. 58 (Pt 11), S. 1948-1954.

Ahmad, M. und Cashmore, A.R. 1993. HY4 gene of *A. thaliana* encodes a protein with characteristics of a blue-light receptor. *Nature.* 1993, 366, S. 162-166.

Akbar, S., et al. 2001. New Family of Regulators in the Envrionmental Signaling Pathway Which activates the General Stress Transcription Factor sigma B of *Bacillus subtilis*. *J. Bacteriol.* 2001, 183, S. 1329-1338.

Alexandre, M.T.A., et al. 2007. A based-catalysed mechanism for dark state recovery in the *Avena sativa* phototropin-1 LOV2 domain. *Biochemistry.* 2007, Bd. 46, S. 3129-3137.

Ataka, K., Hegemann, P. und Heberle, J. 2003. Vibrational Spectroscopy of an Algal Phot-LOV1 Domain Probes the Molecular Changes Associated with Blue-Light Reception. *Biophys. J.* 2003, 84, S. 466-474.

Avila-Perez, M., Hellingwerf, K.J. und Kort, R. 2006. Blue light activates the sigmaB-dependent stress response of *Bacillus subtilis* via YtvA. *J. Bacteriol.* 2006, Bd. 188, S. 6411-6414.

Ayers, R.A. und Moffat, K. 2008. Changes in quarternary structure in the signaling mechanism of PAS domains. *Biochemistry.* 2008, 47, S. 12078-12086.

Berera, R., et al. 2012. The Photophysics of the Orange Carotenoid Protein, a Light-Powered Molecular Switch. *J. Phys. Chem.* 2012, 116, S. 2568-2574.

Birge, R.R. 1990. Nature of the primary photochemical events in rhodopsin and bacteriorhodopsin. *Biochim. Biophys. Acta.* 1990, 1016, S. 293-327.

Bocola, M., et al. 2015. Light-Induced structural changes in a short light, oxygen, voltage (LOV) protein revealed by moelcular dynamics simulations - implications for the understanding of LOV photoactivation. *Front. Mol. Biosci.* 2015.

Borgstahl, G.E., Williams, D.R. und Getzoff, E.D. 1995. A structure of photoactive yellow protein, a cytosolic photoreceptor, unusual fold, active site, and chromophore. *Biochemistry.* 1995, 34, S. 6278-6287.

Bourenkov, G.P. und Popov , A.N. 2010. Optimization of data collection taking radiation damage into account. *Acta Crystallogr. D Biol. Cryszallogr.* 2010, 66, S. 409-419.

Bradford, M.M. 1976. A rapid and sensitive method for the quantitation of microgram quantities of protein utilizing the principle of protein-dye binding. *Analytical Biochemistry.* 1976, 72, S. 248-254.

Briggs, W.R. und Christie, J.M. 2002. Phototropin 1 and 2: verastaile plant blue-light receptors. *Trends Plant Sci.* 2002, 7, S. 204-210.

Briggs, W.R., Christie, J.M. and Salomon, M. 2001 a). Photottropins: A new family of flavin-binding photoreceptors in plants. *Antioxid. Redox Signaling.* 2001, Vol. 3, pp. 775-788.

Briggs, W.R., et al. 2001 b). The phototropinfamily of photoreceptors. *Plant Cell.* 13, 2001, S. 993-997.

Brown, J.M. 2007. Tumor hypoxia in cancer therapy. *Methods Enzymol.* 2007, 435, S. 297-321.

Buttani, V., Gärtner, W. und Losi, A. 2007. NTP-binding properties of the blue-light receptor YtvA and effects o the E105L mutation. *Eur. Biophys. J.* 2007, 36, S. 831-839.

Card, P.B. und Gardner, K.H. 2005. Structural basis of ARNT PAS-B dimerization: use of a common beta-sheet interface for hetero- and homodimerization. *J. Mol. Biol.* 2005, 353, S. 664-677.

Chalfie, M., et al. 1994. Green Fluorescent Protein as a Marker for Gene Expression. *Science.* 1994, Bd. 263, S. 802-805.

Chapman, S., et al. 2008. The photoreversible fluorescent protein iLOV outperforms GFP as a repoerter of plant virus infection. *Proc. Natl. Acad. Sci. USA.* 2008, Bd. 105(50), S. 20038-20043.

Chen, M. und Chory, J. 2011. Phytochrome signaling mechanims and the control of plant development. *Trends Cell Biol.* 2011, 21, S. 664-671.

Chen, V.B., et al. 2010. Molprobity: all-atom structure validation for macromolecular crystallography. *Acta Cryst. .* 2010, D66, S. 16-21.

Cheung, J., et al. 2008. Crystal structure of a Functional Dimer of the PhoQ Sensor Domain. *J. Biol. Chem.* 2008, 283, S. 13762-13770.

Christie , J.M., et al. 2015. Plant Flavoprotein Photoreceptors. *Plant Cell Physiol.* 2015, 56, S. 401-413.

Christie, J., et al. 1999. LOV (light, oxygen, voltage) domains of the blue light photoreceptor phototropin (nph1): binding sites for the chromophore flavin mononucleotide. *Proc. Natl. Acad. Sci. USA.* 1999, Bd. 96, S. 8779-8783.

Christie, J.M., et al. 2012. LOV to BLUF: flavorprotein contributions to the optogenetic toolkit. *Mol. Plant.* 2012, 5, S. 533-544.

Christie, J.M., et al. 2007. Steric interactions atabilize the signaling state of the LOV2 domain of phototropin 1. *Biochemistry.* 2007, Bd. 46, S. 9310-9319.

Christie, J.M., et al. 2012. Structural Tuning of the Fluorscent Protein iLOV for improved Photostability. *J. Mol. Biochem.* 2012, 287, S. 22295-22304.

Circolone, F., et al. 2012. Structural Basis for the Slow Dark Recovery of a Full-Length LOV Protein from *Pseudomonas putida*. *J. Mol. Biol.* 2012, Bd. 417, S. 362-374.

Coates, J.D. und Anderson, R.T. 2000. Emrging techniques for anaerobic bioremedation of contaminated environments. *Trends Biotechnol.* 2000, 18, S. 408-412.

Collaborative Computational Project. 2011. Overview of hte CCP4 suite and current developments. *Acta Cryst. .* 2011, D67, S. 235-242.

Conrad, K.C., Bilwes, M. und Crane, B. R. 2012. Light-induced Subunit Dissociation by a Light-Oxygen-Voltage Domain Photoreceptor from *Rhodobacter sühaeroides*. *Biochemistry.* 2012, Bd. 52, S. 378-391.

Conrad, K.S., Manahan , C.C. und Crane, B.R. 2014. Photochamistry of Flavoprotein Light Sensors. *Nat. Chem. Biol.* 2014, 10, S. 801-809.

Coto, P.B., et al. 2008. Origiin of the Absorption Maxima of the Photoactive Yellow Protein Resolved via Ab Initio Multiconfigurational Methods. *J. Phys. Chem. B.* 2008, 112, S. 7153-7156.

Crosson, S. und Moffat , K. 2001. Structure of a flavin-binding plant photoreceptor domain: Insights into light-mediated signal transduction. *PNAS.* 2001, 98, S. 2995-3000.

Crosson, S. und Moffat, K. 2002. Photoexcited structure of a plant photoreceptor domain reveals a light-dreiven molecular switch. *Plant Cell.* 14, 2002, S. 1067-1075.

Crosson, S., Rajagopal, S. und Moffat, K. 2003. The LOV domain family: photoresponsive signaling modules coupled to divers output domains. *Biochemistry.* 2003, 14, S. 2-10.

de Sanctis, D., et al. 2012. ID29: a high-intensity highly automated ESRF beamline for macromolecular crystallography experiments exploiting anomalous scattering. *J. Synchrotron Radiat.* 2012, Bd. 19, S. 455-461.

Dejonghe, W., et al. 2001. Bioaugmentation of soils by increasing microbial richness: missing links. *Environ. Microbiol.* 2001, 3, S. 649-657.

Drepper, T., et al. 2010. Flavin Mononucleotide-Based Fluoerscent Reporter Proteins Outperform Green Fluorescent Protien-Like Proteins as Quantitative In Vivo Real-Teime Reporters. *Appl. Env. Microbiol.* 2010, Bd. 76, S. 5990-5994.

Drepper, T., et al. 2007. Repoerter proteins for in vivo fluorescence without oxygen. *Nature Biotech.* 2007, 25, S. 443-445.

Efremov, R., et al. 2006. Time-resolved microspectrometry on a single crystal of bacteriorhodopsin reveals lattice-induced differences in the photocycle kinetics. *Biophys J.* 2006, Bd. 91, S. 1441-1451.

Eitoku, T., et al. 2005. Conformational dynamics of phototropin 2 LOV2 domain with hte linker upon photoexcitation. *J. Am. Chem. Soc.* 2005, 127, S. 13238-13244.

El-Arab, K., Pudasaini, A. und Zoltowski, B.D. 2015. Shot LOV Proteins in *Methylocystis* Reveal Insight sinto LOV Domain Photocycle Mechanisms. *PLoS ONE.* 2015.

Eltzschig, H.K. und Carmeliet, P. 2011. Hypoxia and inflammtion. *N. Engl. J. Med.* 2011, 364, S. 656-665.

Emsley, P. und Cowtan, K. 2004. Coot: model-building tools for molecular graphics. *Acta Crystallogr. D Biol. Crystallogr.* 2004, Bd. 60, S. 2126-2132.

Endres, S., et al. 2015. Structure and function of a short LOV protein from marine phototrophic bacterium *Dinoroseobacter shibae. BMC Micorbiology.* 2015.

Endres, Stephan. 2013. Bakterielle LOV-Blaulichtrezeptoren und deren Verwendung als Fluoreszenzreporter und Photosensilisatoren. 2013.

Ernst, J.F. und Tielker, D. 2009. Responses to hypoxia in fungal pahtogens. *Cell. Microbiol.* 2009, 11, S. 183-190.

Evans, P.R. 2011. An introduction to data reduction: space-group determination, scaling and intensity statistics. *Acta Cryst. .* 2011, D67, S. 282-292.

Evans, P.R. und Murshudov, G.N. 2013. How good are my data and what is the resolution. *Acta Cryst.* 2013, D69, S. 1204-1214.

Federov, R., et al. 2003. Crystal Structure and Molecular Mechanism of a Light-Induced Signaling Switch: The Phot-LOV1 Domain from Chlamydomonas reihnhardtii. *Biophys. J.* 2003, 84, S. 2474-2482.

Fenno, I., Yizhar, O. und Dessenroth, K. 2011. The development and application of optogenetics. *Annu. Rev. Neurosci.* 2011, 34, S. 389-412.

Flot, D., et al. 2010. The ID23-2 structural biology microfocus beamline at the ESRF. *J. Synchrotron Radiat.* 2010, Bd. 17, S. 107-118.

Franke, D. und Svergun, D.I. 2009. DAMMIF, a program for rapid ab-initio shapedetermination in small-angle scattering. *J. Appl. Cryst.* 2009, 42, S. 342-346.

Franklin, K.A. und Quail, P.H. 2010. Phytochrome functions in *Arabidopsis* development. *J. Exp. Bot.* 2010, 61, S. 11-24.

Freddolino, P.L., Diitrich, M und Schulten, K. 2006. Dynamic switchin mechanisms in LOV1 and LOV2 domains of plant phototropins. *Biophys J.* 2006, 91, S. 1067-1075.

Freddolino, P.L., Gardner, K.H. und Schulten, K. 2013. Signaling mechanisms of LOV domains: New insights from molecular dynamics studies. *Photochem. Photobiol. Sci.* 2013, 12, S. 1158-1170.

Fudim, R., et al. 2015. Photoinduced formation of flavin radicals in BLUF domains lacking the central glutamine. *FEBS J.* 2015, 282, S. 3161-3174.

Gomelsky, M. und Klug, M. 2002. BLUF: a novel FAD-binding domain involved in sensory transductionin microorganism. *Trends Biochem. Sci.* 2002, 27, S. 497-500.

Greenbaum, L., et al. 2000. Green Fluorescent Protein Photobleaching: a Model for Protein Damage by Endogenous and Exogenous Singlet Oxygen. *Biol. Chem.* 2000, 381, S. 1251-1258.

Halavatny, A. und Moffat, K. 2007. N- and C-terminal Flanking Regions Modulate Light-Induced Signal Transduction in the LOV2 Domain of the Vlue Light Sensor Phototropin 1 from Avena sativa. *Biochemistry.* 2007, Bd. 46, S. 14001-14009.

Harper, S.M., Christie, J.M. und GArdner, K.H. 2004. Disruption of the LOV-J helix interaction activates phototropin kinase activity. *Biochemistry.* 43, 2004, S. 16184-16192.

Harper, S.M., Neil, L.C. und Gardner, K.H. 2003. Structural basis of a phototropin light switch. 2003, 301, S. 1541-1544.

Hassett, D.J., et al. 2009. *Pseudomonas aeruginosa* hypoxic or anaerobic biofilm ind´fections within cystic fibrosis. *Trends Microbiol.* 2009, 17, S. 130-138.

Hefti, M., et al. 2004. The PAS fold. A redefinition of the PAS domain based upon structural prediction. *Eur. J. Biochem.* 2004, Bd. 271, S. 1198-1208.

Heintzen, C, Loros, J.J. und Dunlap, J.C. 2001. The PAS protein VIVID defines a clock-associated feedback loop that represses light input, modulates gating, and regulates clock resetting. *Cell.* 2001, 104, S. 453-464.

Henry, J.T. und Crosson, S. 2011. Ligand binding PAS domains in a genomic, cellular, and structural context. *Annu. Rev. Microbiol.* 2011, 65, S. 261-286.

Herrou, J. und Crosson, S. 2012. Function, Structure, and mechanism in bacterial photosensory LOV proteins. *Nat. Rev. Microbiol.* 2012, Bd. 9(10), S. 713-723.

Huala, E., et al. 1997. *Arabidopsis* NPH1: a protein kinase wiht a putative redox-sensing domain. *Science.* 1997, 19, S. 2120-2123.

Huang, Z.J., Edery, I. und Rosbash, M. 1993. PAS is a dimerization domain common to *Drosophila period* and several transcription factors. *Nature.* 1993, 364, S. 259-262.

Imaizumi T., et al. 2003. FKF1 is essential for photoperiodic-specific light signalling in *Arabidopsis*. *Nature.* 2003, 426, S. 302-306.

Iwata, T., Tokutomi, S. und Kandori, H. 2002. Photoreaction of the cysteine S-H group in the LOV2 domain of *Adiantum* phytochrome3. *J. Am. Chem. Soc.* 2002, 9, S. 11840-18841.

Jacques, D.A., et al. 2012. Publication guidelines fo structural modelling of small-anlge scattering data from biomolecules in solution. *Acta Cryst. D.* 2012, 68, S. 620-626.

Jentzsch, K., et al. 2009. Mutual exchange of kinetic properties by extended mutagenesis in two short LOV domain proteins from *Pseudomonas putida*. *Biochemistry.* 2009, Bd. 48, S. 10321-10333.

Jones, M.A., et al. 2006. Mutational analysis of phototropin 1 provides insights into the mechanism underlying LOV2 signal transmission. *J. Biol. Chem.* 2006, 282, S. 6405-6414.

Kabsch, W. 1988. Evaluation of Single.Crystal X-ray Diffraction Data from a Position-Sensitive Detector. *J. Appl. Cryst.* 1988, 21, S. 916-924.

Kabsch, W: und Sander , C. 1983. Dictionary of Protein Secondary Structure - Pattern-Recognition of Hydrogen-Bonded and Geometrical Features. *Biopolymers.* 1983, Bd. 22(12), S. 2577-2637.

Kabsch, Wolfgang. 2010. XDS. *Acta Cryst.* 2010, Bd. D66, S. 125-133.

Kantardjieff, K.A. und Rupp, B. 2003. Matthews coefficient probabilities: Improved estimates for unit cell contens of proteins, DNA, and protein-nucleic acid complaex crystals. *Protein Sci.* 2003, 12, S. 1865-1871.

Karakashew, D., Thomsen, A.B. und Angelidaki, I. 2007. Anaerobic biotechnnological approaches for production of liquid energy carrers from biomass. *Biotechnol. Lett.* 2007, 29, S. 1005-1012.

Katoh, S. 2013. MAFFT multiple sequence alignment software version 7: improvements in perfomrance and usuablility. *Mol. Biol. Evol.* 2013, 30, S. 772-780.

Katzke, N., et al. 2010. A novel T7 RNA polymerase dependent expression system for high-level protein production in the phototrophic bacterium Rhodobacter capsulatus. *Protein Expr. Purif.* 2010, 69, S. 137-146.

Kay, C.W.M., et al. 2003. Blue light perception in plants. Detection and characterization of a light-induced neutral flavin radical in a C450M mutant of Phototropin. *J. Biol. Chem.* 2003, 278, S. 10973-10982.

Key, J., et al. 2007. Structure of the Redox Sensor Domain of *Azetobacter vinelandii* NifL at Atomic Resolution: Signaling, Dimeriation, and Mechanism. *Biochemistry.* 2007, 46, S. 3614-3623.

Kinoshita, T., et al. 2001. Phot1 and Phot2 mediate blue light regulation of stomatal opening. *Nature.* 414, 2001, S. 656-660.

Kirilovsky, D. 2007. Photoprotection in cyanobacteria: the orange carotenoid protein (OCP)-related non-photochemical-quenching mechanism. *Photosynth. Res.* 2007, 93, S. 7-16.

Kliebenstein, D.J., et al. 2002. *Arabidopsis* UVR8 Regulates Ultraviolet-B Signal Transduction and Tolerance and Contains Sequence Similarity to Human Regulator of Chromatin Condensation 1. *Plant Phys.* 2002, 130, S. 234-243.

Konarev, P., et al. 2003. PRIMUS - a Windows-PC based system for small-angle scattering data. *J. Appl. Cryst.* 2003, Bd. 36, S. 1277-1282.

Kottke, T., et al. 2003. Irreversible photoreduction of flavin in a mutated Phot-LOV1 domain. *Biochemistry.* 2003, Bd. 42, S. 9854-9862.

Kottke, T., et al. 2003. Phot-LOV1: photocycle of a blue-light receptor domain from the green algal *Chlamydomonas reinhardtii*. *Biophys. J.* 2003, Bd. 84, S. 1192-1201.

Kozin, M. und Svergun, D. 2001. Automated matching of high- and low-resolution structural models. *J. Appl. Cryst.* 2001, 34, S. 33-41.

Kraulis, P. 1991. MOLSCRIPT: a program to produce both detailed and schematic plots of protein structures. *J. Appl. Crystallogr.* 1991, Bd. 24, S. 946-950.

Krauss, U., et al. 2009. Distribution and Phylogeny of Light-Oxygen-Voltage-Blue-Light-Signaling Proteins in the three kingdoms of Life. *J. Bacteriol.* 2009, Bd. 191, S. 7234-7242.

Krauss, U., et al. 2005. Inititial characterization of a blue-light sensing, phototropin-related protein from *Pseudomonas putida*: a paradigm fro an extended LOV construct. *Phs. Chem. Chem. Phys.* 2005, 7, S. 2804-2811.

Krissinel, E. und Henrick, K. 2007. Inference of macromolecular assemblies from crystalline state. *J- Mol. Biol.* 2007, Bd. 372, S. 774-797.

Kurokava, H., et al. 2004. A Redox-controlled Molecular Switch Revealed by the Crystal Structure of a Bacterial Heme PAS Sensor. *J. Biol. Chem.* 2004, 7, S. 20186-20193.

Kutta, R.J., et al. 2015. A search for radcial intermediates in the photocycle of LOV domains. *Photochem. Photobiol. Sci.* 2015, 14, S. 288-299.

Laemmli, U.K. 1970. Cleavage of structural proteins during the assembly of the head of bacteriophage T4. *Nature.* 1970, 227, S. 680-685.

Lamb, J.S., et al. 2008. Time-resolved Dimerization of a PAS-LOV protein measured with photocoupled small angle X.ray scattering. *J. Am. Chem. Soc.* 2008, 130, S. 12226-12227.

Lee, B.C., et al. 2001. Folding and signaling shaer the same pathway in a photoreceptor. *Proc. Natl. Acad. Sci. USA.* 2001, 98, S. 9062-9067.

Liscum, E. und Briggs, W.R. 1995. Mutations in the NPH1 locus of *Arabidopsis* disrupt the perception of phototrophic stimuli. *Plant Cell.* 1995, 7, S. 473-485.

Löffler, F.E. und Edwards, E.A. 2006. Harnessing microbial activities for environmental cleanup. *Curr. Opin. Biotechnol.* 2006, 17, S. 274-284.

Lokhandwala, J., et al. 2015. Structural biochemistry of a fungal LOV domain photoreceptor reveals an avolutionary conserved pathway integrating ligth and oxidative stress. *Structure.* 2015, 23, S. 116-125.

Losi, A. 2004. The bacterial counterparts of plant phototropins. *Photochem. Photobiol. Sci.* 2004, 3, S. 566-574.

Losi, A., et al. 2002. First Evidence for Phototropin-Related Blue-Light-Receptors in Prokaryotes. *Biophys. J.* 2002, 82, S. 2627-2634.

Losi, A., Quest, B. und Gärtner, W. 2003. Listening to the blue: the time-resolved thermodynamics of the bacterial blue-light receptor YtvA and its isolated LOV-domain. *Photochem. Photobiol.* 2003, Bd. 2, S. 759-766.

Lu, X. und Kang, Y. 2010. Hypoxia and hypoxia-inducible factors (HIFs): master regulatord of metastasis. *Clin. Cancer Res.* 2010, 16, S. 5928-5935.

Masuda, S. 2013. Light detection and signal transduction in the BLUF photoreceptors. *Plant and Cell Phys.* 2013, 54, S. 1171-179.

Matthews, B.W. 1968. Solvent content of protein crystals. *J. Mol. Biol.* 1968, 28, S. 491-497.

McCarthy, A., et al. 2009. A decade of user operation on the macromolecular crystallography MAD beamline ID14-4 at the ESRF. *J. Synchrotron Rad.* 2009, 16, S. 803-812.

McKinlay, J.B. und Harwood, C.S. 2010. Photobiological production of hydrogen gas as a biofuel. *Curr. Opin. Biotechnol.* 2010, 21, S. 244-251.

Merritt, E. und Bacon, D. 1997. Raster3D: photorealisic molecular graphics. *Methods Enzymol.* 1997, Bd. 277, S. 505-524.

Mitra , D., Yang, X. und Moffat, K. 2012. Crystal structure of Aureochrome 1 LOV suggest new desig strategies for optogenetics. *Structure.* 2012, 4, S. 698-706.

Möglich , A. und Moffat , K. 2010. Engeneered phototreceptors as novel optogenetic tools. *Photochem. Photobiol. Sci.* 2010, 9, S. 1286-1300.

Möglich, A. und Moffat, K. 2007. Structural Basis for Light-dependent Signaling in the Dimeric LOV Domain of the Photosensor YtvA. *J. Mol. Biol.* 2007, Bd. 373, S. 112-126.

Möglich, A., Ayers, R.A und Moffat, K. 2009. Structure and signaling mechansim of PER-Arndt-Sim domains. *Structure.* 2009, 17, S. 1282-1294.

Möglich, A., Ayers, R.A. und Moffat , K. 2009. Design and signaling mechanism of light-regulated histidine kinases. *J. Mol. Biol.* 2009, 385, S. 1433-1444.

Möglich, A., et al. 2010. Structre and Function of Plant Photoreceptors. *Annu. Rev. Plant Biol.* 2010, 61, S. 21-47.

Mortimer, C.E. und Müller, U. 2007. *Chemie.* Stuttgart : Georg Thieme Verlag, 2007.

Mukherjee, A., et al. 2013. Characterization of Flavin-Based Fluorescent Proteins: An Emergin Class of Fluorescent Reporters. *PLoS ONE.* 2013.

Myatake, H., et al. 2000. Sensory Mechanism of Oxygen Sensor FixL from *Rhizobium meliloti*: Crystallographic, Mutagenesis and Resonance Raman Spectroscopic Studies. *JMB.* 2000, 301, S. 415-431.

Nambu, J.R., et al. 1991. The *Drosophila single-minded* gene encodes a helix-loop-helix protein that acts as a master regulator of CNS midline development. *Cell.* 1991, 95, S. 1157-1167.

Nash, A. I. , et al. 2011. Structural basis of photosensitivity in a bacterial light-oxygen-voltage/helix-turn-helix (LOV-HTH) DNA-binding protein. *PNAS.* 2011, Bd. 108, 23, S. 9449-9454.

Nash, A.I., et al. 2008. A conserved glutamine plays a central role in LOV domain signal transmission and its duration. *Biochemistry.* 2008, 47, S. 13842-13849.

Nelson, K.E., et al. 2002. Complete genome sequence and comparative analysis of the metabolically versatile *Pseudomonas putida* KT2440. *Env. Microbiol.* 2002, 4, S. 799-808.

Nozaki, D., et al. 2004. Role of Gln1029 in the photoactivation process of the LOV2 domain in *Adiantum* phytochrome3. *Biochemistry.* 2004, 43, S. 8373-8379.

On the role of the crystal Environment on Determining Protein Side-chain Conformations. **Jacobson, M. P., et al. 2002.** 2002, J. Mol. Biol., Bd. 320, S. 597-608.

Palleroni, N. 1984. *Family I. Pseudomonaceae.* Baltimore : Williams and Wilkns, 1984.

Patterson, A.P., Booth, S.A. und Saba, R. 2014. The Emerging Use od in Vivo Optical Imaging in the Study of Neurodegenerative Diseases. *Biomed. Res. Int.* 2014.

Pellequer, J.L., et al. 1998. Photoactive yellow protein: a structural prototype for the three-dimensional fold of the PAS domain superfamily. *Proc. Natl. Acad. Sci. USA.* 1998, 95, S. 5884-5890.

Pernot , P., et al. 2013. Upgraded ESRF BM29 beamline for SAXS on macromolecules in solution. *J. Synchrotron Radiat.* 2013.

Peter, E., Dick B. und Baerle, S.A. 2010. Mechanism of siganl transduction of the LOV2-Ja photosensor from *Avena sativa. Nat. Commun.* 2010.

Petoukhov , M.V., et al. 2012. New developments in the ATSAS program package for small-angle scattering data anlysis. *J. Appl. Cryst.* 2012, Bd. 45, S. 342-350.

Petoukhov, M.V. und Svergun, D.I. 2005. Global rigid body modelling of macromolecular complexes against small-angle scattering data. *Biophys. J.* 2005, 89, S. 1237-1250.

Petoukhov, M.V., et al. 2007. ATSAS 2.1 - towards automated and web-supported small-angle scattering data analysis. *J. Appl. Cryst.* 2007, 40, S. 223-228.

Pettersen, E.F., et al. 2004. UCSF Chimera -- a visualization system for explorattory research and analysis. *J. Comput. Chem.* 2004, 25, S. 1605-1612.

Pongratz, I., et al. 1998. Role of the PAS domain in regulation of dimerization and DNA binding specificity of the dioxin receptor. *Mol. Cell. Biol.* 1998, 18, S. 4079-4088.

Ponting, C.P. und Aravind, L. 1997. PAS: amultifunctuinal domain family comes to light. *Current Biol.* 1997, 7, S. R674-R677.

Potzkei, J., et al. 2012. Real-time determination of intracellular oxygen in bacteria using a genetically encoded FRET-based biosensor. *BMC biology.* 2012, 10, S. 28.

Pudasaini, A., El-Arab, K.K. und Zoltowski, B.D. 2015. LOV-based optogenetic devices: light-driven modules to impart photoregulated control of cellular signaling. *Front. Mol. Biosci.* 2015, Bd. 2:18.

Purcell, E.B., et al. 2007. A photosensory two-component system regulates bacterial cell attachment. *Proc. Natl. Acad. Sci. USA.* 2007, Bd. 104, S. 18241-18246.

Purves, W.K., et al. 2006. *Biologie.* s.l. : Spektrum, 2006.

Quail, P.H. 1998. The phytochrome family: dissection of functional roles and signaling pathways among family members. *Philosophical Transactions of the Royal Society of London. Series B: Biological Science.* 1998, 353, S. 1399-1403.

Raffelberg, S., et al. 2011. Modulation of the Photocycle of a LOV Domain Photoreceptor by the Hydrogen-Bonding Network. *JACS.* 2011, Bd. 133, S. 5346-5356.

Rivera-Cancel, G., et al. 2014. Full-length structure of a monomeric histidine kinase reveals basis for sensory regulation. *Proc. Natl. Acad. Sci. USA*. 2014, 16, S. 17839-17844.

Rizzini, L., et al. 2011. Perception of UV-B by the *Arabidopsis* UVR8 Protein. *Science.* 2011, 332, S. 103-106.

Rockwell, N.C., Su, Y.S. und Lagarias, J.C. 2006. Phytochrome Structure and Siganling mechanism. *Annu. Rev. Plant Biol.* 2006, 57, S. 837-858.

Rustad , T.R., et al. 2009. Hypoxia: a window into Mycobacterium tuberculosis latency. *Cell Microbiol.* 2009, 11, S. 1151-1159.

Sakai, T., et al. 2001. Arabidopsis nph1 and npl1: Blue-light receptors that mediate both phototropism and chloroplast relocation. *Proc. Natl. Acad. Sci. USA.* 98, 2001, 98, S. 6969-6974.

Sakamato, K. und Briggs, W.R. 2002. Cellular and subcellular localization of phototropin 1. *Trends Plant Sci.* 14, 2002, S. 1723-1735.

Salomon, M., et al. 2000. Photochemical an Mutational Analysis of the FMN-Binding Domains of the Plant BLue Light Receptor, Phototropin. *Biochemistry.* 2000, Bd. 39, S. 9401-9410.

Sambrook, J., Fritsch, E. F. und Maniatis, T. 1989. *Molecular Cloning: A Laboratory Manual.* Cold Spring Harbor, New York : s.n., 1989.

de Sanctis, D., Beteva, A., Caserotto, H., Dobias, F., Gabadinho, J., Giraud, T., Gobbo, A., Guijarro, M., Lentini, M., Lavault, B., Mairs, T., McSweeney, S., Petitdemange, S., Rey-Bakaikao, V., Surr, J., Theveneau, P., Leonard, G. A., Mueller-Dieckmann, C. 2012. ID29: a high-intensity highly auotmated ESRF beamline for macromolecular crystallography experiments exploiting anomalous scattering. *J. Synchrotron Rad*. 2012, 19, 455-461

Schleicher, E., et al. 2004. On the Reaction Mechanism of Adduct Formation in LOV Domains of the Plant Blue-Light Receptor Phototropin. *J. Am. Chem. Soc.* 2004, 126, S. 11067-11076.

Schmid, A., et al. 2001. Industrial bioctalysis today anf tomorrow. *Nature.* 2001, 409, S. 258-268.

Schobert, M. und Tielen, P. 2010. Contribution of oxygen-limiting conditions to persitent infection of *Pseudomonas aeruginosa. Future Microbiol.* 2010, 5, S. 603-621.

Schreiber, M., et al. 2006. Quantum mechanical studies on the crystallographic model of bacteriorhodopsin. *Angew. Chem. Int. Ed. Engl.* 2006, 45, S. 4274-4277.

Schwerdtfeger, C. und Linden, H. 2003. VIVID is a flavoprotein and serves as afungal blue light photoreceptor for photoadaption. *The EMBO Journal.* 2003, Bd. 22, S. 4846-4855.

Semenza G.L. 2003. Regulation of mammalian O2 homeostasis by hypoxia-inducible factor 1. *Annu. Rev. Cell Dev. Biol.* 2003, 15, S. 551-578.

Shcherbakova, D.M., et al. 2015. Natural Photoreceptors as a Source of Fluorescent Proteins, Biosensors, and Optogenetic Tools. *Annu. Rev. Biochem.* 2015, Bd. 84, S. 519-550.

Shu, X. Lev-Ram, et al. 2011. A Genetically Encoded Tag for Correlated Light and Electron Microscopy of Intact Cells, Tissues, and Organisms. *PLoS Biol.* 2011.

Song, S.H., et al. 2007. Photo-reduction of flavin mononucleotide to semiquinone form in LOV domain mutants of blue-light receptor phot from *Chlamydomonas reinhardtii*. *J. Photobiol. Photochem.* 2007, 87, S. 37-48.

Spudich, J.L. und Luecke, H. 2002. Sensory rhodopsin II: funcitonal insights from structure. *Curr. Opin. Struct. Biol.* 2002, 12, S. 540-546.

Strong, M., et al. 2006. Toward the structural genomics of complexes: Crystal structure of a PE/PPE protein complex Mycobacterium tuberculosis. *PNAS.* 2006, 103, S. 8060-8065.

Studier, F. W. 2005. Protein production by auto-induction in high density shaking cultures. 2005, 41, S. 207-234.

Surrey, T., et al. 1998. Chromophore-assisted light inactivation and self-organization of microtubules and motors. *Proc. Natl. Acad. Sci. USA.* 1998, 95, S. 4293-4298.

Svergun, D. 1999. Restoring low Resolution structure of biological macromolecules from solution scattering using simulated annealing. *Biophys J.* 1999, S. 1879-2886.

Svergun, D., Barberato, C. und Koch, M. 1995. CRYSOL - a Program to Evaluate X-ray Solution Scatteringof Biological Macromolecules from Atomic Coordinates. *J. Appl. Crystall.* 1995, Bd. 28, S. 768-773.

Svergun, D.I. 1992. Determination of the Regularization Parameter in Indirect-Transform Methods Using Perceptual Critaeria. *J. Appl. Cryst.* 1992, 25, S. 495-503.

Svergun, D.I., Petoukhov, M.V. und Koch, M.H.J. 2001. Determination of domain structure of proteins from X-ray solution scattering. *Biophys. J.* 2001, 80, S. 2946-2953.

Swartz , T.E., et al. 2001. The photocycle of a flavin-binding domain of the blue-light photoreceptor phototropin. *J. Biol. Chem.* 2001, Bd. 276, S. 36493-36500.

Swartz, T.E., et al. 2007. Blue-light-activated histidine kinases: Two-component sensors in bacteria. *Science.* 2007, Bd. 317, S. 1090-1093.

Sycz, G., et al. 2015. Histidine Kinase Modulates the General Stress Response System an Affects the virB Operon Expression in Brucella abortus. *PLoS ONE.* 2015.

Talyor, B. und Zhulin, I. 1999. PAS domains: Internal sensors of oxygen, redox potential, and light. *Microbiol. Mol. Biol.* 1999, Bd. 63, S. 479-506.

Tang, Y., et al. 2010. Interdomain signalling in the blue-light sensing and GTP-binding protein YtvA: a mutagenesis study uncovering the importance of specific protein sites. *Photochem. Photobiol. Sci.* 2010, 9, S. 47-56.

Taylor, D. und Zhulin, I. 1999. PAS domains: internal sensors of oxygen, redox potential, and light. *Microbiol. Mol. Biol. Rev.* 1999, Bd. 63, S. 470-506.

Tielker, D., et al. 2009. Flavin mononucleotide-based fluorescent protein as an oxygen-independent reporter in *Candida albicans* and *Saccharomyces cerevisiae*. *Eukaryot Cell.* 2009, Bd. 8, S. 913-915.

Tilbrook, K., et al. 2013. The UVR8 UV-B Photoreceptor: Perception, Signaling and Response. *The Arabidopsis book.* 2013.

Torra, J., et al. 2015. Singlet oxygen photosensitisation by the novel fluorescent protein Pp2FBFP L30M, a novel derivative of *Pseudomonas putida* flavin-binding Pp2FbFP. *Photochem. Photobiol. Sci.* 2015, 14, S. 280-287.

Tsien, Roger Y. 1998. The Green Fluorescent Protein. *Annu. Rev. Biochem.* 1998, Bd. 67, S. 509-544.

Urzhumtseva, L., et al. 2009. Crystallographic model quality at a glance. *Acta Cryst.* 2009, D65, S. 297-300.

Vagin, A. und Teplyakov, A. 1997. MOLREP: an automated program for moelcular replacement. *J. Appl. Cryst.* 1997, 30, S. 1022-1025.

Vaidya , A., et al. 2011. Structure of Light-Activated LOV Protein Dimer That Regulates Transcription. *Struct. Biol.* 2011.

Vaidya, A.T., et al. 2011. Structure of a Light-Activated LOV Protein Dimer That Regulates Transcritption. *Sci. Signal.* 2011, Bd. 4, 184, S. ra50.

Volkov, V. und Svergun, D. 1984. Computer simulations as a tool for tracing the conformational differences between proteins in solution and crystallie state. *JMB.* 1984, Bd. 167, S. 559-564.

Volkov, V.V. und Svergun, D.I. 2003. Uniqueless of ab-initio shape determination in small-angle scattering. *J. Appl. Cryst.* 2003, Bd. 36, S. 860-864.

Wagner-Döble, I., et al. 2010. The complete genome sequence of the algal symbiont *Dinoroseobacter shibae*: a hitchhiker´s guide to life in the sea. *ISME J.* 2010, 4, S. 61-77.

Wallrabe, H. und Perisamy, A. 2005. Imaging protein molecules using FRET and FLIm microscopy. *Curr. Opin. Biotechnol.* 2005, 16, S. 19-27.

Walter, J., et al. 2012. Flavin Mononucleotide-Based Fluorescent Proteins Function in Mammalian Cells without Oxygen Requirement. *PLoS ONE.* 2012.

Wingen, M., et al. 2014. The photophysics of LOV-based fluorescent proteins - new tools for cell biology. *Photochem. Photobiol. Sci.* 2014, 13, S. 875-883.

Winn, M., et al. 2011. Overview of the CCP4 suite and current developments. *Acta Cryst.* 2011, Bd. D67, S. 235-242.

Wriggers, W. 2010. Using Situs for the Integration of Multi-Resolution Structures. *Biophys. Rev.* 2010, 2, S. 21-27.

Yamamoto, A., et al. 2009. Light Signal Transduction Pathway from Flavin Chromophore to the Ja helix of *Arabidopsis* Phototropin. *Biophys J.* 2009, 96, S. 2771-2778.

Zhulin, I.B., Taylor, B.L: und Dixon, R. 1997. PAS domain S-boxes in Archaea, bacteria, and sensors for oxygen and redox. *Trends Biochem.* 1997, 22, S. 331-333.

Zoltowski , B.D., Vaccaro, B. und Crane, B.R. 2009. Mechanism-based tuning of a LOV domain photoreceptor. *Nat. Chem. Biol.* 2009, Bd. 5, S. 827-834.

Zoltowski, B. D. und Crane, B.R. 2008. Light Activation of the LOV Protein Vivid Generates a Rapidly Exchaning Dimer. *Biochemistry.* 2008, 47, S. 7012-7019.

Zoltowski, B.D., et al. 2007. Conformational switching in the fungal light sensor Vivid. *Science.* 2007, Bd. 316, S. 1054-1057.

7. Appendix

7.1. DNA-Sequences

7.1.1. PpSB1-LOV

```
ATGGGCAGCAGCCATCATCATCATCATCACAGCAGCGGCCTGGTGCCGCGCGGCAGCCATATGATCAACGCGCAATTGCT
GCAATCGATGGTCGATGCGTCCAATGACGGCATCGTGGTTGCCGAAAAGGAAGGCGACGACACCATCCTGATCTACGTGA
ACGCCGCTTTCGAATACCTCACTGGCTACAGCCGTGACGAGATTCTCTACCAGGATTGCCGGTTCCTGCAGGGTGACGAC
CGTGACCAGCTTGGCCGCGCACGCATCCGCAAGGCCATGGCCGAAGGCCGCCCATGCCGCGAAGTGCTGCGCAACTATCG
CAAGGACGGCAGCGCCTTCTGGAACGAGCTGTCGATCACGCCGGTGAAGAGCGACTTCGACCAGCGCACCTACTTCATCG
GCATCCAGAAGGACGTCAGCCGCCAGGTCGAACTGGAACGGGAGCTGGCAGAACTGCGCGCTCGTCCGAAACCCGACGAA
CGCGCCTGA
```

7.1.2. PpSB1-LOV-C53A

```
ATGGGCAGCAGCCATCATCATCATCATCACAGCAGCGGCCTGGTGCCGCGCGGCAGCCATATGATCAACGCGCAATTGCT
GCAATCGATGGTCGATGCGTCCAATGACGGCATCGTGGTTGCCGAAAAGGAAGGCGACGACACCATCCTGATCTACGTGA
ACGCCGCTTTCGAATACCTCACTGGCTACAGCCGTGACGAGATTCTCTACCAGGATGCACGGTTCCTGCAGGGTGACGAC
CGTGACCAGCTTGGCCGCGCACGCATCCGCAAGGCCATGGCCGAAGGCCGCCCATGCCGCGAAGTGCTGCGCAACTATCG
CAAGGACGGCAGCGCCTTCTGGAACGAGCTGTCGATCACGCCGGTGAAGAGCGACTTCGACCAGCGCACCTACTTCATCG
GCATCCAGAAGGACGTCAGCCGCCAGGTCGAACTGGAACGGGAGCTGGCAGAACTGCGCGCTCGTCCGAAACCCGACGAA
CGCGCCTGA
```

7.1.3. PpSB1-LOV-R66I

```
ATGGGCAGCAGCCATCATCATCATCATCACAGCAGCGGCCTGGTGCCGCGCGGCAGCCATATGATCAACGCGCAATTGCT
GCAATCGATGGTCGATGCGTCCAATGACGGCATCGTGGTTGCCGAAAAGGAAGGCGACGACACCATCCTGATCTACGTGA
ACGCCGCTTTCGAATACCTCACTGGCTACAGCCGTGACGAGATTCTCTACCAGGATTGCCGGTTCCTGCAGGGTGACGAC
CGTGACCAGCTTGGCATTGCACGCATCCGCAAGGCCATGGCCGAAGGCCGCCCATGCCGCGAAGTGCTGCGCAACTATCG
CAAGGACGGCAGCGCCTTCTGGAACGAGCTGTCGATCACGCCGGTGAAGAGCGACTTCGACCAGCGCACCTACTTCATCG
GCATCCAGAAGGACGTCAGCCGCCAGGTCGAACTGGAACGGGAGCTGGCAGAACTGCGCGCTCGTCCGAAACCCGACGAA
CGCGCCTGA
```

7.1.4. PpSB1-LOV-R61H/R66I

```
ATGGGCAGCAGCCATCATCATCATCATCACAGCAGCGGCCTGGTGCCGCGCGGCAGCCATATGATCAACGCGCAATTGCT
GCAATCGATGGTCGATGCGTCCAATGACGGCATCGTGGTTGCCGAAAAGGAAGGCGACGACACCATCCTGATCTACGTGA
ACGCCGCTTTCGAATACCTCACTGGCTACAGCCGTGACGAGATTCTCTACCAGGATTGCCGGTTCCTGCAGGGTGACGAC
CATGACCAGCTTGGCATTGCACGCATCCGCAAGGCCATGGCCGAAGGCCGCCCATGCCGCGAAGTGCTGCGCAACTATCG
CAAGGACGGCAGCGCCTTCTGGAACGAGCTGTCGATCACGCCGGTGAAGAGCGACTTCGACCAGCGCACCTACTTCATCG
GCATCCAGAAGGACGTCAGCCGCCAGGTCGAACTGGAACGGGAGCTGGCAGAACTGCGCGCTCGTCCGAAACCCGACGAA
CGCGCCTGA
```

7.1.5. DsLOV

```
ATGCGCAGACATTATCGCGACCTGATACGGAACACGCCCATGCCCGACACACCGCAAGACATCGCAGACCTCCGCGCCCT
TCTGGACGAGGACGAGGCCGAGATGAGCGTCGTCTTCTCCGACCCGTCGCAGCCCGACAACCCGATGATCTATGTCAGCG
ACGCCTTCCTGGTCCAGACCGGCTACACCCTCGAAGAGGTGCTGGGCCGCAACTGCCGTTTCCTGCAGGGGCCCGACACC
AACCCCCATGCGGTCGAGGCGATCCGCCAGGGCCTGAAGGCCGAAACCCGCTTCACCATCGACATCCTGAATTACCGCAA
GGACGGCTCGGCCTTCGTCAACCGCTTGCGCATCCGTCCGATCTATGACCCCGAGGGCAACCTGATGTTCTTCGCAGGCG
CCCAGAACCCGGTCCTCGAGCACCACCACCACCACCACTGA
```

7.1.6. DsLOV-M49S

```
ATGCGCAGACATTATCGCGACCTGATACGGAACACGCCCATGCCCGACACACCGCAAGACATCGCAGACCTCCGCGCCCT
TCTGGACGAGGACGAGGCCGAGATGAGCGTCGTCTTCTCCGACCCGTCGCAGCCCGACAACCCGAGCATCTATGTCAGCG
ACGCCTTCCTGGTCCAGACCGGCTACACCCTCGAAGAGGTGCTGGGCCGCAACTGCCGTTTCCTGCAGGGGCCCGACACC
AACCCCCATGCGGTCGAGGCGATCCGCCAGGGCCTGAAGGCCGAAACCCGCTTCACCATCGACATCCTGAATTACCGCAA
GGACGGCTCGGCCTTCGTCAACCGCTTGCGCATCCGTCCGATCTATGACCCCGAGGGCAACCTGATGTTCTTCGCAGGCG
CCCAGAACCCGGTCCTCGAGCACCACCACCACCACCACTGA
```

7.1.7. DsLOV-M49I

```
ATGCGCAGACATTATCGCGACCTGATACGGAACACGCCCATGCCCGACACACCGCAAGACATCGCAGACCTCCGCGCCCT
TCTGGACGAGGACGAGGCCGAGATGAGCGTCGTCTTCTCCGACCCGTCGCAGCCCGACAACCCGATTATCTATGTCAGCG
ACGCCTTCCTGGTCCAGACCGGCTACACCCTCGAAGAGGTGCTGGGCCGCAACTGCCGTTTCCTGCAGGGGCCCGACACC
AACCCCCATGCGGTCGAGGCGATCCGCCAGGGCCTGAAGGCCGAAACCCGCTTCACCATCGACATCCTGAATTACCGCAA
GGACGGCTCGGCCTTCGTCAACCGCTTGCGCATCCGTCCGATCTATGACCCCGAGGGCAACCTGATGTTCTTCGCAGGCG
CCCAGAACCCGGTCCTCGAGCACCACCACCACCACCACTGA
```

7.1.8. DsLOV-C72A

```
ATGCGCAGACATTATCGCGACCTGATACGGAACACGCCCATGCCCGACACACCGCAAGACATCGCAGACCTCCGCGCCCT
TCTGGACGAGGACGAGGCCGAGATGAGCGTCGTCTTCTCCGACCCGTCGCAGCCCGACAACCCGATGATCTATGTCAGCG
ACGCCTTCCTGGTCCAGACCGGCTACACCCTCGAAGAGGTGCTGGGCCGCAACGCGCGTTTCCTGCAGGGGCCCGACACC
AACCCCCATGCGGTCGAGGCGATCCGCCAGGGCCTGAAGGCCGAAACCCGCTTCACCATCGACATCCTGAATTACCGCAA
GGACGGCTCGGCCTTCGTCAACCGCTTGCGCATCCGTCCGATCTATGACCCCGAGGGCAACCTGATGTTCTTCGCAGGCG
CCCAGAACCCGGTCCTCGAGCACCACCACCACCACCACTGAG
```

7.2. Protein sequences

7.2.1. PpSB1-LOV

```
(-19) MGSSHHHHHHSSGLVPRGSHMINAQLLQSMVDASNDGIVVAEKEGDDTILIYVNAAFEYLTGYSRDEILYQDC
RFLQGDDRDQLGRARIRKAMAEGRPCREVLRNYRKDGSAFWNELSITPVKSDFDQRTYFIGIQKDVSRQVELERELA
ELRARPKPDERA* (142)
```

7.2.2. PpSB1-LOV-C53A

```
(-19) MGSSHHHHHHSSGLVPRGSHMINAQLLQSMVDASNDGIVVAEKEGDDTILIYVNAAFEYLTGYSRDEILYQDA
RFLQGDDRDQLGRARIRKAMAEGRPCREVLRNYRKDGSAFWNELSITPVKSDFDQRTYFIGIQKDVSRQVELERELA
ELRARPKPDERA* (142)
```

7.2.3. PpSB1-LOV-R66I

```
(-19) MGSSHHHHHHSSGLVPRGSHMINAQLLQSMVDASNDGIVVAEKEGDDTILIYVNAAFEYLTGYSRDEILYQDC
RFLQGDDRDQLGIARIRKAMAEGRPCREVLRNYRKDGSAFWNELSITPVKSDFDQRTYFIGIQKDVSRQVELERELA
ELRARPKPDERA* (142)
```

7.2.4. PpSB1-LOV-R61H/R66I

```
(-19) MGSSHHHHHHSSGLVPRGSHMINAQLLQSMVDASNDGIVVAEKEGDDTILIYVNAAFEYLTGYSRDEILYQDC
RFLQGDDHDQLGIARIRKAMAEGRPCREVLRNYRKDGSAFWNELSITPVKSDFDQRTYFIGIQKDVSRQVELERELA
ELRARPKPDERA* (142)
```

7.2.5. DsLOV

(1) MRRHYRDLIRNTPMPDTPQDIADLRALLDEDEAEMSVVFSDPSQPDNPMIYVSDAFLVQTGYTLEEVLGRNCR
FLQGPDTNPHAVEAIRQGLKAETRFTIDILNYRKDGSAFVNRLRIRPIYDPEGNLMFFAGAQNPVLEHHHHHH* (146)

7.2.6. DsLOV-M49S

(1) MRRHYRDLIRNTPMPDTPQDIADLRALLDEDEAEMSVVFSDPSQPDNPSIYVSDAFLVQTGYTLEEVLGRNCR
FLQGPDTNPHAVEAIRQGLKAETRFTIDILNYRKDGSAFVNRLRIRPIYDPEGNLMFFAGAQNPVLEHHHHHH* (146)

7.2.7. DsLOV-M49I

(1) MRRHYRDLIRNTPMPDTPQDIADLRALLDEDEAEMSVVFSDPSQPDNPIIYVSDAFLVQTGYTLEEVLGRNCR
FLQGPDTNPHAVEAIRQGLKAETRFTIDILNYRKDGSAFVNRLRIRPIYDPEGNLMFFAGAQNPVLEHHHHHH* (146)

7.2.8. DsLOV-C72A

(1) MRRHYRDLIRNTPMPDTPQDIADLRALLDEDEAEMSVVFSDPSQPDNPMIYVSDAFLVQTGYTLEEVLGRNAR
FLQGPDTNPHAVEAIRQGLKAETRFTIDILNYRKDGSAFVNRLRIRPIYDPEGNLMFFAGAQNPVLEHHHHHH* (146)

Erklärung

Ich versichere an Eides Statt, dass die Dissertation von mir selbstständig und ohne unzulässige fremde Hilfe unter Beachtung der „Grundsätze zur Sicherung guter wissenschaftlicher Praxis an der Heinrich-Heine-Universität Düsseldorf“ erstellt worden ist.

Die Dissertation in der vorgelegten oder in ähnlicher Form wurde noch bei keiner anderen Institution eingereicht. Ich habe bisher keine erfolglosen Promotionsversuche unternommen.

Viersen, den _____ _____

Katrin Röllen